UNIVERSITY OF BIRMINGHAM

A STUDY OF A MODULAR MICROFLUIDIC STABILISER SYSTEM USING FLUIDIC CIRCUIT ANALOGY

BY

WUYANG ZHUGE

A THESIS SUBMITTED TO

THE COLLEGE OF ENGINEERING AND PHYSICAL SCIENCES

THE UNIVERSITY OF BIRMINGHAM

DOCTOR OF PHILOSOPHY

Department of Mechanical Engineering

School of Engineering

College of Engineering and Physical Sciences

The University of Birmingham

March 2023

ABSTRACT

The thesis presents my PhD study about a novel flow-control solution for typical lab-on-a-chip systems. The design, fabrication, and analysis of a Lego-like modular microfluidic stabiliser system are discussed. This system can provide controllable, amplitude-adjustable features for microfluidic systems and offer steady and accurate flow control solutions. The study has three main contributions: (1) it provided a generalised and standardised stabiliser system with adjustable working curves; (2) it established a simplified fluid circuit analogy to present a prediction model for all stabiliser systems; and (3) it improved the universality of microfluidic systems for different applications.

For contribution (1), the thesis presents a Lego-like modular stabiliser system. Inspired by Lego toys, the devices are standardised, pluggable and exchangeable. With a simplified design iteration, the 3D-printed modular microfluidic stabiliser system can be quickly assembled with twelve adjustable working states and tunable resistance and capacitance constants (RC constants) ranging from 3.24 s to 12.57 s. The Lego-like design can enlarge the working range of stabilisers and provide more generalised design iterations for microfluidic stabilisers.

For contribution (2), by studying the deflection of membranes, this work uses a recursive method to summarise a simplified circuit model for microfluidic

stabiliser systems. By borrowing the transfer function and amplitude response law from the digital circuit analogy, the established model has an R-square value of 0.95, which proves the model's accuracy.

For contribution (3), to evaluate the system's effectiveness and improve the universality of all microfluidic chips with a common flow-control solution, the stabiliser system is tested when working with typical fluid providers such as gas pumps, piezoelectric pumps, and syringe pumps. The Lego-like system can provide controllable working curves with an optimal stabilisation ratio of less than 1%. The amplitude feature can be controlled numerically by linking different combinations of devices. Furthermore, droplet generation experiments coupled with the proposed system are conducted and discussed. By using the novel flow-control solution, the polydispersity of droplets reduced from 0.13 to 0.07 by using a typical cross-junction droplet generator. The standard deviation of the droplet distribution reduced by over 40% when compared with its original working state without stabilisers.

In summary, this thesis presents a novel flow-control solution based on a Lego-like microfluidic stabiliser system with a predictable working curve. The system's adjustability and universality, combined with the simplified prediction model established in this study, make it a valuable tool for a wide range of microfluidic applications.

ACKNOWLEDGEMENTS

I would like to express my heartfelt gratitude to my PhD supervisors, Professor Kyle Jiang, Professor Xing Cheng and Doctor Carl Anthony, for granting me this opportunity, providing me with support and guidance during my most challenging moments, and generously sharing their knowledge and advice both in academics and personal life. Furthermore, I would like to thank Dr Weihao Li, my research collaborator, for collaborating with me on innovative ideas, which makes the research better.

I am also indebted to my colleagues, Dr Tianchu Jiang, and Dr Luo Yun for their valuable insights on how to commence research, and how to lead a fulfilling life during daily routines. Furthermore, I wish to express my sincere gratitude to my parents, who have been my pillars of support throughout life's struggles and provided me with a warm home during my childhood and beyond, no matter where they are.

I would also like to thank my friends, who have stood by me. Furthermore, I am grateful to my beloved cat Douhua, who always sleeps behind my keyboard and gives me happiness while I work.

Finally, thanks to Janet Hingley, who proofread my thesis for language conventions, spelling, and grammar through Janet's Proofreading Service.

TABLE OF CONTENTS

LIST OF FIGURES

LIST OF TABLES

LIST OF ABBREVIATIONS

ABS	Acrylonitrile butadiene styrene
FSI	Fluid structure interaction
FDM	Fused deposition modelling
LPF	Low pass filter
LSM	Least squares method
MSS	Modular stabiliser system
PDMS	Polydimethylsiloxane
PLA	Polylactic acid
PMMA	Polymethyl methacrylate
PTFE	Polytetrafluoroethylene
RC	Resistance and capacitance
RCL	Resistor capacitor inductor
SLA	Stereolithography
SLS	Selective laser sintering

LIST OF VARIABLES

A	Cross sectional area of pipe
A_i	Amplitude or oscillation of initial flow
A_s	Amplitude or oscillation of stabilised flow
C	Capacitor
$C_{chamber}$	Fluidic capacitance of chamber
$C_{deflection}$	Fluidic capacitance of deflection
C_f	Fluidic capacitance
$C_{geometry}$	Geometry constant
C_i	Capacitance at node i
C_{MSS}	Capacitance of modular fluidic system
C_{pump}	Capacitance of pump
C_{total}	Total capacitance of the fluidic circuit
E	Young's modulus
E_m	Elastic modulus
f	Frequency of input
g	Gravity acceleration
h	Thickness of the membrane
$I(t)$	Current at time t
j	Imaginary number
K	Bulk modulus
K_m	Geometric index of fluidic capacitor
L	Length of pipe
P	Pressure
Δp	Pressure difference
P_0	Pressure when the capacitor is fully charged
P_c	Pressure of MSS at steady state
P_{c0}	Pressure of node 0 at steady state

$P_{ci}(t)$	Pressure at node i
P_f	Pressure of fluid
P_{in}	Inlet pressure
P_{head}	Water head pressure
P_r	Poisson's ratio.
Q	Volumetric flow rate
Q_0	Flow rate caused by the water head pressure
$Q_{average}$	Average steady state flow rate
Q_e	Electronic amount
Q_{f}	Flow rate across the membrane
Q_{f1}	Volumetric flow rate at time point 1
Q_{f2}	Volumetric flow rate at time point 2
Q_H	Flow rate when the capacitor is charged with full potential energy
Q_L	Flow rate when the discharging process of the capacitor ends
Q_{max}	Average maximum flow rate
Q_{min}	Average minimum flow rate
R	Radius of pipe
R_0	Background resistance
R_A	Amplitude response ratio
R_{Af}	Ratio between the input and output signal
R_C	Resistance of fluidic capacitor
$R_{capacitor}$	Resistance of the equivalent capacitor
R_{dis}	Amplitude response ratio of displacement
R_h	Fluidic resistance
R_H	Fluidic resistance of the chamber
R_f	Fluidic resistance of the fluidic system
R_i	Resistance at node i
$R_{loading}$	Resistance of the loading pipe

R_m	Radius of membrane
R_{MSS}	Resistance of modular fluidic system
R_{ohm}	Electric resistance
$R_{overall}$	Overall resistance of the circuit
R_{pump}	Resistance of the pump
R_{system}	Resistance of fluidic system
R_{total}	Total resistance of the fluidic circuit
s	Imaginary number
t	Time
T_0	Time when the fluidic capacitor started discharging
u	Velocity of fluid
v	Viscosity
V_0	Total circuit voltage
V_f	Fluid volume
V_m	Volume of fluidic chamber
w	Width of the membrane
μ	Dynamic viscosity
ρ	Density
σ	Deflection of membrane
σ_d	Displacement of the device
σ_o	Oscillation of the device
τ	RC constant
ω	Angular velocity
∇	Laplace operator

CHAPTER 1 INTRODUCTION

1.1 Introduction

This thesis presents my PhD work about a new flow control solution based on a Lego-like modular stabiliser system. By studying fluidic stabilisers in a systematic way using membrane deflection features of the stabiliser and the digital circuit analogy, a novel plug-and-play stabiliser system with adjustable and predictable working curve for typical microfluidic systems is offered. In this study, how to design and fabricate discrete pluggable modular stabiliser devices which looks like a Lego toy is discussed. In the experimental part, the characteristics of each device are tested. How the input frequencies, the oscillation, and levels of stabilisers influence the working curve of the Lego-like system are provided. Then, the simplified RC circuit model borrowed from digital circuit analogy is studied to improve the predictability of this modular system. The system response with different working states for providing a range of RC constants in a discrete manner is studied by using the model. With a more accurate model established to explain the working curve, the system can be used to improve the universality of different situations which require an adjustable flow-control solution. In addition, experiments about how the system can improve the behaviour of typical unsteady flow sources are discussed. A typical droplet generation experiment is studied and provides a

diameter distribution with 40% less standard deviation.

This chapter serves as an introduction. Section 1.2 introduces the study's background and motivation. Section 1.3 demonstrates the aim and objectives of the research. Section 1.4 contains the outline of the thesis.

1.2 Background and motivation

Flow control solutions[1] based on microfluidic stabilisers[2] and their design process have provided a steady flow input for a number of applications during the past few decades[2, 3]. Illustrated in Fig. 1-1, a typical flow control system includes the pump, the functional microfluidic device, the sensor and the computer for data collecting. To fit customised flow-control requirements for different applications, researchers have established different kinds of flow stabilising systems[4-6]. However, even with the establishment of these different systems, the fluctuation of the flow signals and the system’s background vibration continues to affect the performance of microfluidic chips[7]. Further improvements about the flow control performance inside the microfluidic chips with a more standardised solution are required.

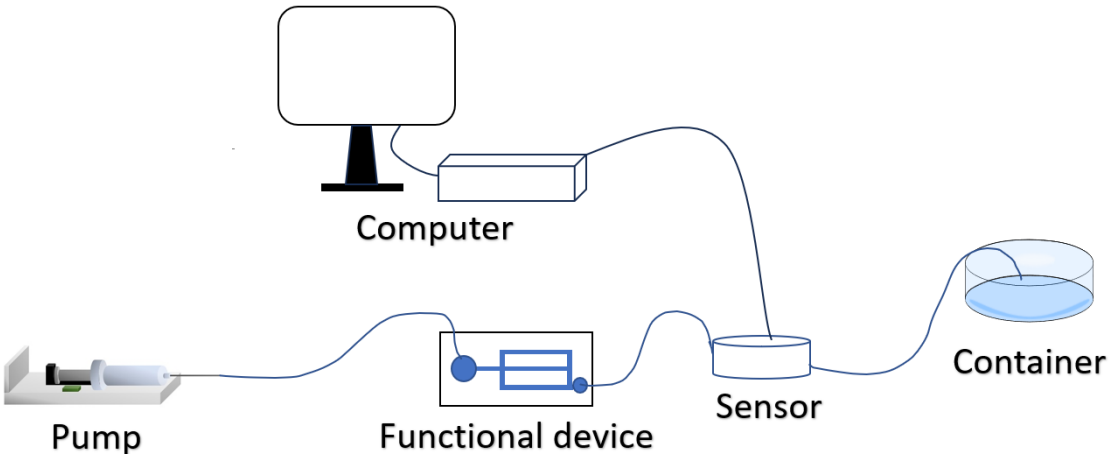

Fig. 1-1 Illustration of typical flow control system.

Besides, with the expansion of the requirement for microfluidic chips working with different flow conditions[3, 8, 9], stabilisation solutions designed for a specific condition have limited the universality of microfluidic systems. For example, a stabiliser designed for a hand-powered injector[6] may not be suitable for a piezoelectric pump because the size of the devices, the flow rate, the input frequency, and the output curve vary in different microfluidic systems[10, 11]. To fit different working conditions and enlarge the working range of microfluidic stabilisers[12], how to establish a more generalised system with adjustable features and the standardised devices which can work in different situations has become crucial.

Additionally, to provide an easier and low-cost way to design microfluidic devices[13], the fabrication process of the microfluidic system should be improved. The typical way of fabricating microfluidic devices usually includes photolithography[14], injection modelling[15], etching, and polyd-

imethylsiloxane (PDMS) reversed moulding[16]. The verification of fabrication iteration is both time and resource costly. Rather than a traditional fabricating method, 3D printing[12, 17, 18] enables the rapid fabrication of modular devices at a lower cost and with less difficulty than conventional injection modelling fabrication or soft-lithography[19-21], hence simplifying the design iterations for fabrication. However, even though the research about 3D printed microfluidic devices has been rapidly developed[22, 23], the research for a 3D printed modular fluid stabiliser system still remains at the beginning stage[18, 24]. How to take advantages of novel flexible materials[25, 26] and the development of 3D printing to give better performance and have simpler design iterations for stabiliser systems needs to be studied further.

Moreover, a simplified mathematical model which can describe the flow stabilising characteristics of stabilisers is in demand. Models borrowed from digital circuit analogy[27, 28] need to be considered in describing the flow characteristic of stabiliser systems. Researchers have been studying the topic of signals inside microfluidic devices and have established different models[1, 7, 29, 30] to describe a microfluidic system. However, a successful combination of theory and application for all microfluidic stabiliser systems still remains unsolved. An accurate model which can describe all microfluidic stabiliser systems is required for a more precise flow control process. For example, the modulation's nature of the fluidic circuit and microfluidic

stabilisers has not been adequately examined[31, 32], making it hard to forecast the behaviour of the microfluidic stabiliser throughout the design process. To obtain the accurate functioning curve of stabilisers, researchers must often examine the behaviour of a certain fluidic device through extra experimentation after constructing the prototype to get the response of each situation[33-35]. Thus, a simplified model that can describe the working curve of all stabiliser systems needs to be improved to provide a more accurate description for the flow stabilising process.

1.3 Aims and objectives

In this work, the universality and compatibility of microfluidic systems is improved by establishing a more generalised microfluidic stabiliser system with enlarged working curves and a simplified prediction model. The pluggable microfluidic stabiliser system can provide further solutions to fill the gaps mentioned in the background. The overall aim is to provide a novel flow stabilising solution for microfluidic systems with a controllable fluctuation reduction ability to give precise fluid control for multiple applications. The objectives of the study are listed below.

1. Establish combined 3D-printed stabilisers to reduce the oscillation error in a rapid and low-cost way. The microfluidic stabiliser should have a variable operating curve in the frequency domain to reduce the

oscillation error of microfluidic systems. Besides, the stabilisation ratio should reach the best stabilised flow in previous literature.

2. Analyse the characteristic of each device and study the physical principles behinds. Study how the geometry characteristic of the stabiliser membrane influences the amplitude response.

3. Establish a pluggable modular stabiliser system (MSS) with an adjustable RC constant to fit different working conditions. The MSS needs to be controllable with multi-working stages to satisfy different amplitude modulation requirements.

4. Analyse the MSS by studying the physical nature, the displacements and the stabilisation ratio of the MSS. Establish and verify a simplified fluidic circuit to give more adequately predicted working curves. A simplified circuit model describing the working curve should be established by studying the relationship between oscillation and stabilisation ratio.

5. Illustrate how to benefit from the new MSS system and simplified analysing method. How to get better performance by using the MSS in microfluidic systems should be proved. How to get better fluctuation reduction performance by benefiting from the new MSS system and the simplified analysis method should be discussed.

1.4 Thesis outline

The thesis includes seven chapters, Chapter 1 is an introduction to present the motivation and background of the study. The Aims and objectives are listed in Section 1.3. Then the outline as an overview of the thesis is given here.

Chapter 2 is a literature review. In this chapter, what is microfluidic stabiliser; the development of the microfluidic stabiliser; the research about digital circuit analogy used in fluidic circuits and how 3D printing influenced microfluidic devices are reviewed by time line.

Chapter 3 introduces the theory used to describe a microfluidic system, including the working principles of a fluidic capacitor, a fluidic resistor, a fluidic stabiliser and the membrane theory.

Chapter 4 presents the design and analysis of the 3D-printed modular fluidic stabilisers. The characteristics of the fluidic stabiliser such as the stabilisation ratios, the RC constants and the membrane's oscillation are studied, helping the model validation process.

Chapter 5 presents the assembled 3D printed Lego-like modular microfluidic stabilisers, focusing on their characteristics across various working states. A simplified circuit model is introduced and analysed, providing a basis for model validation through empirical data comparison with theoretical

predictions. This approach ensures the accuracy of the model and supports the development of effective stabilisation systems.

Chapter 6 presents the experiments and discussion about how to benefit from the stabiliser system. To take advantage of the fluctuation reduction ability of the MSS, droplet generation experiments with reduced polydispersity were analysed as an example of microfluidic applications to highlight the system's contribution to fluctuation reduction in flow control situations.

Chapter 7 includes a summary of the thesis and introduces the future works. It discussed the conclusions derived from the study and some options about future research in this fields.

CHAPTER 2 LITERATURE REVIEW

2.1 Introduction

This chapter reviews the development of microfluidic stabilisers, the circuit analogy used in studying microfluidic circuits and the 3D printing technology in microfluidic devices. Section 2.2 talks about the definition of a microfluidic stabiliser and why the stabiliser is important in the field of microfluidic systems. While Section 2.3 summarises some of the gaps which have limited the development of microfluidic systems. In Section 2.4 an overview of typical fluidic stabilisers is presented. Section 2.5 discusses how the digital circuit analogy helped to develop theories which describe the microfluidic circuit in a predictable way. Section 2.6 reviews the development of 3D-printed microfluids and gives a brief introduction about how to take advantage of 3D printing in the design and fabrication of microfluidic devices. Finally, Section 2.7 summarises the whole review.

2.2 Introduction to the microfluidic stabiliser and microfluidic system

A microfluidic stabiliser is an essential device designed to regulate fluid flow within microfluidic channels or circuits[5]. It is a key component in microfluidic systems because precise control over signals and flow rates is paramount for

the successful operation of various microfluidic applications[19, 27, 36]. To address this need, researchers have engineered a variety of microfluidic stabiliser structures[37, 38] aimed at delivering a consistent and controllable flow to the active functional components integrated within microfluidic chips. With the growing demand for microfluidic systems, microfluidic stabilisers with a better flow control-ability have become crucial[29]. To delve deeper into the subject of fluidic stabiliser systems, it is beneficial to first establish a foundational understanding of a typical microfluidic system and the evolving significance of stabilisers in the field of microfluidic technology.

The microfluidic system, usually called lab-on-a-chip system[37], includes a series of devices designed to process or control small amounts of liquid or particles under specific conditions[11, 39].Typically, the microfluidic chip system consists of the chip itself as well as a driven source to provide fluid flow or other input signals to active functional components, sensors for monitoring variables, and a computer for modifying or analysing the output of the experimental procedure. Structures inside the chips usually include microchannels and other functional components with dimensions ranging from tens to hundreds of micro-metres[19], for example, microvalves[40], micropumps[33], and micromixers[22] have been designed by various researchers to achieve specific tasks.

According to the data from the Web of Science, publications containing the

terms "microfluidic," "microfluid," or "fluidic" and "chip" increased from 1 to 2 papers per year to over thousands of publications per year from the 1980s to the 2020s (Fig. 2-1). It can be clearly seen that the utilisation of microfluidic chips has gained popularity according to the growth of the number of publications. In particular, the applications of microfluidic systems have expanded to encompass a wide range of fields, such as biological engineering[41], optical analysis[42], and electro-engineering[12].

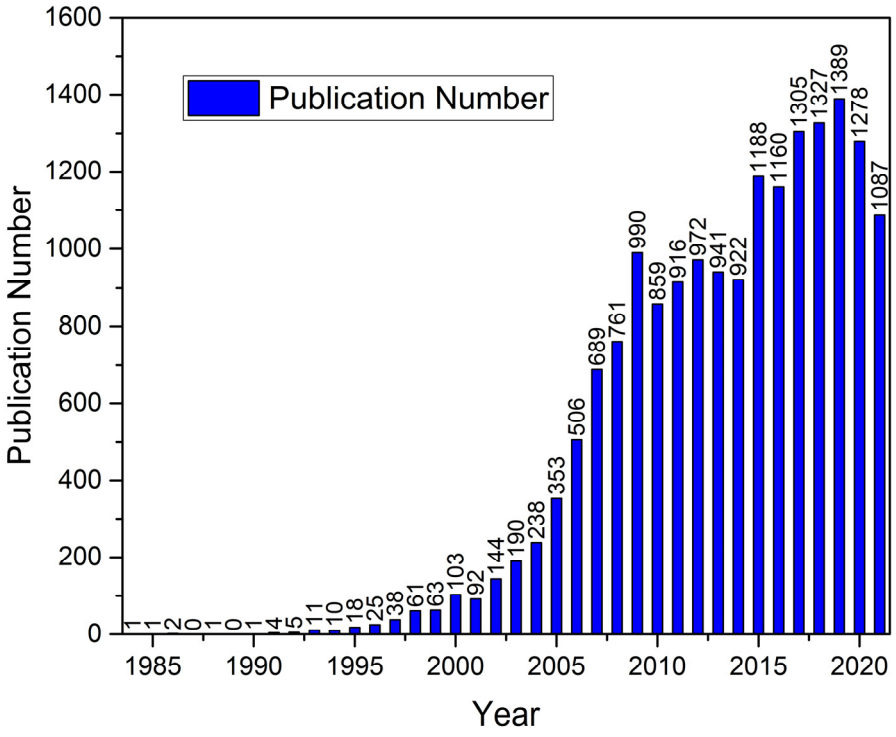

Fig. 2-1 Publication numbers in each year including the key words “microfluidic” or “microfluid” or “fluidic” and “chip”, data recorded from the Web of Science.

At the same time, the versatility in various applications made the demand for accurately controlled microfluidic devices expand. A growing number of researchers have started to use multiple types of microfluidic chips which requires more accurate flow control solutions in various applications. However,

the flow inside the microfluidic chips, often occurs with unpredictable fluctuations, is limiting the portability and broader application of these systems. In other words, the flow stability has direct effects on the expected functional performance in a wide range of application. For example, accurate flow control units are required in microfluidic applications such as drug delivery[19, 43], droplet generation[4, 44, 45], concentration separation[27], chemical mixing[3, 23], soft robots[46-48], and signal fitting [28, 35, 49]. But a common solution for steady flow control still remains unsolved. The fluctuation of different pumping systems needs to be controlled precisely by stabilisers. Thus, with the development of microfluidic systems, microfluidic stabiliser systems start to play an important role in microfluidics. By reducing fluctuations inside the microfluidic chips, stabilisers allows researchers to use microfluidic chip technology in applications which requires precise flow control, such as cell manipulation[32], controlled drug delivery[43] and particle synthesis[50]. In summary, the development of microfluidic stabiliser systems provides a more stable and controllable flow control solution for lab-on-a-chip applications[7, 51]. Stabilisers have started to help researchers maintain a steady and uniform flow in microfluidic chip systems, reducing variability and increasing the accuracy and reliability of experimental results[2, 49, 52].

2.3 Limitations of microfluidic chips

Microfluidic chips have become an increasingly popular platform for various lab-on-a-chip applications due to their ability to perform complex, analytical processes in a compact and efficient manner. In Fig. 2-2, typical applications of lab-on-a-chip systems are illustrated. However, the limitations of the flow-control process inside the microfluidic chips are still hindering the progress of becoming a "lab inside a chip" and making a lot of chips only work inside a laboratory[3, 11, 29, 53]. For example, some of the microfluidic chips lack consistency, portability[3, 42, 54] and predictability[55-57] for steady functional responses. Typically, to gain a steady performance, the chips must be connected to external equipment such as gas pumps with complex controllers, detecting sensors, computers, and wires in order to perform their function correctly inside a laboratory.

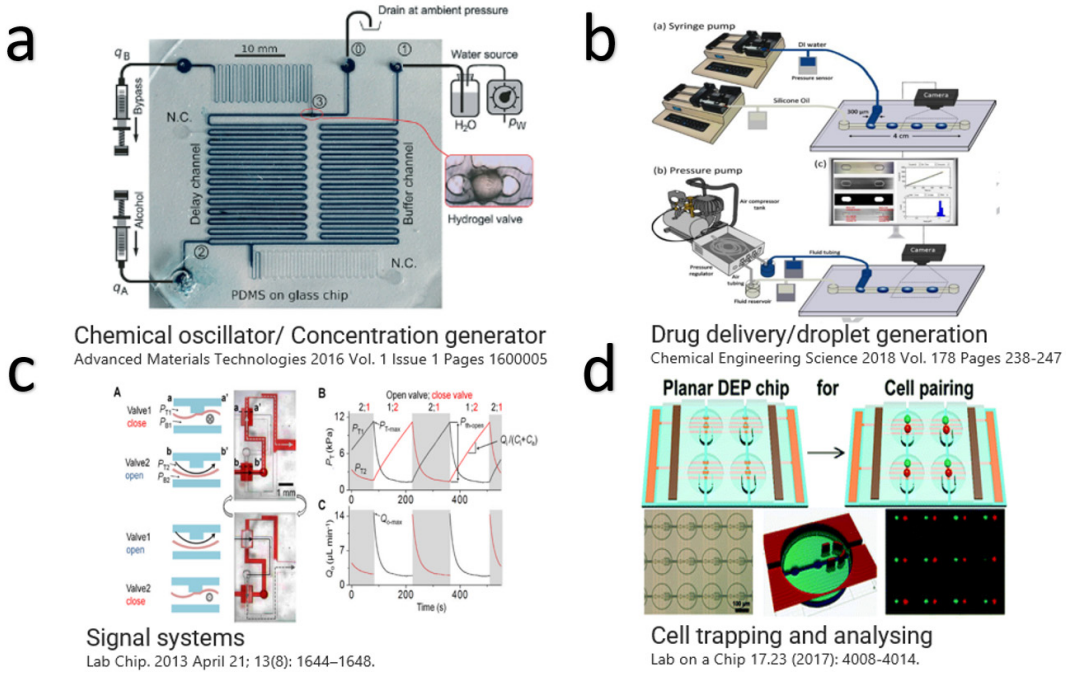

Fig. 2-2 Illustration of typical microfluidic devices and applications: (a) chemical oscillator system[58]; (b) microfluidic drug delivery system[52]; (c) a signal system on microfluidic chip[59]; (d) microfluidic cell trapping system[60].

In general, the limitation which slows down the improvement of mobility, predictability and universality of microfluidic chips is mainly caused by the unsteady and unpredictable fluctuation of flow inside the chip. In Fig. 2-3, limitations of Lab-on-a-chip system are exhibited. The limitations can be discussed as following:

a

Flow control

b

Bulky and expensive power sources

Fluctuations of inside fluid

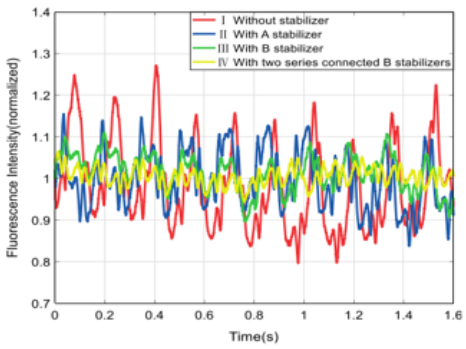

MICROFLUIDICS AND NANOFLUIDICS 2019 Vol. 23 Issue 2

c

Design & Fabrication

d

Complex design iterations and fabrication methods

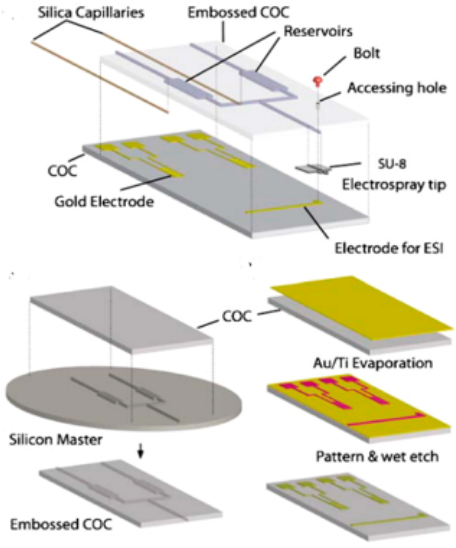

Chemical reviews 2013 Vol. 113 Issue 4 Pages 2550-2583

Lack of Universality

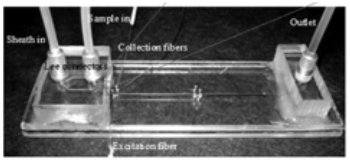

JOURNAL OF FLUIDS ENGINEERING-TRANSACTIONS OF THE ASME 2012 Vol. 134 Issue 11

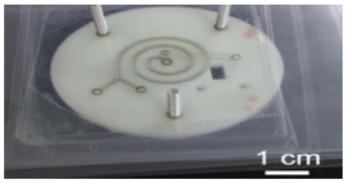

BIOSENSORS-BASEL 2022 Vol. 12 Issue 1

Fig. 2-3 Limitations of lab-on-a-chip systems; (a) bulky power sources; (b) fluctuation and low accuracy flow control inside the chip(reproduced with permission of springer-Verlag GmbH Germany[50]); (c) complex fabrication iterations[3]; (d) devices with different connectors which lack universality and standardisation[6, 8].

First, there is the influence of unsteady input signals; for instance, chips are usually connected to a pump with a huge volume, low stability, and unpredictable output flow[61, 62] as shown in Fig. 2-3(a) and (b). Various power sources such as gas pumps, syringe pumps, piezoelectric pumps, and even hand-powered injectors are used, particularly in cases where working pressure, flow rate, and viscosity are different[6, 63]. Given the sensitivity of microfluidic chips to minute alterations in flow rate or pressure, it follows that the experimental outcomes of passive microfluidic chips are significantly influenced by the stability of the input flow. Under such circumstances, researchers are compelled to seek a real-time flow control solution for ascertaining the system's status. Typically, different pressures and flow rates supplied to microfluidic chips change in different applications with various frequencies[42, 64-66]. Due to the compressibility of air inside the tube and the inaccuracy of the pump, the output oscillation ranges over a wide span from 5 to 50 percent[6, 7, 63, 67], an example of unsteady flow is given in Fig. 2-3(b). To avoid the influence of unsteady input signals in microfluidic systems, it is necessary to develop a kind of device which can assist researchers in determining the state of the system in real-time, and to optimise the flow control mechanism to minimise the influence of unsteady input signals.

Second, the fabrication of lab-on-a-chip devices should be carried out in a more cost-effective and rapid manner. The fabricating process limits the potential for simplified low-cost design iterations. The traditional fabrication process of microfluidic devices usually contains photolithography[54], modelling[12], etching and gluing[16, 19], which is time-consuming and costly[42] just as illustrated in Fig. 2-3(c). For example, to create microscale structures, Si-based channels or polydimethylsiloxane (PDMS) tunnel modelling templates[7] are commonly utilised, which require chemical etching[29], e-beam writing[31], or lifting off[68] to generate a smooth and flat surface with a precise height and width[54]. On the other hand, as given in Fig. 2-3(d), different microfluidic devises lack a standardised design and an efficient connecting structure, different researchers use various outside designs for their microfluidic chips and thus a combination of different lab-on-a-chip systems is nearly impossible. In other words, the time and cost involved make it almost impossible to build a large number of demo chips in a short time. And the iterative improvement of the chip will be limited.

Furthermore, the predictive model that explains the nature of the behaviours between the input and output of the fluidic circuit needs further development. Researchers use membrane theory to describe nonlinear systems with complex physical explanations[5, 30, 32] because most of the stabilisers contains flexible membranes. Researchers have established different models

such as fluidic low pass filters[7] and fluidic RC circuits[34] to explain the relationship between input and output signals. But a specific model that works for most of the stabilisers to obtain a more accurate operating curve has still not been developed[69-72] because the theories are usually used to explain the systematic response of a microfluidic circuit. The error between theory and experimental data remains over 10%[26, 73]. Developing a suitable model for the design process of stabilisers can simplify their design procedure, improving the predictability of flow inside all the microfluidic chips. In summary, the progression of microfluidic chip technology necessitates the following modifications to address existing gaps:

1. For a more accurate flow control unit inside functional devices, the microfluidic chips require a steadier and more controllable flow control method with less fluctuation.

2. The fabrication of the chip can be replaced with a low-cost method to reduce the cost of trial and error during the design process. Researchers can focus on the functional characteristics rather than the fabrication by using a simplified design technology.

3. The design of connectors between different microfluidic chips and devices needs to be improved to make microfluidic systems standardised and more universal.

4. The model used to describe the flow stabilising process between the input and output signals still needs to be improved, developing a more simplified model is required.

2.4 Microfluidic stabilisers

2.4.1 Introduction to the microfluidic stabiliser

After discussing the importance of microfluidic stabilisers and why a modular low-cost stabiliser with a predictable model should be established, the development of stabilisers should be examined. Before the modern microfluidic stabilisers were established, researchers used flow regulators to provide a steady flow for applications such as drug delivery process[74]. Similar to the regulator, a microfluidic stabiliser is a kind of device designed to improve the stability and universality of microfluidic systems[7]. Researchers have been working on designing different types of stabilisers[7, 32, 50, 65, 67, 75-80] to adjust the amplitude features[9, 10, 33, 64, 81-86] of the microfluidic circuits. Basically, there are two types of stabilisers working with different principles. One kind works with flexible membranes to control the unsteady flow[2, 5]. The other kind is based on air chambers or bubbles[50]. Both of these stabilisers can be designed as single-stage or multistage stabilisers. With different numbers of stabiliser chambers, the stabilisers can provide different stabilisation ratios. To illustrate typical stabilisers, Fig. 2-4 shows the

working states of the typical stabilisers.

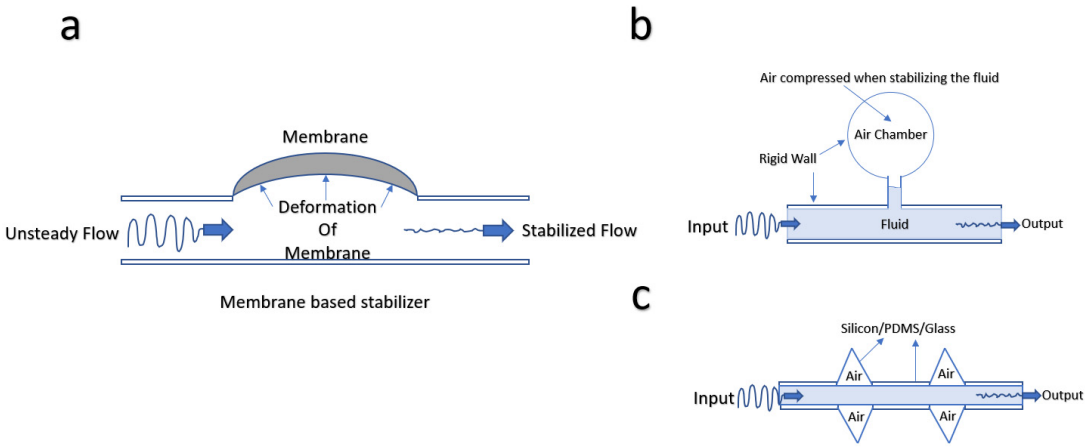

Fig. 2-4 Illustration of typical stabilisers: (a) typical membrane-based flow stabiliser at working state[87]; (b) working state of air chamber flow stabiliser[50]; (c) working state of gas damper stabiliser[67].

2.4.2 Membrane-based stabilisers

Membrane-based microfluidic stabilisers take advantage of a flexible membrane to store and control the passive flow inside microfluidic systems. Illustrated in Fig. 2-4(a), a typical membrane-based stabiliser contains a flexible membrane and a fluid chamber for passive flow. The deformation of the membrane absorbs the extra kinetic energy of the passing unsteady flow and reduces actuation of the input. The number of flexible chambers also influences the stabilisation ratio. In 2005, B. Yang and Q. Lin first identified the membrane based microfluidic device that is now known as the microfluidic stabiliser[2] as shown in Fig. 2-5(a). In their paper, the stabiliser for a microfluidic system is defined as a device with single or multi-compliant PDMS membranes that can passively reduce the oscillation for microfluidic

systems which require a constant flow rate. Their PDMS stabiliser works for typical syringe pumps with sine wave input working at a frequency of 2.5 Hz. The average flow rate of the stabilised flow is 50 μl/min with an amplitude of 20 μl[2]. To identify the input and output oscillations of the stabiliser, stabilisation ratio is calculated by dividing the oscillation of output by the oscillation of input. The stabilisation ratio is used to identify the stabilisation ability of stabilisers in the following publications to make a comparison between different researches. As the first reported membrane-based stabiliser, it has a stabilisation ratio ranging from 20% to 5%[2] for various input scenarios without a static model explanation. The stabilisation ratio of first stabiliser is quite low when today's stabilisers can provide a stabilisation ratio less than 2.5%[7]. In 2009, additional work about membrane-based stabilisers pointed out that, by establishing a lumped parameter model for analysing the dynamic performance of stabilisers[5], stabilisation ratios can be predicted. The lumped parameter model shown in Fig. 2-5(b) couples the fluid flow with vibration of membranes for the first time, by using mathematical induction, the relationship between stabilisation ratio and fluidic amplitude is described. But the error between the theory and experimental data ranges from 11.4% to 19.8% as shown in Fig. 2-5(c), which can be improved for a more precise explanation.

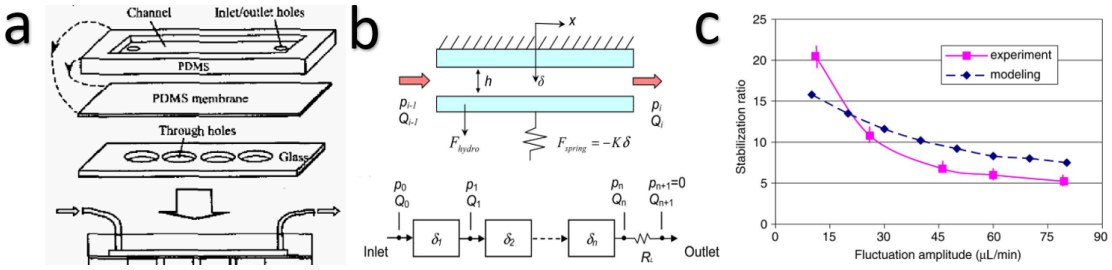

Fig. 2-5 Typical membrane-based stabiliser and its physical model: (a) PDMS stabiliser[2]; (b) mechanism of membrane-based stabiliser[5](reproduced with permission,#© 2009, IEEE); (c) compare between modelling and experimental data[5](reproduced with permission,#© 2009, IEEE).

After inventing the stabiliser, how to minimise the volume and cost of stabilisers became important. To reduce the cost of flow suppliers and provide a solution for experiments under primitive, resource-poor conditions, researchers established simpler stabiliser systems such as hand-powered fluidic stabiliser[63] which is exhibited in Fig. 2-6(a). A typical working curve for hand-powered stabiliser is shown in Fig. 2-6(b). By using different PDMS membranes with diameters ranging from 200 μm to 800 μm, the fluctuation ratio is reported to be smaller than 6% for hand-powered injections[63]. But the working conditions of such a kind of stabiliser are limited. The suitable flow rate is smaller than 1.5 ml/min, the minimum deviation of the stabiliser could reach 1.81% of the original fluctuation only under a 50 kPa threshold condition[63]. By replacing the syringe pump in a sample injection, hand-powered injectors obviously provide greater mobility for microfluidic chips with smaller volume. By reducing the cost of stabilisers, “lab on a chip” drug delivery devices work without passive flow pumps and enlarge the working

situations of stabilisers. But the hand-powered stabiliser is still limited by its working situation. Due to the unchangeable chamber inside the stabiliser, it can only work at a limited flow rate ranging from 1.2 to 2.5 ml/min without exchangeable working curves for different situations[6, 7, 63]. As a result, stabilisers with enlarged working range and better stabilisation ratio are required.

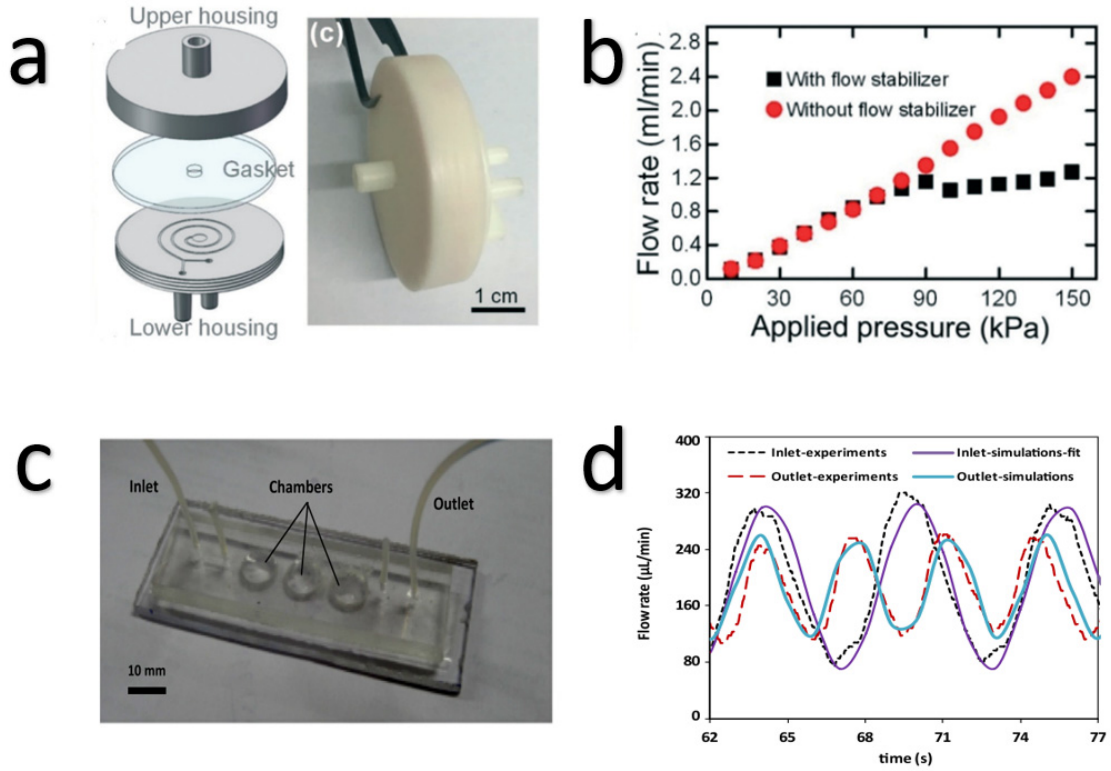

Fig. 2-6 Exhibition of hand-powered stabiliser and multi-chamber stabiliser: (a) example of single-chamber hand-powered stabiliser[6]; (b) working curve of hand-powered stabiliser[63]; (c) multi-chamber PDMS stabiliser[73]; (d) working curve of multi-chamber PDMS stabiliser[32].

With the growth of demand for a steady flow, stabilisers with a bigger stabilisation ratio and a predictable numerical working curve are required. To provide smaller oscillation, researchers start to use multi-chamber stabilisers

to enhance the stabilisation ratio. A typical multi-chamber stabiliser is illustrated in Fig. 2-6(c). Stabilisers with multi-chambers could provide larger stabilisation ratio when compared with single stage stabilisers[73]. In 2015, a multi-chamber PDMS-made fluidic stabiliser designed on Ansys fluent simulation iterations are mentioned[73]. In their work, with solving continuity and momentum equations, their predictive model leads to a 10% error between experimental data and simulation results, which is better than previous publications[2,7]. Comparing Fig. 2-5(c) and Fig. 2-6(d), it is noticed that the degree of fitting in Fig. 2-6(d) is improved by using the Ansys coupling solver. In their work, a 2 mm height PDMS chamber with PMMA (Polymethyl methacrylate) substrate covered by a 150 μm membrane with a diameter of 4 mm was used for forming each flexible chamber[73]. By studying the attenuation factor of the flow rate of both single-stage stabilisers with one chamber and multi-stage stabilisers with two or three chambers, researchers point out that a non-linear increase of the stabilisation ratio can be observed by increasing the number of chambers[73]. The single-stage stabiliser showed a 0.27 attenuation factor, while the three-stage stabiliser showed a 0.05 attenuation factor[73]. With smaller attenuation factor, the new design performed better. By summarising their work, it can be noticed that the chamber size and the membrane thickness can influence the stabilisation ratio. The results highlight that for PDMS-based stabilisers, series connected

stabilisers provide a larger amplitude adjusting range. However, to improve the predictability and enlarge the stabilisation ratio of microfluidic stabiliser based on this conclusion, the geometric feature of the flexible chamber needs to be further studied. How the thickness and volume of the chamber will influence stabilisers' stabilisation ratios should be studied in more detail. Additionally, the phase shift phenomenon observed between the output and input was not explained clearly during this stage of research, making it critical to provide a more precise predictive working curve for stabiliser systems.

The membrane-based stabiliser is not limited to the flow and pressure reducing process, the feature of reducing the input flow could give solutions for the signal stabilising process in microfluidic applications. For example, by taking advantage of membrane fluidic stabilisers, in 2019, noise reduction inside wearable microfluidic sensors are reported[51]. A damping sensor which can filter the noise by 9 dB is fabricated with flexible, soft and transparent material[51]. With PDMS hemispherical mechanical eye models used to give equivalent fluctuation of human eyes, the sensor is filled with different liquids such as water and oil to store the energy of deflection caused by lens based intraocular pressure (IOP) [51]. Rather than using a complex physical model, by building a hydraulic resistance and capacitance model for the noise reducer, the sensor is numerically studied by a typical electrical equivalent RC circuit. By controlling the time constant of the sensor, the

suppressed behaviour of the sensor changed from 7.8 dB to 9 dB[51]. The results point out that with a model equivalent to an electric circuit, the signal to noise ratio of fluidic stabilisers can be predicted more accurately. However, how the membrane's physical features influence the signal-to-noise ratio is not mentioned in the study. And the electric model is only suitable for this specific PDMS sensor.

By summarising the development of the flexible-membrane-based stabilisers, three possible areas for microfluidic stabiliser to be improved could be identified. Firstly, fluidic stabilisers usually work for a specific frequency and flowrate without a precise predictive model. How to design novel microfluidic stabilisers to enlarge the working curve in both frequency domain and flow rate domain need to be studied.

Second, the lack of numerical studies about of the nature of an elastic membrane's fluctuation stabilising behaviours has limited the development of stabilisers. By summarising the papers, the stabiliser appears to provide a greater stabilisation ratio as the amplitude of flow fluctuations increases. It is speculated that the output was influenced by the spring stiffening effect of the flexible membrane. A further study about how the working curve of stabilisers changes with different amplitudes and different frequencies has become important for all microfluidic stabilisers. A study of novel and simple predictive model for all stabilisers needs to be researched. Researchers need more

knowledge about how the displacement of the membrane, the input flow rate, the pressure, and the signal phase shift will influence the stabilisation ratio of the devices. If the membrane's vibrations could be tested and coupled with the amplitude response ratio, a clear explanation of the non-linear behaviour of stabilisers could be discovered. With simple equations applied to the model of the membrane, the study of how the flexible membrane will impact the stabilisation ratio can reduce the difference between the theory and the real case.

Thirdly, the microfluidic stabilisers lack modularity to suit different working conditions. A standardised modular design and analysing method of stabiliser systems need to be established to evaluate the performance of different types of devices by the same standard.

2.4.3 Gas damper stabiliser

Rather than a stabiliser based on membranes, researchers also consider using air as the stabilising medium. As shown in Fig. 2-4(b) and Fig. 2-7(a), a fluid chamber filled with air is designed to stabilise the passive flow by taking advantage of the compressed air damper. In 2016, a gas damper[88] is introduced for portable microfluidic circuits in a low-cost manner by using SU-8 moulding and light lithography methods. The damper works as a pressure stabiliser for conditions between 1 and 100 kPa in passive microfluidic

systems. The damper is constructed with two layers of elastic membrane made by PDMS. The chamber of the damper has a 100 μm height, 500 μm width cross-section area[88]. The design was claimed to be low-cost and the mechanism behind the device can be regarded as an equivalent low pass filter consisting of a capacitor and resistor in a digital circuit. The damper was tested by two variables: the average pressure of the input and the frequency of the input. In conclusion, a low-cost pressure damper based on PDMS membranes and the equivalent capacitor behaviour of the air chamber is established by using the mechanism of compressed air. With an average flow rate error of 5.7% and 20%-10% variation of pressure at different frequencies[88], the air damper stabiliser enlarged the working range of the microfluidic stabiliser in the frequency domain. Regarding the system as an RC signal filter, the working curve of the damper stabiliser helps to study how the input influences the relative variation of the damper system.

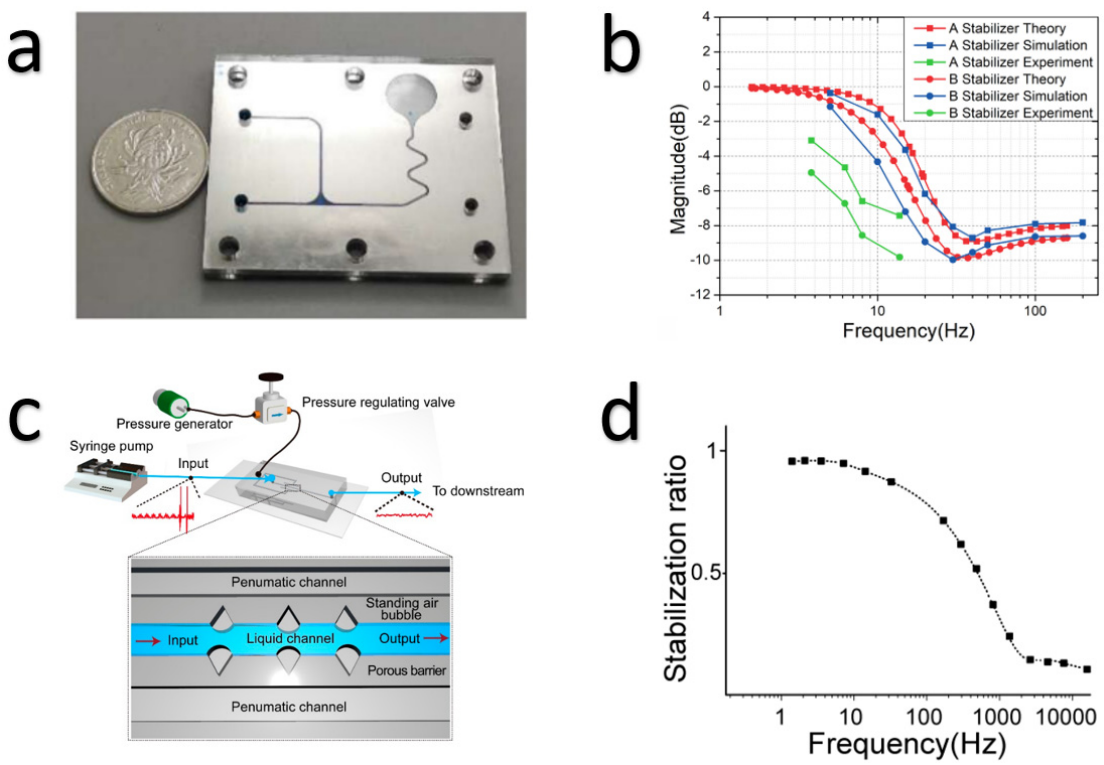

Fig. 2-7 Air damper stabilisers: (a) single-chamber air damper stabiliser (reproduced with permission of Springer-Verlag GmbH Germany[50]); (b) working curve and simulation curve of air damper stabiliser (reproduced with permission of Springer-Verlag GmbH Germany[50]); (c) air bubble stabiliser[67]; (d) working curve of the air bubble stabiliser[67].

However, even though the RC amplitude response model is used to describe a typical stabiliser system, the comparison between the experimental data with the theoretical RC circuit still remains unclear and the extraction of RC constant and amplitude response is still missing. As shown in Fig. 2-7(b), how the frequency, the amplitude response and the RC constant control the fluid inside the channels are unsolved. And the degree of fitting is limited and not numerically mentioned in previous work.

In 2019, a numerical model based on Euler laws was established to provide a link between air-based dampers and circuit model[50]. An air chamber-based

fluctuation stabiliser was developed to minimise the periodic oscillation caused by the stepper motor mechanism within the syringe pump. They reported that serially connected air-bubble stabilisers have the ability to cut the system’s amplitude response to less than 14% of the input signal[50]. Their work inspired that for both single-stage and double-stage stabilisers, the fluctuation amplitude can be defined as the output fluctuation divided by the amplitude of inlet vibration. By replacing stabilisation ratio with fluctuation amplitude, it is more intuitive to compare different stabilisers. To model the dynamic behaviours of the air-based capacitor, a Euler-equation-based description of the frequency response of the damper is provided in their study[50]. The features which are similar to an electrical equivalent band-pass-filter is mentioned in the numerical discussion to explain why the devices can only operate with frequencies higher than a limit. By studying the relationship between the output's magnitude and the frequency of the input signal, their device's operating frequency range is limited from 4 Hz to 100 Hz. The stabilisation ratio decreases from 46% to 14% as the input frequency increases from 6.2 Hz to 13.8 Hz[50]. Even though the gas damper can provide less stable flow when compared with membrane-based stabilisers, it enlarged the working range of stabilisers and provided a novel method of using air as the elastic damper for stabilisers. By summarising their work, it can be pointed out that the air damper stabiliser is potentially efficient for

different applications in microfluidic systems by changing the volume of the damping air or other actuating mediums.

As shown in Fig. 2-4(c) and Fig. 2-7(c), another kind of stabiliser based on a multiple gas damper has been designed and analysed for higher frequency conditions. In 2020, an air-bubble-based micro-hydraulic stabiliser for a syringe pump is established[67]. Tuneable micro-bubbles sized $8 \times 10^{-9} m^3$ attached to a porous barrier inside a pneumatic micro-channel formed the functional part of the damper. The shape of the bubbles attached inside the channel changed with the squeezing of the periodic unsteady flow. Because the kinetic energy of the flow transformed into potential energy of the bubble when the fluid flowed across the damper, the stability of the flow rate was increased by the damper. Without a passive power supply to drive the stabiliser, the normalised standard deviation of the stabiliser was reduced to 24.3% by three pairs of air-bubbles[67]. According to the experimental result given in the paper, the micro-hydraulic stabiliser showed equivalent characteristics to a filter with a cut-off frequency. The stabilisation ratio of the stabiliser changed from 100% to less than 13.7% when the frequency exceeded over 1000 Hz as shown in Fig. 2-7(d). However, the comparison between the established model and experimental data still remains missing. How to predict stabilising ratio at different input frequencies is uncertain.

2.4.4 Summary of microfluidic stabilisers

In summary, microfluidic stabilisers continue to have a significant impact on microfluidic systems by reducing the fluctuation inside microfluidic chips because the flow stability in microchannels has direct effects on the expected functional performance in a wide range of applications. The development of stabilisers also contributes to the acceleration of fluidic circuit research. The type of stabiliser can be distinguished by the chamber number, the working frequency, the characteristics of oscillation reducing materials, and the amplitude adjusting features. In Table 1, information about typical stabilisers is given. Table 1 and the review indicates that the development of microfluidic stabilisers exhibits numerous common conclusions as in the following:

Table 1 The summary of different types of stabilisers.

Stabiliser	Materials	Fabrication methods	Model explanation	Working situation	Best stable flow	Stabilisation ratio	Working frequency (Hz)
Bozhi Yang Group in 2005[2]	PDMS; PMMA; Glass	Spin-coating; Chemical bonding; Gluing; CNC drilling.	Hydrodynamics of the liquid film	Syringe pump	50±3 μL/min	40% to 6%	2.5
Bozhi Yang Group in 2009[5]	PDMS; PMMA; Glass	Photolithography; Gluing; Ironic bonding.	In/out pressure based $Q_{i-1}+Q_i=(h+\delta_i)^3(p_{i-1}-p_i)/6\mu$ $Q_{i-1}-Q_i=A\dot{\delta}_i$.	Syringe pump	50±1.4 μL/min	40% to 3%	2.5

Y. J. Kang and S. Yang, 2012[34]	PDMS; Glass	Clamping; Fixed plunger; Photolithography; Gluing.	Fluidic low pass filter sin wave $Q_{out}(t) = Q_{ave} + Q_{alt}\sin\left(\frac{2\pi t}{T} - \tan(\tau_f\omega)^{-1}\right)$	Syringe pump	40±3.64 mL/h	17% to 8%	$\frac{1}{140}$ to $\frac{1}{60}$
V Iyer, A Raj Group, 2015[73]	PDMS; PMMA	Spin-coating; Ionic bonding; Gluing; Photolithography; Material injection.	N/A, define stabilization ratio as $\text{Attentuation Factor (AF)} = \left(\frac{Q_{o,\max} - Q_{o,\min}}{Q_{i,\max} - Q_{i,\min}}\right)$	Syringe & Piezoelectric pump	40±4 µL/min	27% to 8%	0.2 to 0.6
Zhonghua Ni Group, 2016[88]	PDMS; SU8	Multilayer soft lithography; SU8 moulding.	low-pass filter $A = \frac{1}{\sqrt{1 + (2\pi f\tau)^2}}$	Gas pump	9.64±0.27 µL/min	35% to 2.8%	0.5 to 5
Zeheng Jiao Group, 2019[50]	Stainless steel; PMMA	CNC; Chemical etching; Laser cutting.	Pressure based stabilisation model $\eta = \frac{\Delta Q_1}{\Delta Q} = \frac{\Delta Q_1}{\Delta Q_1 + \Delta Q_2} = \frac{\rho l_2 s^2 + AR_2 + \frac{\rho_0 A}{V_0}}{\rho(l_1 + l_2)s^2 + A(R_1 + R_2)s + \frac{\rho_0 A}{V_0}}$	Syringe pump	60±4.8 µL/min	46% to 8%	3.8 to 13.8
N.Xiang, Z.Ni Group, 2019[63]	Silicon gasket; PDMS; Resin	Stereolithography; 3D printing; UV laser cutting; Spin-coating.	N/A, system error as constant Q $\left(Q = \frac{P}{R} = \frac{P + \Delta P}{R + \Delta R}\right)$	Hand-powered injector	1214±22 µL/min	7.53% to 1.81%	0.25 to 0.5
Y. Zhou, et al Group, 2020[67]	PDMS; Glass	Teflon treating; Gluing; Photolithography; Clamping.	Pressure based stabilization $\lambda = \frac{\Delta Q_1}{\Delta Q_1 + \Delta Q_2} = \frac{\frac{\rho_0 A}{V_0} - 2\rho l_2 s^2}{\rho(l_1 - 2l_2)s^2 + 2AR_1 s + \frac{\rho_0 A}{V_0}}$	Syringe pump	N/A	100% to 13.7%	Over 1000 to 10000

1. The input frequency, flow rate, and pressure all affect the devices' fluctuation ratio. Typically, as frequency increased, the performance of the stabilisers improved relative to their low frequency performance. In the future,

using power supplies with a higher working frequency may help scientists to extract the full potential of stabilisers.

2. Depending on the application, the stabilisation ratio for microfluidic stabilisers varies widely, typically from over 30% to less than 5% to accommodate the diverse requirements of different applications. As indicated in Table 1, the optimal stabilised flow is achieved within a narrower range of 1.81% to 13.7% of the average flow. Conventional stabilisers are characterised by a single operating frequency domain curve, which may not be sufficient for the complex demands of next-generation microfluidic systems. Future advancements in flow-control devices should focus on incorporating variable working curves within the frequency domain, offering a more adaptable and dynamic response rather than relying solely on a specific device with a fixed working curve.

3. The universality and modularity of stabilisers need to be enhanced as a result of the fact that all of the researchers created their stabilisers as unique fluctuation-controlling solutions for unique power sources such as gas pumps, syringe pumps, and hand-powered blowers. A novel solution for precise flow control should be studied in order to increase its adaptability to various working conditions.

4. The explanatory models outlined in Table 1 demonstrate limitations in their

adaptability. For example, using the liquid field model[2] mentioned in Table 1 necessitates the precise measurement of the membrane displacement, material thickness and pressure difference across microfluidic chambers, which is nearly impossible for air chamber stabilisers with opaque materials. Furthermore, pressure-based models continue to exhibit a discrepancy between theoretical predictions and experimental results, with errors exceeding 10%[5,50,67] while multiple pressure sensors are required for data recording, which cannot satisfy the growing demand for precise flow control.

To elucidate the dynamics of the fluctuation reduction process and minimise errors between theory and experimental data, an investigation into fluidic circuit analogies becomes imperative. Drawing parallels between digital circuit theory and microfluidic stabilisers could unveil the physical characteristics of microfluidic circuits, warranting additional study.

2.5 Digital circuit analogy in microfluidic circuits

2.5.1 Introduction

In Section 2.4, it was outlined how some of the researchers had started to use models borrowed from digital circuit analogy to explain the behaviour of microfluidic stabilisers. The numerical study of the stabilising ratio in a stabiliser system needs a comprehensive examination of the interplay between the input and output of the microfluidic circuit. Some scientists have

been trying to connect microfluidic circuits with digital circuits using analogies[1, 9, 27, 28, 51] to obtain numerical studies between fluidic signals. The application of the digital circuit analogy proves instrumental in both the design and analysis of microfluidic circuits and stabilisers. For example, a fluidic circuit model such as band-pass[37] and Ohm’s law[27] borrowed from digital circuit analogy have helped researchers to design flow control units which can investigate the relationship between the input and output of microfluidic systems[68, 89].

The analogy between digital and fluidic circuits has assisted in the prediction of fluid systems’ behaviours. One of the advantages of using digital circuit analogy is that researchers can simulate, and optimise a complex microfluidic system without extensive calculations about capillary force utilizing Poiseuille's law and Navier–Stokes equations[28, 35, 49]. The behaviour of fluid channels within a microfluidic chip can be represented with an equivalent digital circuit based on Ohm's law, Kirchhoff laws, Faraday's law, etc.

2.5.2 Fluidic resistor in circuits

The integration of hydraulic circuits with electrical circuits dates back to the early 2000s. In 2001, a microfluidic component with a linear output flow was established[90]. A linear relationship between flow rate and pressure was discovered in the research conducted at that time. The device's flow rate

increased proportionally with the driving pressure. The results suggest that the elastic PDMS channel behaves similar to a resistor in an electrical circuit[90].

Comparatively, in 2002, S. Ghosal developed a lubrication theory to describe the flow within tiny channels with elastic walls[91]. Special geometries with an expanded cross-section are characterised by nonlinear relationships between pressure and flowrate.

In 2004, Armand Ajdari and colleagues proposed the exploration of fluidic circuits using an analogy borrowed from an electric circuit[92]. In their work, extending beyond considerations of channels and materials, they highlighted that most fluidic circuits exhibit similar characteristics under low Reynolds number conditions[92]. In their experiment, the relationship between pressure difference and flow rate is linear, and all the flow pumps can be considered either a pressure source or a flow source, similar to an electric power supplier in a digital circuit.

In 2006, the idea of demonstrating a microfluidic resistor[93] is mentioned. A microchannel with a height of 50 μm and a width of 400 μm wide was fabricated using PDMS[93]. As a conclusion, the channel's height could be reduced to increase flow resistance. With the steady-state flow rate Q and driving pressure P measured at Reynolds number Re<1, the Ohmic

resistances of this apparatus are described as $R = \frac{\mathrm{dP}}{\mathrm{Q}}$[93]. With the equation, the precise calculation of flow rate and resistance in different circuits becomes possible. By fabricating a fluidic resistor and predicting the output of a typical resistance, the microfluidic resistor array[93] enables precise flow control within microfluidic chips. The discovery of the microfluidic resistor illustrated the possibility of using a simplified resistive circuit model to replace the fluidic circuit model. Inspired by their work, fluidic Ohm's law can be used to determine resistance rather than using the complex Navier–Stokes equations, which can simplify the predictive model of fluidic circuits. The comparison between the traditional elastic model and fluidic circuit Ohm's law is illustrated in Fig. 2-8. While pressure, flow rate, thickness of the membrane, geometric features of the fluidic channel are needed for elastic model in Fig. 2-8(a), the simplified electric model in Fig .2-8(b) only records the flow rate and pressure difference to predicting the behaviour of fluid.

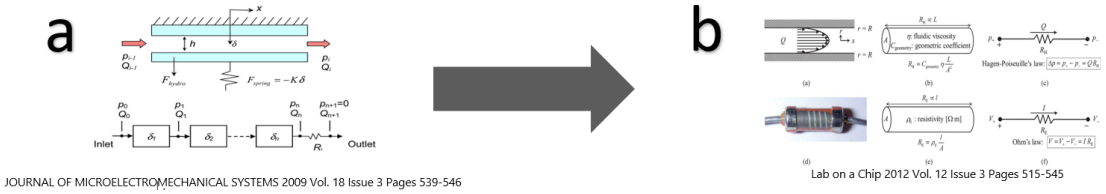

Fig. 2-8 Comparison between traditional model and fluidic circuit model: (a) elastic model using Hooke's law[5](reproduced with permission,#© 2009, IEEE); (b) fluidic circuit model based on Ohm's law[27].

With a fresh perspective on microfluidic circuits, researchers began to reconfigure the fundamental unit of microfluidic devices to resemble a unit

found in digital circuits. For example, in 2009, microfluidic gradient generators based on a dilution model were established[35]. Their findings demonstrated a linear correlation between the length of the microfluidic resistor and the circuit's resistance, equivalent to the resistance law $R_{ohm} = \frac{\rho L}{S}$[94]. According to their theory, fluctuation of mixing flows is considered in the solution equations and concentrations of each branch are calculated with the method. Their method provided a single module or arbitrary gradients[35] with a large number of modules, ranging from simple linear to sophisticated non-linear forms[35].

2.5.3 Fluidic capacitor and RC circuit

Rather than only considering fluidic resistance, fluidic circuits featuring flexible channels and chambers can be conceptualised as fluidic capacitors[30, 35]. Fluidic capacitors are defined to characterise fluidic circuits in accordance with Faraday's capacitor law. The performance of a capacitor in a digital circuit closely mirrors that of a frequency-affected fluidic circuit. For example, the compliance features of the soft tube and flexible membranes of a fluidic circuit have performed similarly to the RC constant and time response features in circuit analogy. The frequency of input, amplitude response ratio, and phase shift in fluidic circuits can be explained by the capacitor law.

In 2006, the Dongshin Kim group published a study of a dynamic fluidic

system by using a model containing a capacitor and resistor to present the behaviours of a microfluidic circuit[30]. They found that there is a rise time to start the functional devices of a fluidic circuit, which is similar to capacitance in circuit analogy[30]. Their work illustrated that calculating the flow rate through the resistance and capacitance of fluidic devices is reasonable. Studying fluidic circuits in an analogical way can simplify the calculation process. For example, the equivalent circuit In Fig. 2-9(b) can replace the complex elastic model in Fig. 2-9(a). Detailed equations about fluidic circuits are explained in Chapter 3.

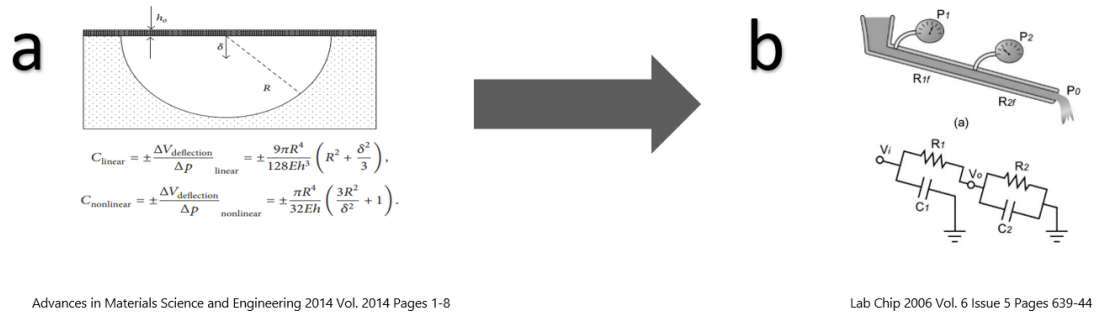

Fig. 2-9 Comparison between membrane theory and fluidic capacitor model: (a) elastic model based on membrane theory[26]; (b) fluidic circuit model based on capacitor model[30].

However, the computation of both resistance and capacitance for each device is fraught with complexity and inaccuracy due to the multitude of variables involved[26]. A more straightforward approach is to document the system's response to fluidic signals. In 2009, Daniel C. Leslie, et al[95] determined that the problem of controlling fluid movement according to complicated patterns in space and time with sufficient precision remained unsolved. To investigate the

nature of frequency-specific flow control technology in a systematic view, they utilised the passive elastomeric properties of membranes. The nature behind the behaviours of the fluidic capacitor is explained as the volume stored under the deformed film per unit of pressure. By combining the characteristics of both the resistor and the capacitor, these researchers built the first fluidic diode[95] working with a non-linear function of pressure. They highlighted that the pressure-flow interrelations are heavily contingent upon the geometrical features, which is often difficult to ascertain accurately. In summary, the researchers have underscored that the investigation of microfluidic circuits can be grounded in algorithms that are strikingly analogous to those employed in the design of electronic circuits. The concept of leveraging the systematic characteristics of a fluidic circuit to delineate the behaviour of the output is deemed efficient across all membrane-based systems. However, there remains a significant gap in the realm of accurately extracting the RC constant. The precise methodology for deriving data from circuit models necessitates further exploration and study.

2.5.4 Filter system and logic array in fluidic circuits.

A fluidic circuit system can be studied as a complicated signal system rather than independent devices. With equivalent circuit analogies and signal treatment circuits such as band filters, improving the usability and capabilities

of microfluidic technologies by standardised control methods for microfluidic circuits has become possible. Table 2 lists typical fluidic devices and their equivalent digital circuits by timeline to show how to transfer a digital circuit analogy into a fluidic circuit. Fluidic resistor, capacitor, valve, transistor, band pass and other logic gates are listed.

Table 2 Summary of typical fluidic circuit devices and modelling.

Researchers	Fluidic devices	Equivalent electric circuits	Illustration
A. Groisman Group in 2003[72]	Fluidic memory device	Resistor	Linear resistance model[72] 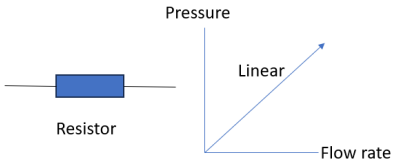
D. Kim Group in 2006[30]	Flexible chambers	Capacitor	Capacitance model[30] 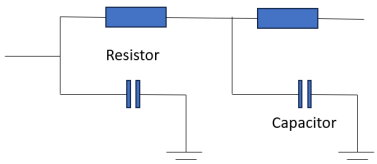
D. C. Leslie Group in 2009[35]	PDMS channels and chambers	Valve & Band pass	High-pass-filter model[35] 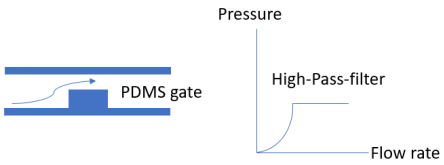
B. Mosadegh Group in 2010[28]	Flexible Chambers	Transistor & Band pass	P-channel transistor model[28] 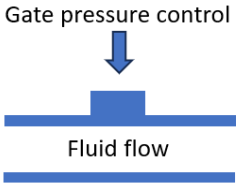

S.-J. Kim Group in 2013[59]	Valve and flexible membranes	Oscillator	Feedback circuit model[59] 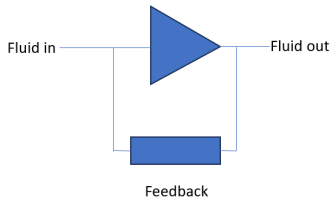
S. Tsuda Group in 2015[96]	Channels and flexible chambers	Programmed register	Flip-flop model[96] 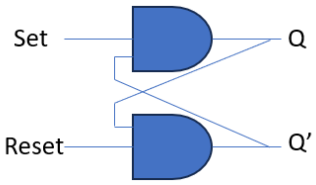
I. E. Araci Group in 2019[51]	Flexible chambers	Noise suppressor; Digital RC circuit	Circuit model[51] 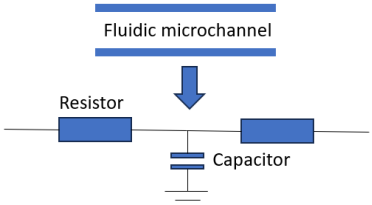
Zhou Group in 2021[100]	Flexible actuator; capacitor; resistor	Control chip with digital signals	Digital signal model[100] 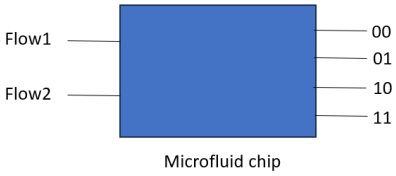

Rather than focus on single fluidic unit, in 2007, a microfluidic logic gate based on tension-based passive pumping[97] were introduced. The And/OR logic gate built via a fluidic circuit was explored since then. With a pump driving a flexible membrane, a CMOS-like gate[97] regulating the output 0/1 of a fluidic circuit was investigated[97]. With logic circuits, it is possible to design fluidic circuits with a high throughput. To enable more integrated functionality, a system consisting of fluidic logic gate-connected devices will be of interest to researchers.

With the concept of adopting solutions from logic circuits to characterise fluidic

systems, researchers began employing analogous models such as transistors and bandpass filters to analyse these systems. In 2009, flow control solutions based on passive elastomeric microfluidic chips within a frequency domain are published[35]. The research delved into the non-linear behaviours of fluidic capacitors and fluidic bandpass filters. A significant milestone is achieved by fabricating a chip containing gates and two fluidic capacitors functioning with distinct frequency features, thereby creating the first fluidic band-pass filter[35]. Their work specified a passive band ranging from 1 Hz to 10 Hz, clearly defining time constants and fluidic capacitance by borrowing principles from time constant laws and RC circuit equations in digital circuits[35]. This marked the first instance where a complex fluidic circuit could be numerically designed with an anticipated output. However, the precise delineation of the input-output relationship through the transfer function within microfluidic circuits remains an unresolved challenge. There is a notable absence of extracting features from RC circuit, for example, the transfer function and the time constants, which are fundamental for accurately modelling the system.

Not limiting in the research to resistors and capacitors, other fluidic circuits are studied numerically by borrowing analogy from digital circuits. For example, in 2010, B. Mosadegh, et al. presented their theory of autonomous regulation of sequential and oscillatory flow in microfluidic[98]. Their work presents an

integrated elastomeric component whose behaviour resembled that of a p-channel transistor[98]. As the driving signal, their experiment analyses the phase shift and time relied output of the system. By using their results, it can be noticed that by using only a transistor component, fluidic circuits are capable of implementing any circuit process.

In 2012, a fluidic low pass filter (LPF) designed by Yang Jun Kanga and Sung Yang was reported[34]. They constructed a simplified LPF with an air compliance volume ranging from 0 to 4 ml using a lumped parameter model[34]. Using fluidic resistance for an adequate preload and air compliance unit, the LPF demonstrates an RC constant between 5 s to 150 s. According to their proposed identification approach, the pulsation index[34] and RC constant of a fluidic circuit can be extracted. With the angular momentum defined within the framework, deriving the time constant from the input frequency and the differential between the input and output flow rates became a more tractable task. This methodology facilitated the computation of the system response for a specific microfluidic device. However, the RC constants exhibit a wide variability, and the correlation between these constants and the input-output dynamics of the system remains an unresolved issue.

To take advantage of fluidic circuit analogy, researchers started to use capacitors, resistors, and logic gates to create microfluidic automation

systems without the usage of huge external controllers[49]. For example, in 2015, fluidic oscillator arrays were reported[99]. The resistor-connected microfluidic oscillator array is driven by a fluid-filled container placed at a higher level than the chip. The container generates the square wave signal, which is then integrated by the array. By segregating the actuation fluid, the controller requires just 3-7 kPa, or 0.3-0.7 m of water head[99] to operate. Due to the array's reduced size restrictions, it can be utilised on a standard lab bench or other incubator set-up.

The creation of a more compact controller for microfluidic networks is fulfilling the demand for portable lab-on-a-chip devices. In 2016, researchers from the University of Washington developed an AC controller by mixing fluidic resistors, inductors, and capacitors to form RLC networks with band-pass resonance[33]. By adding inductors to an RC circuit, a band pass filter with sharper signals can operate at high frequency domain. In their work, the circuit of the controller is a tiny substrate with PDMS membrane and a piezoelectric disc. In contrast to existing actuators, which operate at a low frequency range of 10 Hz to 100 Hz, this chip can readily operate at a frequency range of 500 Hz to 1000 Hz with less space and greater mobility[33].

On the other hand, design of microfluidic circuits using the digital circuit analogy can also give an advantage in high-throughput microfluidic devices.

With the idea of a high-throughput fluidic circuit array, a multistage digital-to-analogy chip was manufactured in 2021[100]. A network of 3D-printed soft actuators connected to a modular flow control unit formed a calculator with 4-bit data storage[100]. With 16 combinations, the signal output varies from code 0000 to code 1111, which made programming with fluidic chip become possible. With the development of a fluidic calculator, electronic devices may be replaced with microfluidic processors in the future, in situations with high electric or magnetic fields.

2.5.5 Summary of digital circuit analogy in microfluidic circuits

In Section 2.5, the progression of fundamental units in fluidic circuits is reviewed through a timeline with typical fluidic circuit units visually represented in Table 2. Laws describing the behaviours of microfluidic resistors, capacitors, oscillators, inductors, logic gates, and signal systems are presented in order to accurately forecast the microfluidic circuit's output during the last 20 years. By summarising their research, one can entertain the concept that employing analytical formulas for the resistor and capacitor components of a digital circuit model in micro-channels driven by periodic inputs or pulses represents a significant stride in the formulation of predictive models. The analysing based on circuit analogy can contribute to the

advancement of analytical devices.

The study of digital circuit analogy in fluidic circuits points out that not only independent devices should be considered, but also the fluidic circuit can be studied as a whole signal system. By using RC circuit law, resistor-capacitor-inductor (RCL) circuit law and amplitude adjusting features, solutions using microfluidic controllers for common applications are now simpler and more accurate due to the new prediction methods borrowed from signal systems. The development of stabilisers and the study about the physical nature of fluidic circuit has also enhanced the universality of lab-on-a-chip systems. However, it is currently unclear how to improve the stability and mobility of various fluidic arrays. The model which can present the fluidic stabiliser system accurately is still unsolved. If a common design methodology or analysis equation can be established, a standard fabrication process for microfluidic circuits could be established.

2.6 Modular design and 3D printing in microfluidic devices

2.6.1 Introduction of the 3D printing design process

3D printing, also known as addictive manufacturing[101], has a rapid and low-cost design iteration for microfluidic fabrications[13]. It has the ability to make highly accurate and complex structures in 3D micro-fluidic chips with 20-1000

μm features[102] when compared with material injection[29, 103], laser writing[38] or lift-off moulding[29]. To design and fabricate modular stabiliser devices, 3D printing is an ideal choice. With the development of additive manufacturing, a rapid design iteration changed the recipe of microfluidic devices; this made rapidly configurable and scalable microfluidic devices became possible.

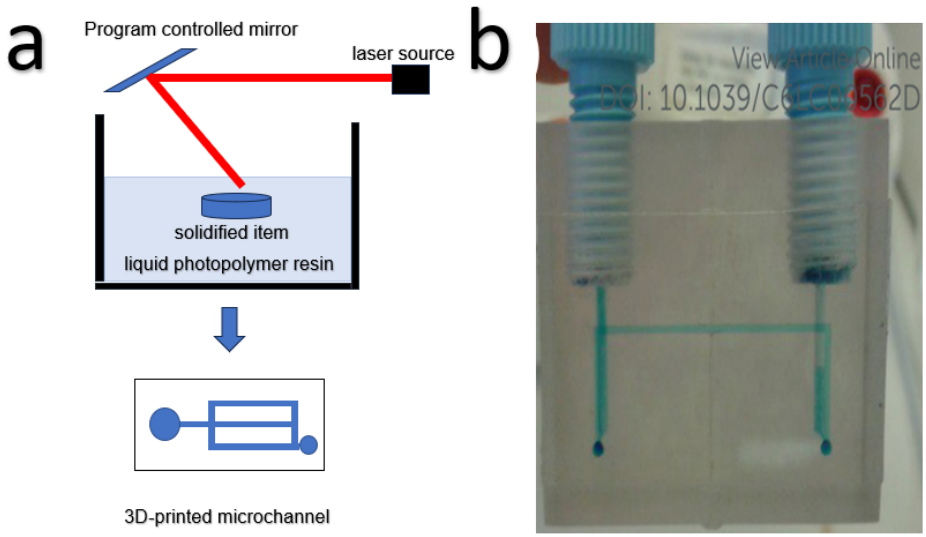

Fig. 2-10 Illustration of SLA process: (a) the SLA process by laser beam and liquid polymer[17]; (b) an example of 3D printed microfluidic channels[15].

Typical 3D printing technologies used for microfluidic applications are stereolithography (SLA)[12], fused deposition modelling (FDM)[12, 104], selective laser sintering (SLS)[41], and inkjet 3D printing[24]. Back in the 1980s, the first 3D printed item was fabricated based on SLA technology by Charles Hull[104]. As shown in Fig. 2-10(a), SLA uses a laser beam to transfer liquid materials into the solid-state layer by layer. The mirror

controlled by programming can transfer laser light into the place where material needs to be solidified. In today's applications, SLA is mostly used for resin materials[105]. The accuracy often ranges from 20 to a few hundred micro-meters[17, 106, 107]. For example, 3D printed microfluidic channels by using SLA are illustrated in Fig .2-10(b).

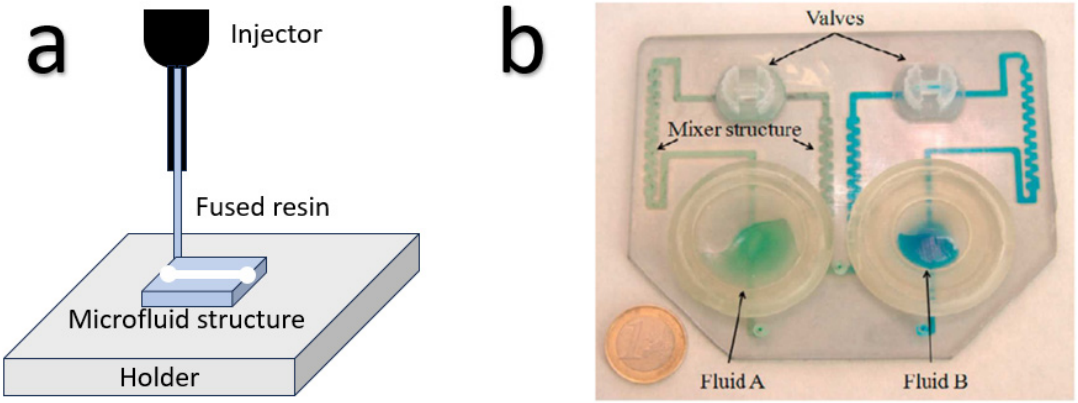

Fig. 2-11 Illustration of FDM process: (a) the FDM process by heating and squeezing polymers[12]; (b) an example of microfluidic mixer printed by FDM[18].

Meanwhile, FDM, which was reported in the late 1980s by Scott Crump[105], usually works for the 3D printing process of thermoplastic materials with an accuracy of over 100 μm nowadays[105, 108], which is rougher than SLA. By squeezing melted materials into a holder layer by layer, the FDM can fabricate polymers such as PLA (Polylactic acid) and PMMA into various microchannels as shown in Fig. 2-11(a). An example of FDM item is illustrated in Fig. 2-11(b).

Rather than FDM, SLS is similar to SLA. SLS usually works for metal powder and solid-state polymer particles with higher speed than other methods[104, 105, 109]. As illustrated in Fig. 2-12(a), by using a high-energy laser or power

source moving on slide rails, SLS can fabricate channels with materials that have a high melting point and hardness. In microfluidic fields, SLS can achieve an accuracy of around 50-100 μm[109]. When the item needs to work in high-pressure conditions or requires a glass channel, SLS will be a suitable choice. An example of metal microchannels fabricated by SLS is given in Fig. 2-12(b). However, the cost of SLS is more expensive and the multi-material ability of SLS is poor when compared with FDM and SLA[105], which limits the application scenarios. Thus, SLS is not widely used in rapid and low-cost microfluidics.

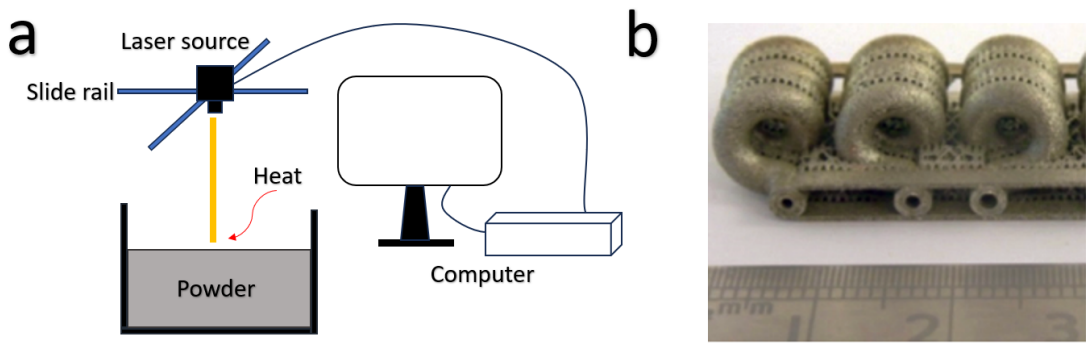

Fig. 2-12 Illustration of SLS process: (a) the SLS system at working state; (b) metal microfluidic channels printed by SLS[110].

Inkjet printing uses a microneedle or microjet to generate small droplets on the holder to form different structures. As illustrated in Fig. 2-13(a), the jet generates droplets at the right place to form designed structures and then cured by different light sources or temperatures. Inkjet printing usually uses low viscosity polymers with an accuracy of 20-500 μm[105, 110]. It is a rapid fabrication process when compared with FDM and SLS. For example, in Fig.

2-13(b), an item with 500 μm channels inside a 2x2x1 cm block could be fabricated by inkjet printing within 1 hour[111].

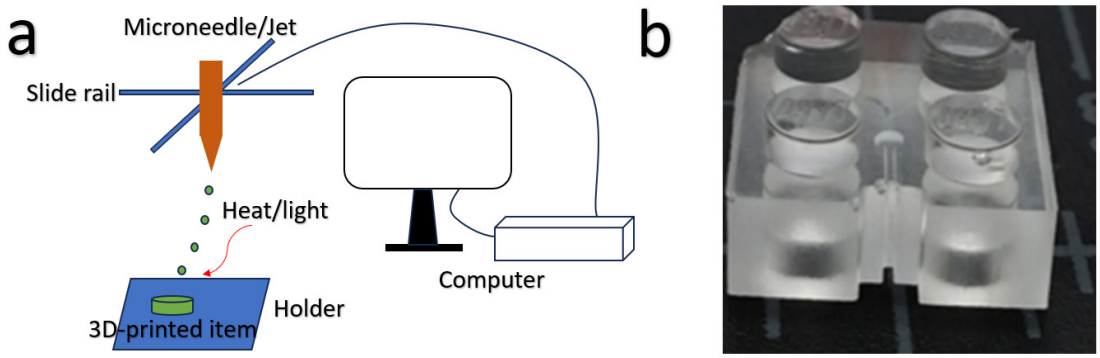

Fig. 2-13 Illustration of inkjet 3D printing: (a) the inkjet system at working state; (b) example of printed devices with microchannels[111].

In summary, 3D printing is suitable for fabricating microfluidic devices and will be a useful tool for designing modular microfluidic devices because the accuracy range of 20-1000 μm exactly fits the requirements of most of the microfluidic channels. With a rapid and low-cost design iteration, 3D printing could help researchers focus on the design of functional structures inside the microfluidic chip rather than the fabrication process, which leads to a simpler solution for modularised stabilisers.

2.6.2 3D printing in modular microfluids

As described in Section 2.4, microfluidic devices usually contain complex channels and functional structures with micro-scale characteristics, which are costly and time-consuming if fabricated by traditional methods[112]. To take advantage of 3D printing, reduce the design iterations and increase the

mobility and universality of microfluidic systems, researchers have been focusing on utilising modularly designed devices to reduce the difficulties of managing various microfluidic chips[16, 109, 113]. Table 3 listed typical 3D-printed modular microfluidic devices by timeline, detailed description is given in the following paragraphs.

Table 3 Typical 3D-printed modular microfluidic devices.

Researcher	Method	Material	Minimum feature size	Modularity
Philip J. Kitson Group 2012[21]	FDM	Polypropylene; PMDS	800 μm	No modular connector
Anthony K. Au Group in 2014[17]	SLA; Plastic moulding	PDMS; WaterShed resin	267.2 μm	No modular luer inlet; Glue bonding
K. C. Bhargava Group in 2014[23]	SLA	Polyether ether ketone	500-750 μm	Discrete components
Kevin Vittayarukskul, Abraham Phillip Lee in 2017[111]	PDMS negative impression based on 3D-printed mould	PDMS	500 μm	Discrete components

Yujin Lee Group in 2018[114]	Photoresist mould; PDMS replica moulding	PDMS	1000 μm	Modular blocks
Pojchanun Kanitthamniyom Group in 2020[113]	SLA & FDM moulding	Acrylonitrile butadiene styrene (ABS); Teflon; Polydopamine	Not mentioned	Lego-like outside

In 2012, the first modular microfluidic micro-reactors with 800 μm channels inside by 3D printing were fabricated[21]. A rapid fabrication process within four hours and a cost of only 0.5 dollars for a 3D-printed micro-reactor are reported. With low design skills required and no clean room needed, 3D printing offers a cost-effective and versatile approach to microfluidic device manufacturing[42]. For example, a simple microreactor with the same channel made by PDMS may need three fabrication processes[17]: the modelling of the motherboard of the PDMS channel; the lift-off of PDMS membranes; and the etching and combining of the substrate and the layer. As shown in Fig. 2-14, the design iterations of 3D printing and a typical micro-fabrication method are compared. 3D printing avoids complex design and analysing processes of multi-layer fabrication. Without mask fabrication and the substrate layer bounding process, 3D printed devices cost less time and money. Even though the minimum featured size is rough to 800 μm, which

has a lower resolution than photolithography, 3D-printed microchannels still provide a rapid assembling solution for microfluidic chips.

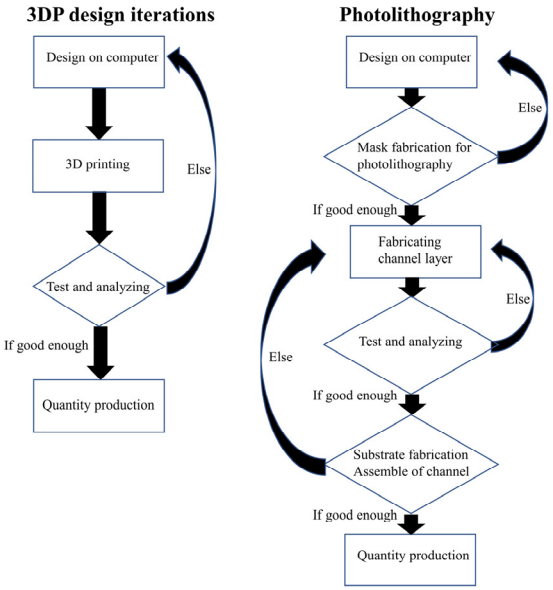

Fig. 2-14 Comparison of 3D-printed design iterations and typical photolithography design process

Besides the simplified procedure, the characteristics of materials used in the 3D printing process are exchangeable in microfluidic systems. When compared with silicon or PDMS membrane chips, 3D-printed devices are more customised. For example, PLA, PMMA, and other resins used in 3D printing have adjustable Young's modulus and different light transmittances[1, 20], which could be customised for specific cases.

To take further advantage of 3D printing for modular microfluids, in 2014, customised micro-channels and Luer-connectors[17] with high light transmittance materials were reported. In their study, a comparison of glass micro-tunnels and 3D-printed micro-tunnels points out that the 3D-printed

devices nearly give the same optical performance as the glass tunnels with fewer design iterations. This feature has made easy access to mass manufacturing in the microfluidic fields possible. On the other hand, 3D printing devices can provide acceptable optical characteristics and biocompatibility for bio-applications such as cell caption[112] or droplet generation[96].

What is more, 3D printing can accelerate the development of the modular design process for microfluidic devices. In 2014, discrete elements used for establishing a rapid assembly of 3D microfluidic systems[23] were reported. With the idea of modular assembly systems, 3D-printed microfluidic devices have the ability to be assembled within a very short time (even less than one hour) when compared with monolithic devices.

For modular devices, there is a special design called the Lego-like microfluidic devices[110]. In 2017, Kevin Vittayarukskul and Abraham Phillip Lee presented a modular microfluidic platform called a truly Lego®-like modular microfluidics platform[111]. They firstly made a 3D-printed master mould and a tin-based silicon-negative model with micro-channels for PDMS moulding. Then they used the urethane master mould to fabricate PDMS based Lego®-like devices. Some simple microfluidic channels were modified inside their Lego-like devices. Their work provides evidence that a platform resembling like a Lego toy can accelerate the experimental process with enhanced

performance. Even though the link between each unit still needs extra connectors such as O-rings or a gluing process, their work still started the expanding development in the field of modular microfluids.

To reduce the moulding process for making modular devices, Yujin Lee presented a new way to fabricate modular devices in 2018[114]. Rather than making the channels and functional parts inside the Lego-like blocks, they decided to only print the exteriors of the modular devices. Then, a 3D-printed plastic housing was inserted with optical or fluidic devices to take advantage of the quickly assembled platform. By only using the plastic outside, researchers can simply buy commercial optical or fluidic devices to assemble a modular block with 3D-printed functional microchannels. By using this design, researchers can further increase the accessibility and affordability of microfluidics technology by avoiding designing specific electronic devices inside microchannels.

In applications that do not require extremely accurate optical analysis of functional microfluidic devices such as bioanalysis[19] or gradient generators[1], a fully 3D-printed modular device without any modelling or mask fabrication process can be attractive. In 2020, Pojchanun Kanitthamniyom and his colleagues established a 3D-printed modular digital microfluidic architecture with magnetic features for on-demand bioanalysis[113]. By measuring the data off-chip and taking advantage of

computer visualisation and imaging analysis methods, a directly 3D-printed modular system provides a possible solution for rapid assay development. Their work takes a further step in simplifying the fabrication of modular microfluidic systems.

In conclusion, the inception of 3D printing within the field of microfluidic devices commenced with the production of individual devices, subsequently evolving towards the development of modular connector designs. The conceptualisation of modular devices characterised by similar shapes and connectors was subsequently introduced. Presently, the pervasive adoption of the modular design has become prevalent in contemporary design iterations, facilitating the expeditious assembly of microfluidic systems capable of operating effectively across different working conditions. Even though the minimum featured size of 3D printing is not as accurate as photolithography and the modular design still consists of extra linkers and sealing materials such as O-rings, the modular microfluidic chip still makes flexible and plug-and-play systems possible. The utilisation of 3D printing in stabiliser systems should involve the consideration of a modular design incorporating standardised linkers and outer blocks for the next generation of plug-and-play stabilisers.

2.6.3 Summary of 3D printing and modular microfluid

In Section 2.6, the development of modular microfluids, and the influence of 3D-printed microfluidic systems and devices are reviewed. Modular design makes rapid assembly of microfluidic devices possible. By using 3D printing, researchers can focus on customised functional units or characteristics rather than paying too much attention to the fabrication processes. For the idea of modular microfluids, Lego-like devices have several advantages such as a rapid assembling process and enhanced performances in a low-cost manner. But the existing modular designs still lack the ability to establish highly automated manufacturing processes with limitless degrees of reproducibility and customisability.

2.7 Summary

In this chapter, the development of microfluidic stabilisers is reviewed via the timeline of the history of research. As described in the beginning of Section 2.1, the definition of microfluidic devices is given and the three main gaps between further accurate microfluidic control solutions and today's characteristics of microfluidic devices are given in the following Sections 2.2 and 2.3. In summary, some of the microfluidic systems need mobility and stability because the unsteady flow input will influence their functional performance. Secondly, the prediction model for microfluidic systems remains

inaccurate. Thirdly, a new design and fabrication method with a simplified and low-cost solution is required for the development of microfluidic stabiliser systems to replace the complex fabrication process.

In Section 2.4, how to provide a controllable flow-control system and how to develop different kinds of stabilisers are reviewed. Basically, there are two types of typical stabilisers. For stabilisers based on flexible materials, there are single-stage and multi-stage stabilisers. By changing chamber volume and chamber numbers, the performance can be controlled. However, even the stabilisation ratio can be less than 2%, the capacity of chambers is limited at a maximum of three, and the operational frequencies are restricted to a relatively low band, with an upper limit of 10 Hz. In the case of air damper stabilisers, the performance can be enhanced to achieve operational frequencies from 100 Hz to 1000 Hz. However, the predictive model of air-damper devices exhibits a non-negligible discrepancy when compared with experimental outcomes, and the optimal stabilisation ratio of air-chamber-based stabilisers exceeds 5%, which can be further developed.

Section 2.5 reviews how to use different circuit models to describe the signals' behaviours inside microfluidic channels. To study the behaviours of microfluidic systems, scientists analysed different fluidic models in both modules and in a systematic way. Fluidic circuits were first to be studied as signal systems with the flow units as a fluidic capacitor, resistor, transistor,

and other control units. Researchers have identified simplified circuit analogies to explain the majority of the relationships between input and output signals within a microfluidic circuit. However, a specific and accurate analogy for fluidic stabilisers remains unsolved. The extraction of fluidic resistance and capacitance is difficult, and the existing equivalent circuit analogies still have significant inaccuracies that require further refinement.

Section 2.6 discussed the evolution of modular design processes and the advancement of 3D printing within microfluidic systems, focussing on how these novel manufacturing iterations influence the construction and design of microfluidic systems. In summary, 3D printing has expedited the development of microfluidic devices, enhanced their performance and reduced their cost. However, further research is required to develop 3D-printed microfluidic stabiliser systems with adjustable characteristics, unified interfaces, and modular connectors. This is particularly important in terms of developing standardised devices across different microfluidic systems and establishing a microfluidic stabiliser-specific model via digital circuit analogy that can more accurately predict the experimental outcomes during the designing process. Furthermore, the optimal stabilisation ratio needs to be improved to expand the working situations of microfluidic stabilisers.

CHAPTER 3 THEORIES ABOUT FLUIDIC CIRCUIT AND SYSTEMS

3.1 Introduction

This chapter introduces the theories used in the experimental sections. The theories about fluidic circuits are used to simplify complex membrane theory to improve the universality of microfluidic stabiliser systems. To accurately explain the features of stabiliser systems, knowledge from digital circuit analogy is transferred into the basic setup of fluidic analogy. By borrowing circuit analogy to describe fluidic circuits, the theories in this chapter include the following parts:

1. How to use circuit analogy to describe fluidic capacitors and fluidic resistors.
2. How to analyse fluidic stabilisers and describe the fluidic circuit by using the RC circuit law.
3. How to describe the efficiency of a fluidic stabiliser and how to study the mechanism of flexible membranes.

3.2 Fluidic resistor

The basic units of fluid circuits are similar to electric circuits. Ohm’s law in

circuit analogy describes the linear relationship between current and voltage; resistors from digital circuits can be described in a numerical way by this law. Similar to fluidic circuits, to describe the relationship between flow amount and flow rate, a fluidic resistor law is chosen to link the “voltage” and “current” of fluidic circuits and to give a definition of fluidic resistors. To define the significance of fluidic resistors, the value of fluid resistance is defined from Hagen-Poiseuilles’s law[115, 116]:

$$\Delta p = \frac{8\mu LQ}{\pi R^4} = \frac{8\pi\mu LQ}{A^2} = QR_h \qquad (3-1)$$

$$R_h = \frac{\Delta p}{Q} = C_{geometry}\mu\frac{L}{A^2} \qquad (3-2)$$

where:

- Δp is the pressure drop,
- μ is the dynamic viscosity,
- L is the length of pipe,
- Q is the volume flow rate,
- R is the pipe radius,
- A is the cross section arear of the pipe,
- R_h is the fluidic resistance,
- $C_{geometry}$ is the geometry constant

In equation (3-1), regard the pressure difference Δp in the fluidic circuit as the difference of voltage and regard the flow rate Q as the current. The fluid resistance R_h can be calculated from the pressure difference Δp and the flow amount Q in equation (3-2). The physical definition of fluid resistance is how difficult is it for a unit of pressure drop to cross a fluid channel.

3.3 Fluidic capacitor

In a digital circuit, capacitance is defined as the ability of storing electrons when charging the device. The capacitance C is $C = \frac{\Delta Q_e}{\Delta V_e}$, where Q_e is amount of held electrons, V_e is the electric potential. The fluidic capacitor is similar to a digital circuit, the fluidic capacitance can be defined as the ability of storing fluid at a unit pressure drop. Following the idea of the digital circuit, if Q_e replaced by the amount of held fluid in volume V_f, and replace V_e by pressure drop P, the fluidic capacitors could be defined by the flowing equation:

$$C_f = \frac{dV_f}{dP_f} \qquad (3-3)$$

where:

- C_f is the fluidic capacitance,
- $V_f$is the fluid volume,
- P_f is the pressure drop.

Since the membrane used in the microfluidic devices is usually cut into a plate, the plate theory[28] of fluidic capacitance can define the capacitance as the following[117]:

$$C_f = \frac{dV_f}{dP_f} = \frac{6w^6\left(1 - {P_r}^2\right)}{\pi^4 h^3 E} \qquad (3-4)$$

where:

- C_f is the fluidic capacitance,
- $V_f$is the fluid volume,
- P_f is the pressure drop,
- w is the width of the membrane,
- h is the thickness of the membrane,

- E is the Youngs modulus,
- P_r is the Poisson's ratio.

By using the characteristic of the flexible membrane, the capacitance of a capacitor can be defined by both the thin membrane theory and hydraulic equation. The geometry feature of the membrane and the chamber both influence the capacitance of a fluidic capacitor.

3.4 Fluidic RC circuit

Rather than identifying basic units of fluidic circuits, the whole fluid circuit can be regarded as a signal system which is similar to an RC circuit in digital analogy. To describe the features of a fluid system including the stabilisation ability of a stabiliser, RC circuit law is used to present a typical stabiliser system in this section.

A fluidic stabiliser system contains the device, the sensor, the tube, the water container and the pump. The fluidic stabiliser, can be regarded as a fluidic capacitor connected with a fluidic resistor. In reality, defining the exact value of a signal capacitor or resistor is nearly impossible in a fluidic circuit because the system's background noise and resistance carried by the pipes and flow sensors is not ignorable. To reduce the influence caused by unrelated devices in the circuit, describing the whole fluidic system from a higher level is required.

Before discussing the fluidic circuit, the RC circuit law of a typical digital circuit should be considered:

$$V_0 = I(t)R_{ohm} + \frac{Q_e}{C} = I(t)R_{ohm} + \frac{\int_0^{t0} I(t)dt}{C} \qquad (3-5)$$

$$\frac{dV_0}{dt} = \frac{dI(t)R_{ohm}}{dt} + \frac{I(t)_0^{t0}}{C} \qquad (3-6)$$

where:

- V_0 is the total circuit voltage
- I(t) is the current at time t,
- R_{ohm} is the resistance,
- Q_e is the electronic amount,
- C is the capacitor.

In equation (3-5), the relationship between the current; the voltage; the resistance R_{ohm}, the electronic quantum Q_e and capacitor C is given. Similar to the electric capacitor, in fluid dynamics, voltage V_0 can be replaced with fluid pressure difference Δp, I(t) replaced with flow rate Q_f, resistance R_{ohm} replaced with fluid resistance R_f, and then the definition of fluid capacitor C_f and response time $\tau = R_f C_f$ can be attained. According to equation (3-5) and (3-6), as the pressure difference is set to 0 at initial stage, the equation can be written as:

$$\frac{-R_f C_f dQ_f}{Q_f} = dt \qquad (3-7)$$

$$lnQ_f(t) = -\frac{t}{R_f C_f} = -\frac{t}{\tau} \qquad (3-8)$$

Solving equation (3-7), the relationship between the flow rate Q_f, the fluid

resistance R_f and the RC constant $t_0 = \tau = R_f C_f$ can be defined in equation (3-8). The calculation of C_f and R_f become possible. Rather than under theoretical conditions, in real fluidic circuits, the Q_f recorded is actually the water-head pressure-caused flow Q_{total} plus the driven flow Q_f. To reduce the influence of the water head, the fluidic capacitor law can be written as[30, 34]:

$$\ln\left(\frac{Q_f(t)-Q_0}{Q_H-Q_L}\right) = -\frac{t-t_0}{R_f C_f} = -\frac{t-t_0}{\tau} \qquad (3-9)$$

where:

- $Q_f(t)$ is the flow rate recorded at time t,
- Q_0 is the flow rate caused by the water head pressure when the extra flow source is not working, or called the system background flow of the circuit,
- Q_H is the flow rate when the capacitor is charged with full potential energy,
- Q_L is the flow rate when the discharging process of the capacitor ends,
- t is the time,
- t_0 is the time when the fluidic capacitor started to be charged,
- τ is the RC constant of the fluidic system which equals to $R_f C_f$.

Equation (3-9) provides the method to calculate RC constants in fluidic circuits. By fluidic RC circuit law, a typical fluidic circuit can be studied in an analogical way. The following Fig. 3-1 is an example of how to view a typical lab-on-a-chip system as a fluidic RC circuit.

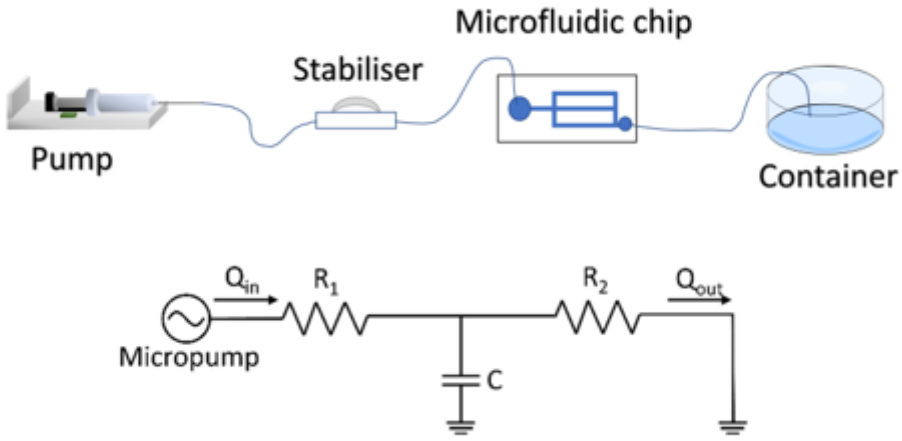

Fig. 3-1 An example of how to simplify a real lab-on-a-chip system as a circuit analogy model.

In a real case, the pump can be regarded as the power supplier for the whole circuit just like a battery. The background noise of the system can be simplified as an extra resistance R_1 in Fig. 3-1. And the stabiliser only provides capacitance C and resistance R_2. The C and R_2 are difficult to calculate, but the total RC constant of the system can be carried out by calculation of system response.

3.5 Membrane theory of stabiliser

To understand the physical nature behind the stabilisation of membrane-based stabilisers, it is necessary to study the movement of membranes. To study how the membrane influences the capacitance and resistance of a stabiliser system, the relationship between the centre displacement of the membrane and the flow rate change is discussed. The following derived formula is given[26, 89]:

$$\sigma = \frac{9{R_m}^2}{64E_m h^3}\Delta \mathrm{p} \qquad (3-10)$$

$$K_m = \frac{9{R_m}^2}{64E_m h^3} \qquad (3-11)$$

$$Q_\mathrm{f} = \frac{\Delta P}{R_H} \qquad (3-12)$$

$$\sigma = K_m Q_\mathrm{f} R_H \qquad (3-13)$$

$$V_m = \frac{\pi\sigma}{6}\left(3{R_m}^2 + \sigma^2\right) \qquad (3-14)$$

$$\frac{dV_m}{dt} = \dot{Q} = \frac{Q_{\mathrm{f}1} - Q_{\mathrm{f}2}}{\Delta t} = \frac{d\left[\frac{\pi\sigma}{6}\left(3{R_m}^2 + \sigma^2\right)\right]}{dt} = \frac{d\left(\frac{\pi{R_m}^2}{2}K_m Q_\mathrm{f} R_H + \frac{\pi}{6}K^3 Q_\mathrm{f}^3 {R_H}^3\right)}{dt}$$
$$= \frac{\pi R^2}{2}K_m \dot{Q}_\mathrm{f} R_H + \frac{\pi}{2}{K_m}^3 Q_\mathrm{f}^2 \dot{Q}_\mathrm{f} {R_H}^3 \qquad (3-15)$$

In equation (3-10), the R_m means the radius of the membrane, E_m is elastic modulus, h is the thickness of the membrane, $\Delta\mathrm{p}$ is the pressure drop on the membrane, and σ is the displacement which occurs at the centre of the membrane. If an index K_m to represent values with nearly no change is set, equation (3-10) can be rewritten as equation (3-13).

From equation (3-10), the displacement at the centre of the membrane can be rewritten as equation (3-13); where R_H is the fluid resistance calculated from H-P law, Q_f is the volume flow rate of fluid.

In equation (3-14), the volume of the capacitor chamber V_m is defined as a function of R_m and σ. Combine equation (3-13) and (3-14), then equation (3-15) defines the change of volume of the chamber where $\frac{dV_m}{dt}$ equals to the

changing rate of the volumetric flow rate. Hence, $\frac{Q_{\mathrm{f1}}-Q_{\mathrm{f2}}}{\Delta t}$ is an example of how to calculate the changing rate of the volumetric flow rate for a time change Δt; Q_{f1} is the volumetric flow rate at time point 1, and Q_{f2} is the volumetric flow rate at time point 2. If V_m and R_m are replaced by equations (3-10), (3-11), (3-12) and (3-13), the final formula will be equation (3-15).

In a non-linear case, equation (3-10) should be written as:

$$\sigma = \left(h\frac{3{R_m}^4}{16E_m h^4}\right)^{\frac{1}{3}}\Delta \mathrm{p} \qquad (3-16)$$

In equation (3-16), the K will change to:

$$K_m = \left(h\frac{3{R_m}^4}{16E_m h^4}\right)^{\frac{1}{3}} \qquad (3-17)$$

and $\dot{Q}$ will be defined as:

$$\dot{Q} = \frac{\pi}{6}({R_m}^2 K {R_H}^{\frac{1}{3}} {Q_{\mathrm{f}}}^{\frac{-2}{3}}\dot{Q}_{\mathrm{f}} + K^3 R_H \dot{Q_{\mathrm{f}}}) \qquad (3-18)$$

As a fluid capacitor, the relationship between flow rate Q(t) and capacitance C is defined as:

$$Q(t) = \mathrm{C}P_0\left(1-\mathrm{e}^{\frac{-t}{\tau}}\right) \qquad (3-19)$$

Where P_0 is the pressure when the capacitor is fully charged. P_0 has a meaning which is similar to the amplitude of a typical capacitor in a digital circuit.

Combine equation (3-15) and equation (3-19), the $\dot{Q}_{\mathrm{f}}$ can be written as:

$$\dot{Q}_{\mathrm{f}} = \frac{CP_0}{\tau}e^{\frac{-t}{\tau}} \qquad (3-20)$$

In a linear condition, the relationship between $\frac{dV}{dt}$ and time t can be written as

$$\frac{dV_m}{dt} = \frac{\pi {R_m}^2}{2} K_m \frac{CP_0}{\tau} e^{\frac{-t}{\tau}} R_H + \frac{\pi}{2} {K_m}^3 C^2 P^2 \left(1 - \mathrm{e}^{\frac{-t}{\tau}}\right)^2 \frac{CP_0}{\tau} e^{\frac{-t}{\tau}} {R_H}^3 \qquad (3-21)$$

If the capacitor C is considered as equal to $\frac{dV_m}{dP}$, and equation (3-18), (3-19), (3-20) and (3-21) are combined, the result is:

$$C = \frac{\mathrm{d}\left[\frac{\pi {K_m}^2}{2}\left(\frac{\sigma}{K_m}\right)^2 {R_m}^2 + \frac{\pi K^3}{6}\left(\frac{\sigma}{K_m}\right)^3\right]}{\mathrm{dp}} = \frac{\pi}{2} K_m \sigma^2 + \pi K_m \sigma {R_m}^2 \qquad (3-22)$$

With the complexity of both the physical nature and the calculation, the equation's working parameters and accuracy are limited[28, 32]. To make the characteristics of stabiliser extractable, a simplified combination of membrane theory and fluidic circuit law should be established in the future.

CHAPTER 4 DESIGN, FABRICATION AND ANALYSIS OF 3D PRINTED MODULAR STABILISERS

4.1 Introduction

In this chapter, the process of design and analysis of a 3D-printed modular fluidic stabiliser system is given. To reduce the gap between unsteady laboratory-developed microfluidic devices and the increasing demand for miniaturisation and standardisation of microfluidic devices, 3D-printed stabilisers are designed and fabricated to fulfil the aim of reducing the oscillation error better in a rapid and low-cost way with adjustable features. The following topics are covered in this section:

1. The first part talks about the design and materials of the 3D printed modular microfluidic stabiliser, including the assembling process and the analysing of stabilisation ratio of the designed stabiliser system.

2. The second part aims to explain the physical nature behind the stabilising process. By studying how the displacement of the membrane influences the input and output signals, fitting curves and transfer functions between input and output are established. The frequency-specified features influenced by the deflection of the

membrane are summarised for setting up a simplified model to explain the stabilisation behaviours.

3. The third part of the experiment includes hypotheses based on part 2, a model based on a simplified fluidic circuit analogy is established in order to characterise the stabiliser system without doing complex calculations. The model is verified by the study based on the extraction of RC constants.

First, Section 4.1 gives an introduction to the whole chapter. Then, in Section 4.2, the design of the modular stabiliser demo is introduced. In Section 4.3, the fabrication process of the devices is discussed, and the characterisation of the designed stabiliser is exhibited. The process includes the extraction of stabilisation ratio and the study of the flexible membrane. To study the physical nature behind the stabilising phenomenon, experiments about the oscillation and displacement of the flexible membrane during working conditions are set to help establish a simplified and common model for explaining all the stabiliser systems. In Section 4.4, the hypothesis of a new model based on digital circuit analogy is explained to link the behaviour of stabiliser systems with a specific variable called the RC constant, which helps to replace the complex calculation from the membrane's features. How to extract the RC constant of a stabiliser system without calculating the resistance and capacitance of the fluidic circuit is introduced, and the tested

degree of fitting is 0.997, which proves the accuracy of the model. Section 4.5 gives the conclusions of the experiments and summarises the characteristics of the system.

4.2 Design of the modular stabiliser

The modular stabiliser system in this thesis is a combination of fluidic resistor substrates and membrane based fluidic capacitors. Different from previous stabilisers, the MSS is pluggable and standardised with lego-like studs. The membrane used in the system was fabricated by Ecoflex0030 with Young's modulus of 0.3 MPa. The Ecoflex0030 has a smaller Young's modulus when compared with PDMS. With 835% expanding ratio, Ecoflex0030 membrane can provide larger capacitance than other resins according to equation (3-22). Table 4 lists typical materials used for fabricating microfluidic devices. The Ecoflex0030 membrane which has largest maximum elongation with Young's modulus smaller than 0.4 MPa can provide larger capacitance and damper volume when compared with other materials according to equations (3-4), (3-10) and (3-14).

Table 4 Young's modulus and maximum elongation of typical flexible materials used for microfluidic devices' fabrication.

Material	Young's Modulus (MPa)	Maximum elongation
Ecoflex0030[118, 119]	0.1-0.4	835%
Ecoflex0010[118]	0.05-0.3	573%

Sylgard184[118]	0.7-1.2	296%
PDMS[118, 120]	1.2-3.0	83%

The design of the stabiliser is shown in Fig. 4-1. The demo contains modular fluidic capacitors and modular substrates. The fluidic capacitor is the main structure of the modular stabiliser which can stabilise the unsteady input flow by transferring the kinetic energy of the fluid into the elastic energy of the membrane.

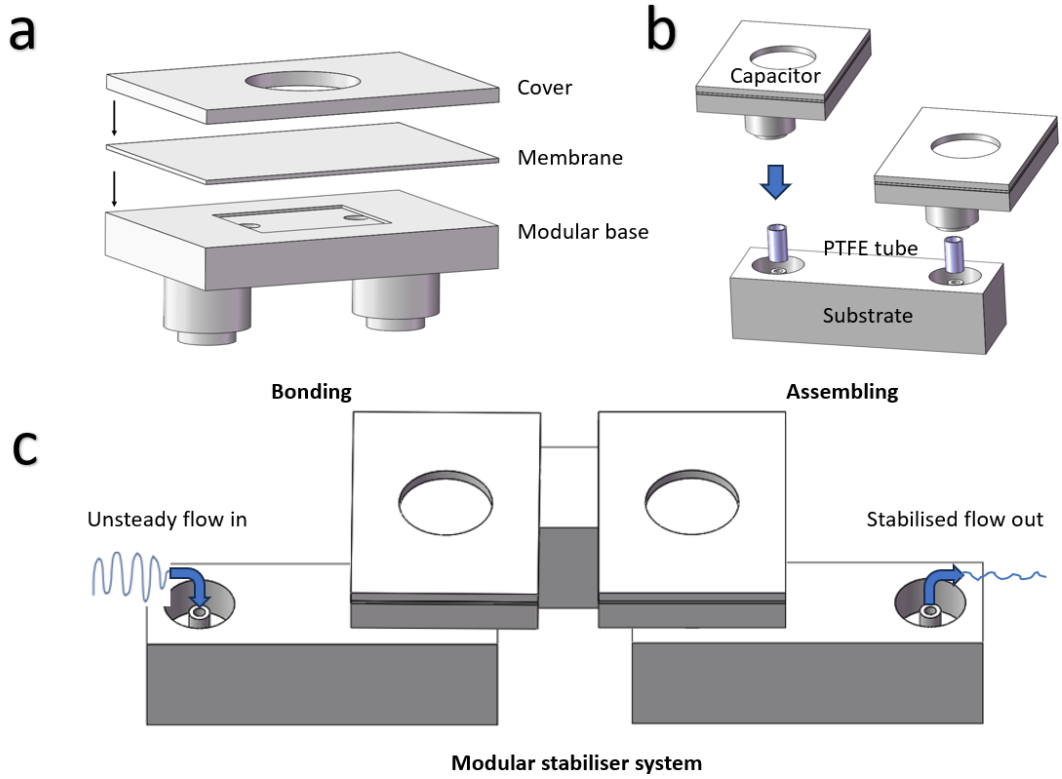

Fig. 4-1 Details of the modular stabiliser system: (a) the modular stabiliser unit; (b) the assembling process of the stabiliser; (c) the assembled stabiliser system.

As shown in Fig. 4-1(a), the capacitor contains a cover part to hold the membrane, a flexible layer with a 500 μm height and 10 mm diameter Ecoflex0030 membrane to provide a fluidic storage chamber. A modular base with $1 \times 1\ mm$ square channels to connect different devices such as fluidic

resistors or flow sensors. To assemble the modular stabiliser, two small polytetrafluoroethylene (PTFE) tubes with a 5 mm length, a 1 mm inner diameter and a 2 mm outer diameter are plugged into the luer-connector inside the modular substrates to provide flexible connections between the capacitor and the substrate. The process is illustrated in Fig. 4-1(b). The assembled stabiliser system is given in Fig. 4-1(c). When the unsteady flow goes into the system, the flexible membrane will expand and store the energy of the fluid as a damper. The output flow will then be stabilised by transferring extra energy to the elastic energy of the membrane.

4.3 Characterisation of the modular stabiliser

4.3.1 The stabilisation ratio

To characterise the stabilisation ratio of the stabiliser, a demo of the designed stabiliser is fabricated and tested. The fabrication process of the stabiliser is illustrated in Fig. 4-2(a). From the design, the 3D printer (Asiga max 365nm, USA) printed modular substrates and capacitors with an accuracy of 100 μm to assemble the stabiliser system. The printing material is Clear V4 resin (Asiga, USA). The stabiliser contains 2 capacitors and 3 substrates to form the Lego-like studs. The devices can be printed and assembled within 5 hours for less than 1 dollar.

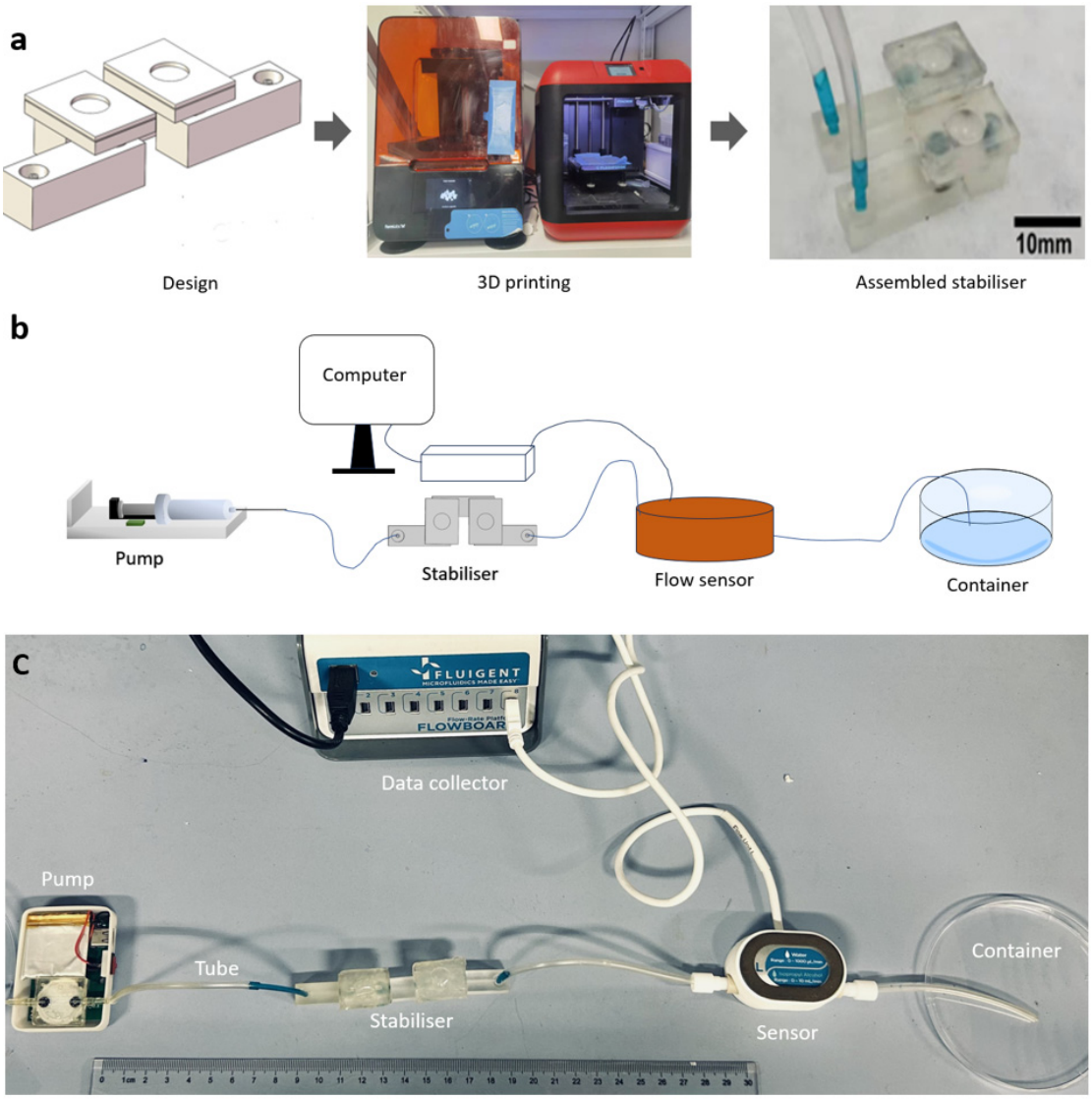

Fig. 4-2 The fabrication process of the modular stabiliser system and the experimental setup: (a) The fabrication process of the stabiliser; (b) the illustration of experimental setup; (c) the devices for experiments.

In order to record the input and output flow of a fluidic system working with the stabiliser and find out the stabilisation ratio, an experiment was set up as shown in Fig. 4-2(b). The testing system uses a pump (Healtell, China) to provide controllable input signals, a computer to record the data collected by the flow sensor, a modular stabiliser to reduce the fluctuation and a container to collect wasted fluid. To extract the stabilisation ratio, the pump provides

different input waves with controllable fluctuation. The illustration of the devices is shown in Fig. 4-2(c). The experiment compares the output flow with the stabiliser and without the stabiliser at the same place in the fluidic circuit to analyse the differences. The flow rate will be recorded when the average flow goes to a steady state to avoid the oscillation error caused by the pump. Each test includes three repeating tests to draw the data with error bars. Both the flowrate and the stabilisation ratio were recoded and calculated. The ratio of amplitude vibration is used to describe the stability of the stabiliser as the amplitude response ratio:

$$R_A = \frac{A_s}{A_i} \qquad (4-1)$$

where:

- R_A is the amplitude response ratio,
- A_s is the amplitude or oscillation of stabilised flow,
- A_i is the amplitude or oscillation of initial flow.

The R_A represents the stabilisation ratio calculated from the recorded amplitude.

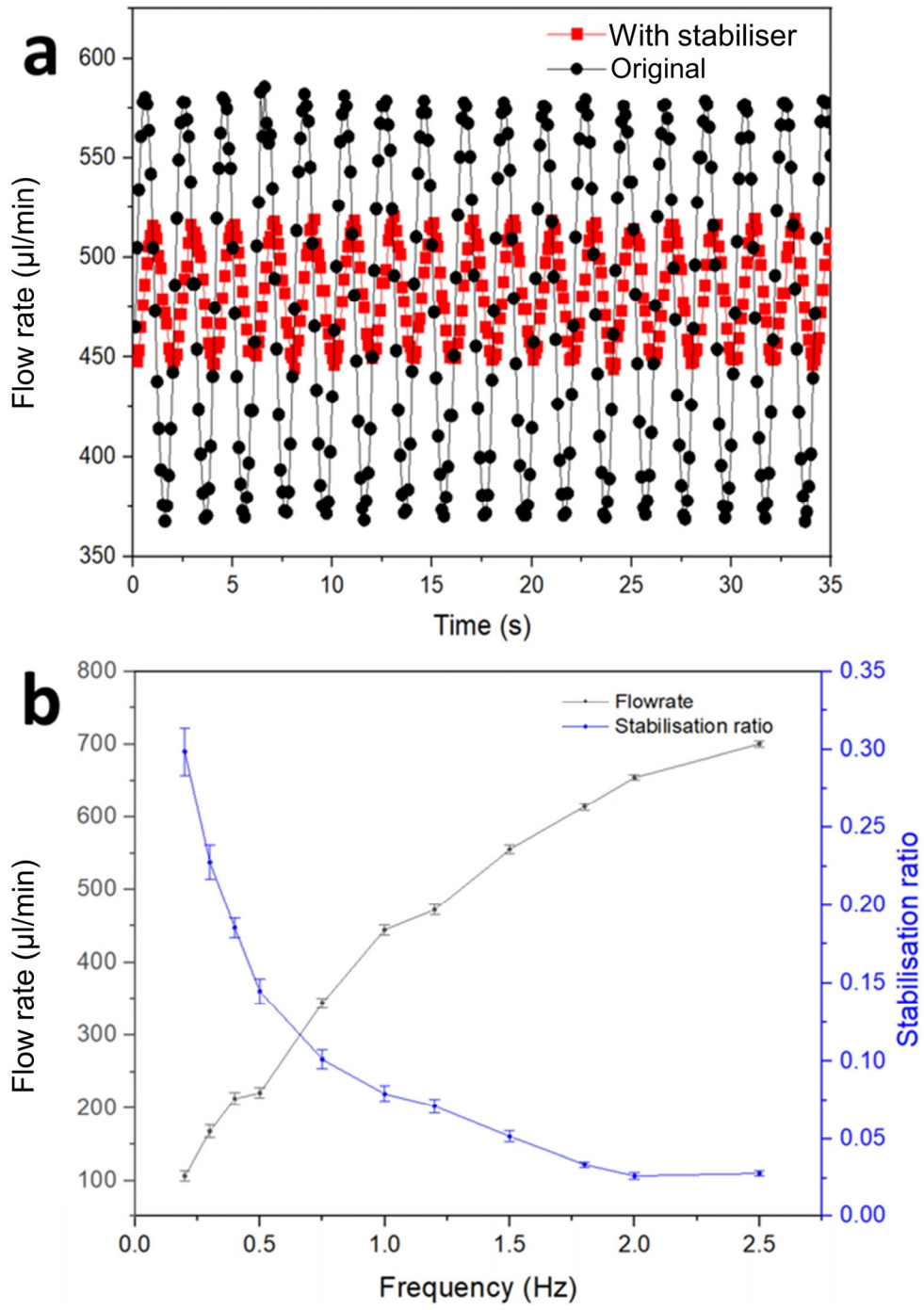

Fig. 4-3 The flowrate and stabilisation ratio of the modular stabiliser: (a) the example of a test with input signal set as 475±100 µl/min; (b) the flowrate and stabilisation ratio calculated at different working frequencies with error bar.

As shown in Fig 4-3(a), the system uses the flowrate recorded with and without the stabiliser to calculate the stabilisation ratio. The amplitude of the signal is defined as the average peak difference between the high peak and

low peak of the recorded signals. To analyse the frequency response of the stabiliser system, the working frequency of the driven flow was changed from 0.2 Hz to 2.5 Hz to provide various flow rates with different stabilisation ratios. The stabilisation ratio is calculated and listed in Fig. 4-3(b). From the results in Fig. 4-3(b), the stabilisation ratio of the system changes with the amplitude and frequency of input signals. As a conclusion from Fig. 4-3(b), the larger the working frequency, the smaller the stabilisation ratio. The stabilisation ratio also decreases with the enlargement of the flowrate. And the stabilisation ratio can change from 29% to less than 2% for this system. Meanwhile, the error of the calculated stabilisation ratio decreases with the increase of input frequency and flowrate with a maximum error of 5.01%. The calculated data is provided to be acceptable. By observing the curve, it can be known that the cut-off frequency is smaller than 0.2 Hz, which means the amplitude response of the stabiliser system can be regarded as a low-pass-filter system.

4.3.2 The deflection of the membrane

According to Section 4.3.1, the stabilisation ratio decreases with the input frequency, which is similar to a LPF. From equations (3-6) and (3-15), it can be known that the displacement of the membrane influences the output signal. To study why the ratio decreases with the increase of frequency and explain the physical nature behind the stabilisation phenomenon, the displacement

and the oscillation of the membrane need to be discussed with frequency-specified. The definitions of displacement and oscillation are shown in Fig. 4-4(a). When the flow goes into the damper chamber, the deformation of the membrane enlarges the volume of fluid and thus transfers the kinetic energy of fluid into the elastic energy of the membrane, which leads to the absorption of unsteady signals. In this experiment, to identify the relationship between the membrane's behaviour and the stabilising process, the oscillation of the membrane during the charging and discharging processes of the stabiliser is detected to study how the displacement of the membrane influences the stabilisation ratio. Besides, how the oscillation and total displacement of the membrane change with different input frequencies were discussed with a laser detector.

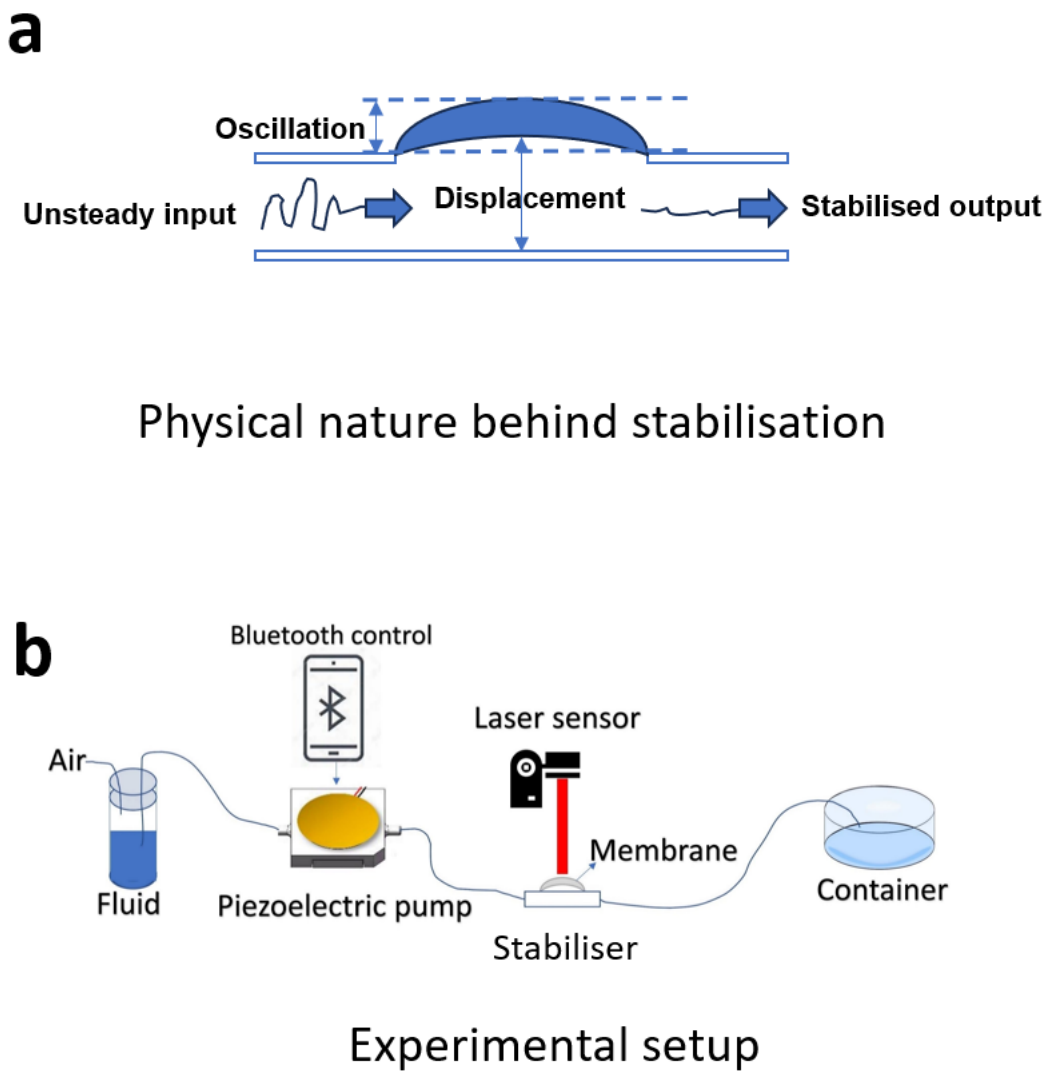

Fig. 4-4 The experimental setup and physical nature of the test: (a) the physical nature behind the stabilisation of the flexible membrane; (b) the experimental set-up for recording the displacement and oscillation of the working state of the stabiliser.

Fig. 4-4(b) illustrates the full setup of the experiment. To provide a direct observation about the deflection and displacement of the flexible membrane in a working state, a laser detector (Keyence, Japan) is prepared to detect the vibration of the membrane. To avoid sampling distortion, the sampling frequency should be high enough to cover all the details of the working state according to Nyquist's theorem. In the experiment, the maximum input signal is 20 Hz, so the sampling frequency is set to 100 Hz to satisfy Nyquist's

theorem. To provide input pulsation, the piezoelectric pump (Healtell, China) is controlled by Bluetooth to give different input signals at different frequencies. Pipes connecting each device are made of PTFE tubes with a 1-mm inner diameter.

To detect the displacement accurately by reflecting the laser light with enough intensity, the fluid was inked to enhance the reflection. The laser sensor was also set to diffuse-reflection model for better accuracy. The input signal of the system was provided by the piezoelectric pump connected to a fluid container. The stabiliser was stationary at the bottom of the laser detector. The laser beam was adjusted to reflect at the centre of the circular membrane in order to detect the largest deformation.

The frequency of input signals provided by the pump varied from 0.05 Hz to 20 Hz in order to cover the most commonly used working situations of the stabiliser. The laser detector recorded the total displacement of the membrane when the pump started to work, and the recording did not end until the input signal disappeared. The whole process of charging, steady working, and discharging of the stabiliser were recorded by this method.

As shown in Fig. 4-5, an example of the whole testing process is illustrated to give a clear view of how the sensor works in the experiment. The input frequency in this example is 2 Hz.

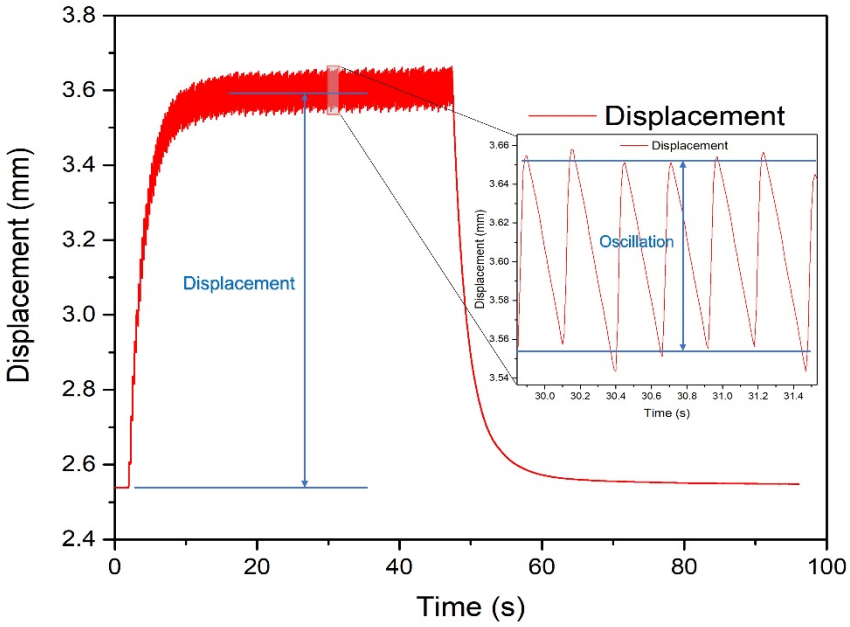

Fig. 4-5 The example of displacement recorded by the laser sensor for a whole charging and discharging process of the stabiliser.

The displacement of the membrane has three stages. Process one is the charging process, which starts with the opening of the piezoelectric pump. In Fig. 4-5, the charging process starts at 0 s and ends around 10 s, when the membrane is deforming with the enlarging flow rate caused by the pulse signal. The change in height of the membrane is defined as the displacement in the figure. In process two, the flow rate becomes steady and the average flow rate stops growing; this stage is defined as the oscillation stage. From 10 s to 45 s in Fig. 4-5, the average displacement of the membrane becomes steady, but the instantaneous oscillation of the membrane is still vibrating. In the enlarged section of Fig. 4-5, the oscillation state is shown. In the last stage, the pump stops working, and the flow rate quickly drops to zero. In the last stage, there is no vibration on the membrane, and the curve of

displacement becomes smooth and quickly drops to the beginning state which is similar to the discharging process of a RC regulator as shown in equations (3-19) and (3-21). Then the sensor and time are reset to the beginning state for the next test.

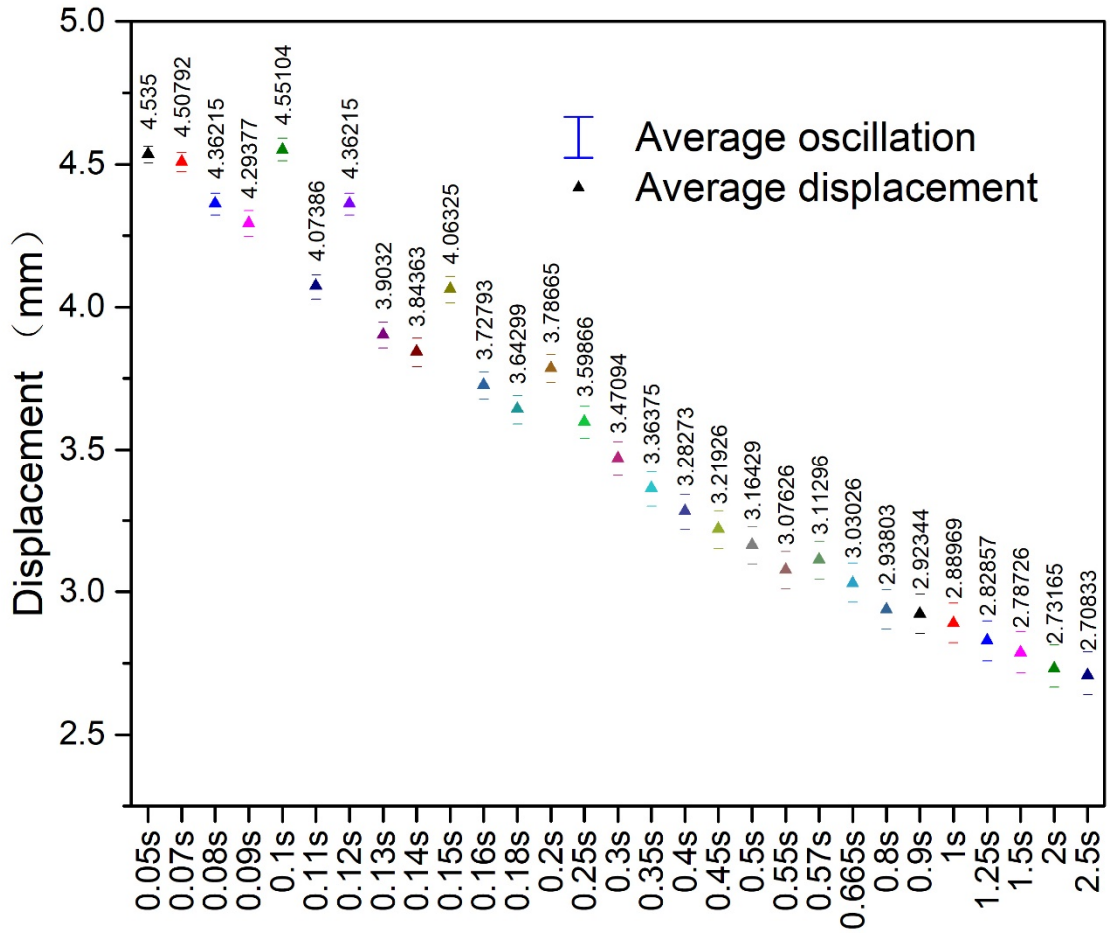

Fig. 4-6 The recorded average displacements of the working stabiliser with different input periods.

The average difference between the high peak and the low peak is defined as the average oscillation as shown in the thumbnail of Fig. 4-5. The average displacement is recorded as the average height difference detected by the laser sensor at the centre of the membrane.

The piezoelectric pump worked from 0.04 Hz to 20 Hz in the experiment to give the frequency response of different working situations. The data recorded from the laser sensor gives different displacement and oscillation curves for each input.

In Fig. 4-6, the average displacement and oscillation of each input signal are exhibited. In the graphic, the centre triangle represents the average displacement of the centre of the membrane at a specified frequency during the steady state of the working process. The x axis in Fig. 4-6 is the input signal's period in seconds, and the y axis means the height of displacement. In the figure, the triangle point means the average displacement detected at the centre of the membrane during the steady working state. There are two small bars around each point, which present the difference between the minimum oscillation and the maximum oscillation of the membrane. It's clear that the average oscillation increases with the increase in input period, and the average displacement decreases with the increase in input period. To have a closer view of the frequency features, the data in Fig. 4-6 is transferred from time domain to frequency domain for comparison in Table 5.

Table 5 The average oscillation and real displacement of the membrane calculated at different input frequencies.

Frequency (Hz)	Oscillation (mm)	Real displacement(mm)
20.00	0.0287	1.9654
14.29	0.0376	1.9361

12.50	0.0419	1.7914
11.11	0.0502	1.7249
10.00	0.0506	1.9832
9.09	0.0597	1.5107
8.33	0.0420	1.7914
7.69	0.0698	1.3331
7.14	0.0726	1.2699
6.67	0.0741	1.4972
6.25	0.0790	1.1549
5.56	0.0872	1.0684
5.00	0.0883	1.2221
4.00	0.1015	1.0601
3.33	0.1069	0.9152
2.86	0.1137	0.8055
2.50	0.1188	0.7218
2.22	0.1259	0.6559
2.00	0.1242	0.6221
1.82	0.1283	0.5130
1.75	0.1284	0.5524
1.50	0.1336	0.4861
1.25	0.1343	0.4028
1.11	0.1367	0.3596
1.00	0.1376	0.3339
0.80	0.1409	0.2653
0.67	0.1442	0.2237
0.50	0.1483	0.1661
0.40	0.1516	0.1405

Since the membrane has an original height in the static state, the real displacement should be the height difference between the average maximum displacement recorded and the original height at the beginning stage. The

calculated oscillation and real displacement are listed in Table 5. The frequency shown in the table is calculated from the reciprocal of the period, so the value is not an integer. The average oscillation at steady state increases with the decrease in frequency, and the real displacement of the membrane decreases with the decrease in input frequency, which inspired us to use a transfer function to describe the relationship between the two variables.

According to equation (3-21), the fluidic chamber volume V_m has a positive correlation with the displacement of the membrane. By referring to equations (3-19) and (3-21), if the hypothesis is correct, the displacement of the membrane at different amplitudes should have an exponential fitting curve with the input frequency. To justify the hypothesis, Fig. 4-7 is drawn to show the fitting curve with error bars.

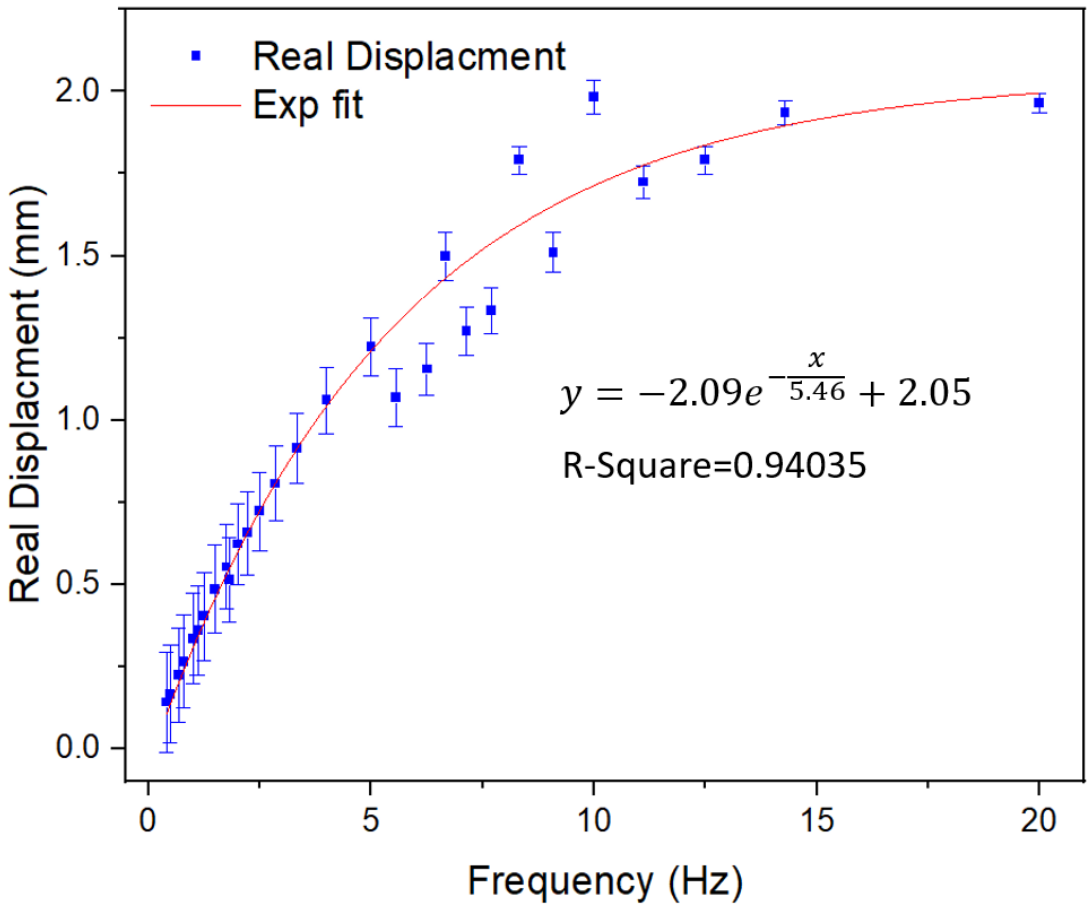

Fig. 4-7 The average real displacement and oscillation in the frequency domain.

Fig. 4-7 shows the oscillation with real displacement in the same frequency domain. By using an exponential fitting curve, the displacement has a similar formula to the amplitude response law with a R square equal to 0.94, which means the response curve can be described with a transfer function transferred from equation (3-19).

In Fig. 4-7, the displacement at high frequency shows a discrete outlier, which is caused by the background noise of the pump. During the experiment, it was found that the output of the pump has more outlier points when the controlling PCB is giving a periodic signal with no integer frequencies. But due to the

limitations of experimental equipment, the following tests were still performed with the same pump.

To further extract the characteristics of oscillation based on equation (3-19), the relationship between oscillation and displacement should be identified. From equations (3-10) and (3-12), it can be known that the displacement of the membrane has a positive correlation with the average flow rate. The average displacement of the working state represents the flow rate Q_f, the oscillation during the steady state presents the instantaneous increase and decrease of the flow rate $Q_f(t)$. Define the amplitude response ratio of the membrane as $R_{dis} = \frac{Oscillation}{Displacement}$, then combine equations (3-8) and (3-13), the relationship between displacement and oscillation can be simplified as:

$$R_{dis} = \frac{\sigma_o}{\sigma_d} = \frac{Q_f(t)}{Q_f} = a_i + b_i e^{-\frac{t-t_0}{\tau}} \qquad (4-2)$$

where:

- R_{dis} is the amplitude response ratio of displacement,
- a_i and b_i are constants,
- σ_d is the displacement,
- σ_o is the oscillation,
- Q_f is the flow rate,
- t is the time,
- t_0 is the time when the fluidic capacitor started to be charged,
- τ is the RC constant of the fluidic system which equals to $R_f C_f$.

If the hypothesis is correct, the oscillation/displacement ratio will perform as an LPF with an exponential fitting curve. To verify equation (4-2), the

amplitude response ratio is calculated and listed in Fig. 4-8.

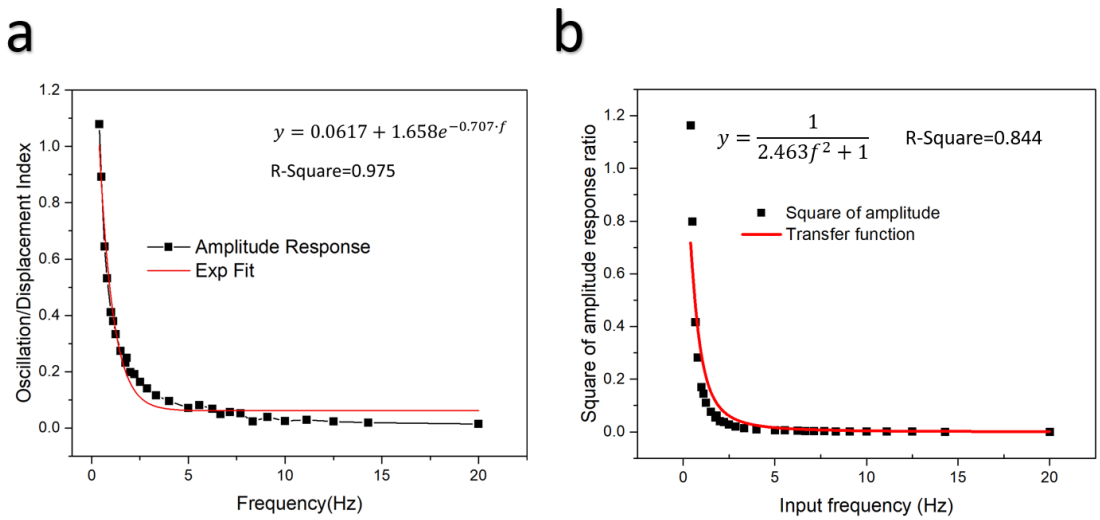

Fig. 4-8 The relationship between average oscillation and displacement at the frequency domain: (a) the exponential fitting curve; (b) the transfer functional fitting curve.

Fig. 4-8(a) illustrates the calculated R_{dis} with input frequencies and Fig. 4-8(b) shows the square of R_{dis}. The amplitude response index mentioned in equation (4-2) shows similar properties to a classic amplitude response for an LPF with an R-square of 0.975. The fitting equation given by the Origin 2021 software in Fig. 4-8(a) is:

$$R_A = 0.0617 + 1.658e^{-0.707f} = 0.0617 + 1.658e^{-0.707 \cdot \frac{\omega}{2\pi}} \qquad (4-3)$$

Where:

- R_A is the amplitude response ratio,
- f is frequency of input,
- ω is $2\pi f$ and means angular velocity.

To simplify equations (4-2) and (4-3), a transform process is done. Notice that equation (4-3) has the formula of an exponential decay function with an

exponential time constant equal to 1.414, inspired by the Laplace transform of a typical exponential decay function $sinf \cdot e^{-f}$, considering that the exponential decay function e^{-t} as the limit of the maximum amplitude of the membrane's displacement. When the input flow is set to frequency f and the $sinf$ is considered as the influenced periodic output wave's amplitude at time t, then $sinf$ can be defined as the vibration function caused by the periodic pulse input wave provided by the piezoelectric pump. To describe the membrane's features in a formula which is similar to transfer functions in electric circuits, a Laplace transform is used to get a formula with an imaginary number s in frequency domain. Here is the process:

Set $R_A = 0.0617 + 1.658e^{-0.707f}$ as function $f(f)$ of time, and do the Laplace transform as:

$$F(s) = \int_0^{\infty} e^{-st} f(f) dt = L[0.0617] + L[1.658 \cdot e^{0.707}] = \frac{0.0617}{s} + \frac{1.658}{s + 0.707} \quad (4-4)$$

Where F(s) is the Laplace transform function, $L[\,]$ is the Laplace transform, and s is an imaginary number. The equation (4-4) can link the transfer function to the fitting curve of R_A in imaginary domain. If the imaginary number s can be replaced by $j\omega RC$, the membrane's behaviour in both time domain and imaginary domain can be described with the common formula $\frac{1}{A_1 j\omega rc} + \frac{1}{A_2 + j\omega rc}$, where A_1 and A_2 are constant numbers. As a similar formula to equation (4-4), the transfer function $|H(j\omega)| = |\frac{1}{1+j\omega RC}|$ can be simplified. To fit the curve,

rewrite the transfer function as following:

$$R_A{}^2 = H^2(j\omega) = \frac{1}{1+\omega^2R^2C^2} = \frac{1}{1+4\pi^2f^2R^2C^2} \qquad (4-5)$$

$H(j\omega)$ is the transfer function, ω is the angular velocity for describing the system, R is the resistance, and C is the capacitance. The fitted curve's RC constant can be calculated using equation (4-5) as 10.198 s without extracting resistance or capacitance.

It can be noticed from the fitting curves that a transfer function from a digital circuit can be used to describe all fluidic circuits in a consistent manner by linking the amplitude response of the output and the frequency of the input.

In summary, the displacement and oscillation of the membrane are defined and calculated in this section. In conclusion, the average oscillation of the stabiliser at steady state increases with the decrease in frequency, and the real displacement of the membrane decreases with the decrease in input frequency. The amplitude response of the stabiliser is defined as the ratio of the output flow's oscillation to the input flow's oscillation, which is performed as an LPF and has a transfer function with a time constant equal to 10.198 and an R square equal to 0.975. The numerical study of the membrane's amplitude response proves the stabiliser system can be characterised by an amplitude response curve without extracting fluidic resistance or capacitance. Inspired by this idea, the simplified transfer function proved to be suitable for

explaining the stabiliser system's amplitude behaviour with the RC constant.

In the experiment, due to the limitations of the equipment and the difficulties of detecting the whole displacement of the membrane, all conclusions are drawn by using the deformation detected at the centre of the membrane. Further studies about the membrane's deformation distribution with more details could be done in the future.

4.4 Model analysis based on characterisation and simplified electric circuit analogy

4.4.1 Hypothesis and model set-up

In Section 4.3, both the stabilisation ratio and the displacement of the membrane were studied. But in the real world, for example, when using wearable micropumps or unsteady flow devices that have limited space for laser sensors and other setups in laboratories, how to extract the characteristics of a fluidic system is a problem. From the results of Section 4.3, it can be noticed that equation (4-5) has a similar common formula with the simplified circuit shown in Fig. 3-1 and equation (3-19). According to the idea, here are the problems that need to be clarified:

Is it possible to represent the characteristics of all stabiliser systems by using a simplified circuit analogy without complex equations such as equations (3-2), (3-4), and (3-22) in fluidic dynamic law? If so, how to extract the

characteristics without calculating the exact resistance, capacitance, and the membrane's displacement? To answer these questions, a model based on extracting the RC constant of the stabiliser system is established in this section to find a simpler way of describing the fluidic circuit without calculating multiple variables.

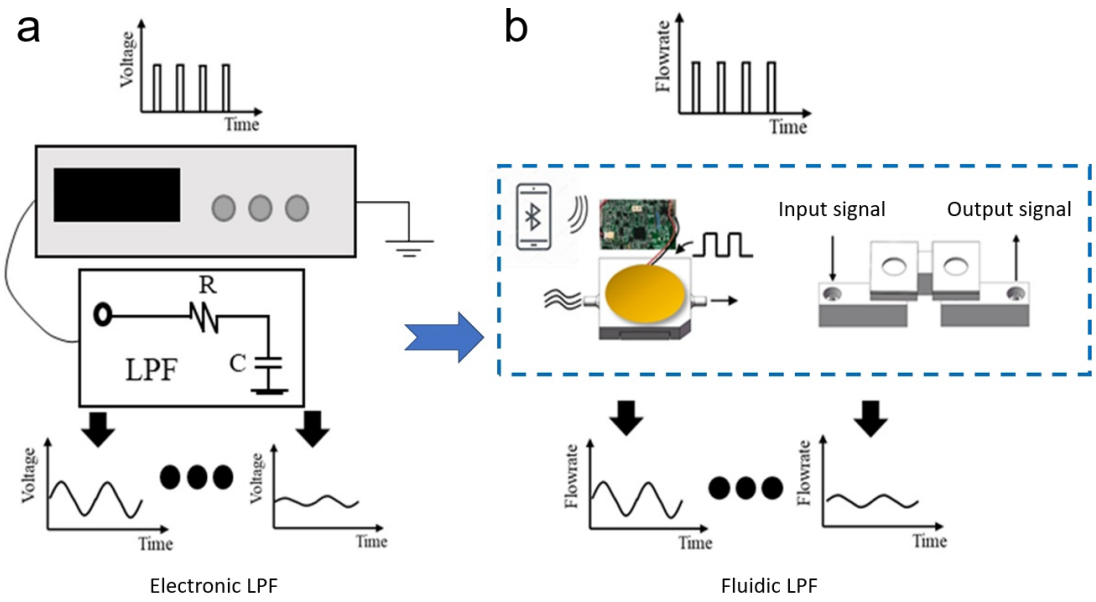

Fig. 4-9 The comparison between electronic LPF and fluidic LPF: (a) the electric circuit low-pass-filter; (b) the fluidic low-pass-filter system.

In Fig. 4-9(a), a typical electric LPF is illustrated. With an oscilloscope-controlled power supplier, the LPF will transfer the input signal into a filtered output signal with a smaller amplitude response. Meanwhile, the fluidic LPF can transfer the unsteady input flow into a filtered steady output flow with a smaller amplitude just like the process shown in Fig. 4-9(b).

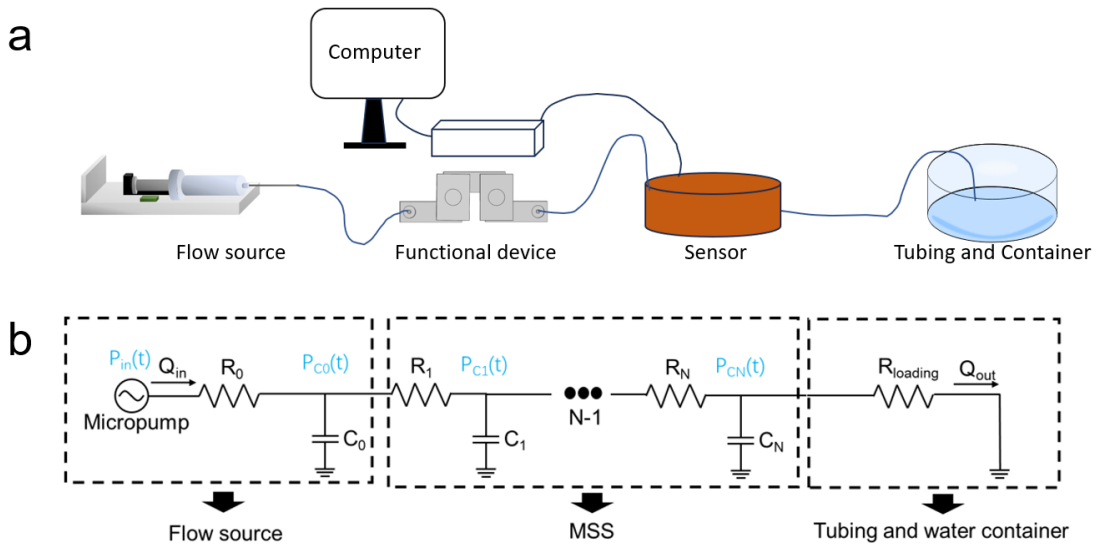

Fig. 4-10 The equivalent electric circuit of a typical fluidic circuit: (a) the typical fluidic circuit including a flow source, the functional devices, a sensor, a computer, a container and tubes; (b) The equivalent electric circuit of the fluidic circuit.

To set up the simplified model, three parts of the fluidic circuit are split into an electric circuit. The flow source in Fig. 4-10(a) is regarded as a pressure inlet with a fluidic resistance R_0 and capacitance C_0 in Fig. 4-10(b). In the same way, fluidic devices linked inside the circuit can be regarded as N nodes of resistance and capacitance, each node includes the pressure of time $P_{ci}(t)$ to describe the pressure drop at node i; R_i and C_i to present the resistance and capacitance at node i. In a fluidic circuit, pressure is similar to voltage and flowrate Q is similar to current in an electric circuit. For example, the MSS in the circuit can be regarded as the N-1 numbers of series-connected RC circuits. The number N depends on the number of devices, each device can be replaced by an RC unit. The tubes and containers inside the fluidic circuit can be regarded as another independent resistance $R_{loading}$ and $C_{background}$. But in real world, detecting the exact resistance and capacitance of each part

of MSS is nearly impossible because sensors, pumps and pipes will all bring extra dynamic resistance and capacitance to the system. Besides, it's also impossible to set up unlimited numbers of sensors at each node of the circuit. To characterise the fluidic circuit, the system needs to be simplified with extractable variables.

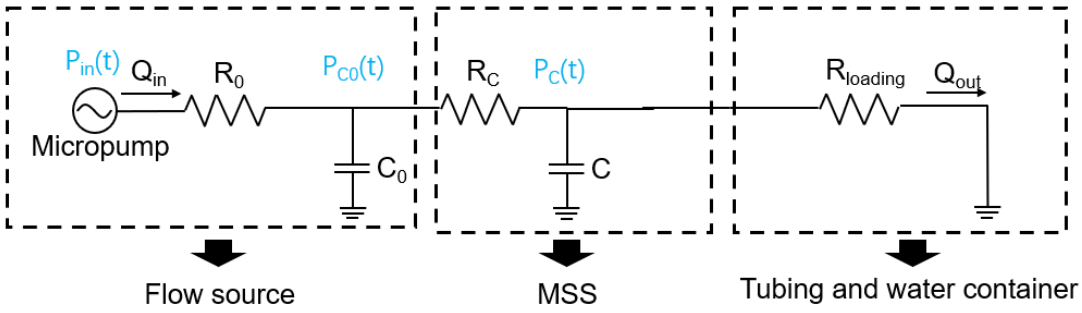

Fig. 4-11 Simplified circuit when node number N equals to 1.

Suppose the system only has one node of circuit, the circuit can be simplified as the circuit in Fig. 4-11. According to the conservation of mass, equation (4-6) shows the relationship between input pressure P_{c0} at node 0 and pressure P_c at node 1:

$$P_{c0}(t) - P_c(t) = R_C C_1 \frac{dP_C(t)}{dt} \qquad (4-6)$$

Where:

- $P_{c0}(t)$ is the pressure of node 0 at time t,
- $P_c(t)$ is the pressure of MSS at time t,
- R_C is the resistance of MSS,
- C_1 is the capacitance of the node 1 MSS.

Solving the differential equations (4-6) by referring to a typical RC circuit like equation (3-6), there will be:

$$P_c(t) = (P_{c0} - P_c)e^{\frac{-t}{R_C C_1}} \quad (4-7)$$

Where:

- P_{c0} is the pressure of node 0 at steady state,
- P_c is the pressure of MSS at steady state.

For each node i, there is:

$$dP_i = P_{ci}(t) - P_{ci-1}(t) = R_i C_i \frac{dP_{Ci-1}(t)}{dt} \quad (4-8)$$

For N nodes, the total pressure of time $P_c(t)$ can be written as:

$$P_{in}(t) = \sum_{i=0}^{N} dP_i = \sum_{i=0}^{N} R_i C_i \frac{dP_{Ci-1}(t)}{dt} \quad (4-9)$$

For series-connected resistors and capacitors, it has the following law:

$$R_{total} = \sum_{i=0}^{N} R_i \quad (4-10)$$

$$\frac{1}{C_{total}} = \sum_{i=0}^{N} \frac{1}{C_i} \quad (4-11)$$

If the total capacitance of each node is replaced by C_{MSS}, and the total resistance of each node is replaced by R_{MSS}, then the simplified circuit can be written as:

$$P_c(t) = (R_{loading} + R_{MSS} + R_{pump}) \frac{(C_{MSS} + C_{pump})}{C_{MSS} C_{pump}} \cdot \frac{dP_C(t)}{dt} \quad (4-12)$$

Where:

- C_{pump} is the capacitance of the pump and tubes,

- C_{MSS} is the total capacitance of the MSS,
- $R_{loading}$ is the total resistance of tubes and connectors,
- R_{pump} is the total resistance of the pump.

By solving equation (4-12), $P_c(t)$ can be written as:

$$P_c(t) = P_{c0} \cdot e^{\frac{-t}{(R_{loading}+R_{MSS}+R_{pump})\frac{(C_{MSS}+C_{pump})}{C_{MSS}C_{pump}}}} \qquad (4-13)$$

By using equation (4-13), the time constant τ of the whole system can be written as $(R_{loading} + R_{MSS} + R_{pump})\frac{(C_{MSS}+C_{pump})}{C_{MSS}C_{pump}}$. And the time constant τ can be extracted without calculating exact resistance and capacitance, which could help characterise the MSS in a simpler way.

4.4.2 Model validation by extracting the RC constant

To measure the RC constant of stabilisers rigorously, the least squares method (LSM)[34] is used to calculate the RC constant τ. For each combination, the RC constant is extracted from the flow rate Q and the time T[30, 34]. To simplify the calculation, the extra background pressure is avoided in the setup by balancing the height of the input and output pipes to set the pressure difference to 0. The extra flow caused by the pressure difference between pipes is set to 0 to minimise the influence of gravity. If the fluid circuit is regarded as an RC circuit, the amplitude of the signal could be replaced by the flow rate of the fluids to get the following simplified equation:

$$Q(T) = (Q_{avg} - Q_L)\exp\left(-\frac{T - T_0}{\tau}\right) \qquad (4-14)$$

In equation (4-14), Q(T) is the flowrate of the system at time T; Q_{avg} is defined as the average flowrate of the working state of the stabiliser system; and Q_L refers to the low point of the flowrate when the pump is stopped, which also represents the flow rate caused by the pressure drop due to gravity (height difference between the inlet and outlet of the experimental set-up). As mentioned in the set-up, the pressure difference is set to be 0 so the Q_L only presents the noise of the background flow; T_0 is the cut-off time of the input signal. The transient behaviour of the fluidic system is characterised by a time constant τ that equals the value of the resistance times the value of capacitance, which is the response time of the fluidic system. To extract the time constant, a ramp-down response of the modular stabiliser is given as shown in Fig. 4-12. With an initial pumping pressure oscillating at 1 Hz, the average flow rate of the microfluidic channel is locked at Q_{avg}= 350 μl/min. The input signal cuts off at T_0, and finally, the flowrate of the system drops to Q_L=0. By rewriting equation (4-14), it can be obtained as:

$$ln\left(\frac{Q(T)}{Q_{avg}}\right) = -\frac{(T - T_0)}{\tau} \qquad (4-15)$$

Here is the analysis process of LSM. To observe the discharging process, the sensor starts to record the flow rate of the output signal by the time the average flowrate is steady. After receiving enough data points, the pump is

turned off to discharge the stabiliser. The Q_L and the flow rate during discharge are recorded. As shown in Fig. 4-12, the steady working state started from time 0, and the discharge process started at $T_0 = 40\ s$.

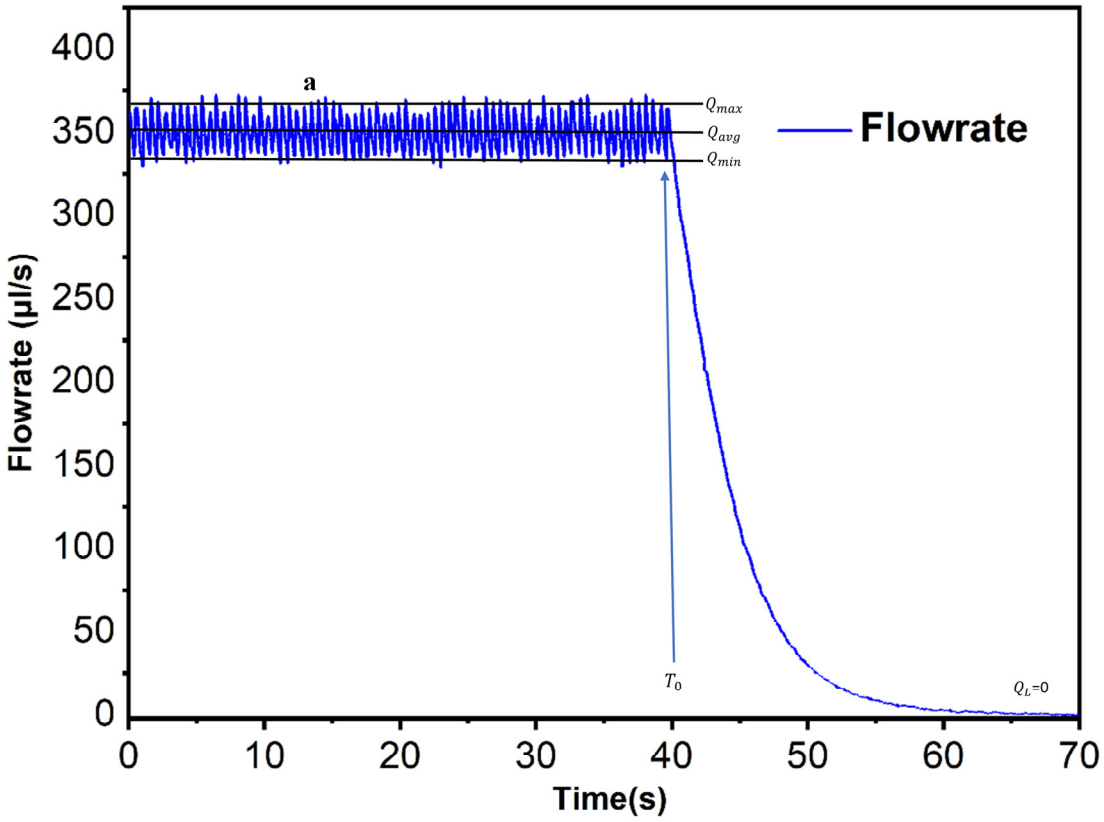

Fig. 4-12 The flow rate recorded for LSM; Q_{min}, Q_{max} , Q_{avg} , Q_L are recorded

In Fig. 4-12, the average lower flowrate of the output flow is recorded as Q_{min},; the average peak flowrate of the output flow is recorded as Q_{max},; the average flow rate of the output is recorded as Q_{avg}.

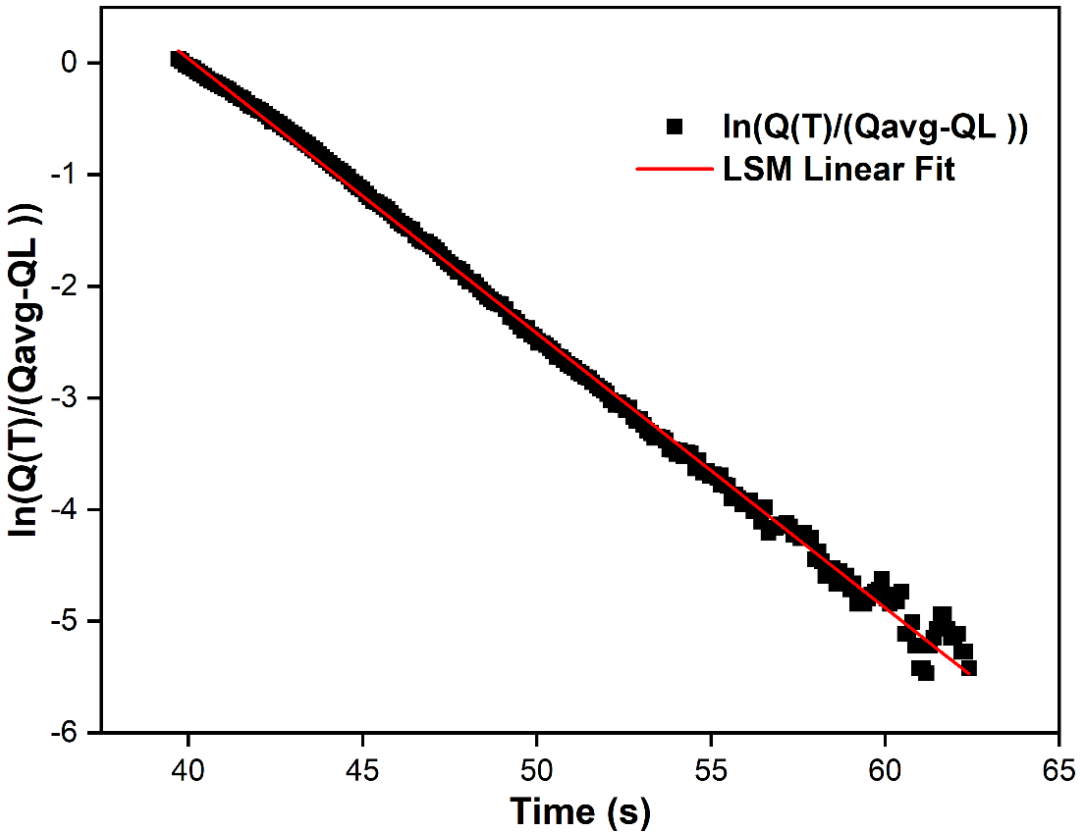

Fig. 4-13 The LSM fitting of the stabiliser system with R = 0.997.

From equation (4-15), Fig. 4-13 is drawn to extract time constant τ. The Y axis means $ln(\frac{Q(T)}{Q_{avg}})$ in equation (4-15) and the X axis means the time of the discharging process, since the discharging started at $T_0 = 40\ s$, the X axis in Fig. 4-13 started from 40 s. The red line presents the fitted line by LSM, the black dot means the experimental model value calculated from equation (4-15). In this case, the slope of the curve refers to $-\frac{1}{\tau} = -0.246$. The RC constant τ is calculated as 4.07 s; and the R-squared of the curve is 0.997, which presents a highly accurate fitting result.

To verify equation (4-14), the calculated RC constant τ=4.07 s is used to calculate the model value of the flow rate during the discharging process of

the stabiliser. The result is shown in Fig. 4-14, the discharging process starts from $T_0 = 40\ s$, with R-square equals to 0.995, the RC constant is proved to be accurate for characterise the stabiliser system.

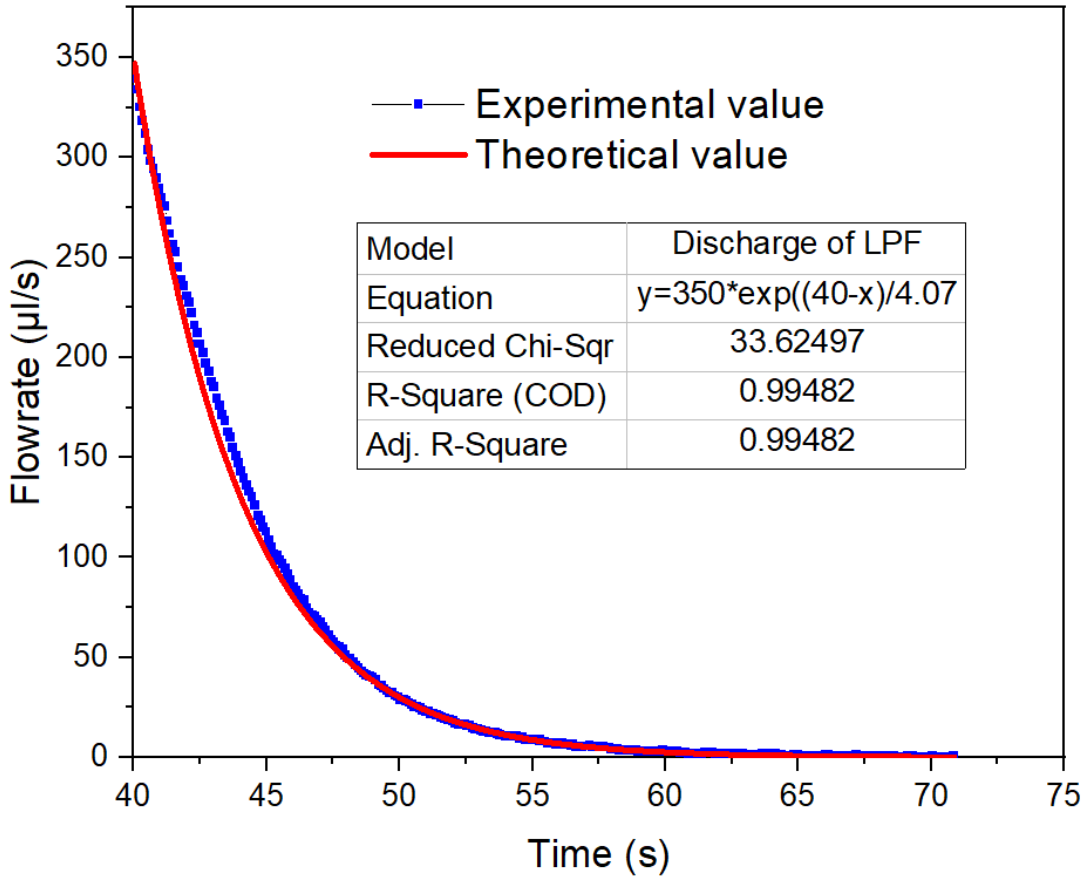

Fig. 4-14 The comparison between theoretical value and experimental value of flow rate.

4.5 Conclusions

In this section, a 3D-printed modular stabiliser system is designed, fabricated and characterised. The 3D printed system is pluggable and easy to assemble. With a fast fabrication process which is less than 5 hours, the fabricated devices only cost 1 dollar. With a flexible membrane as the damper, the stabilisation ratio of the device ranges from 29% to less than 2%, which

reaches the best stabilisation ratio in previous literature's stabilisers listed in Table 1 to the author's knowledge.

Through examining the stabilisation ratio and the vibration characteristics of a flexible membrane, this study establishes and validates a simplified electrical circuit analogy to characterise the performance of the fluidic stabiliser system. By determining the RC constant, which is instrumental in describing the system's low-pass filter behaviour, the analogy elucidates the dynamics of the stabiliser. With an RC constant of 4.07 seconds and an R-square value of 0.997, the model's accuracy is affirmed, streamlining the analysis of fluidic stabiliser systems without the need to calculate individual resistance and capacitance values. This novel approach to analysing stabiliser systems offers promising avenues for integrating the microfluidic stabiliser system with a variety of microfluidic applications, particularly where fluctuation reduction is crucial. The MSS also holds potential for the development of portable, cost-effective, and controllable flow sources tailored to diverse microfluidic scenarios requiring miniaturisation, modularisation and standardisation. However, there is scope for refining the modular stabiliser design to reduce inter-device variability. Additionally, the application of using the RC constant for predicting and controlling the stabilisation ratio more precisely in modular stabiliser systems remains an open question. These challenges and their potential solutions will be explored in depth in Chapter 5.

CHAPTER 5 LEGO-LIKE STABILISER SYSTEM FOR NOVEL FLOW CONTROL SOLUTIONS

5.1 Introduction

In this chapter, how to control the stabilisation ratio with RC constants is presented. A modular stabiliser system called the Lego-like stabiliser system is designed and analysed. The system is capable of delivering tunable stabilisation ratios with a predictable operational curve.

Constructed with standardised 3D-printed exteriors, the Lego-like microfluidic stabiliser system paves the way for a novel approach to microfluidic stabilisation. It facilitates the adjustment of stabilisation ratio and chamber numbers, thereby enabling customised and controllable fine-tuning of the fluid within microfluidic devices. The plug-and-play design of this system is highly adaptable, making it suitable for a wide array of applications where precise control over microfluidic dynamics is essential. The modularised Lego-like MSS has 3 levels of well-fitted working curves with an R-square over 0.94, which can provide a stabilised flow with less than 2% of fluctuation. Consequently, the system offers an accurately determined stabilisation ratio, enhancing the precision and reliability of the stabilisation process within microfluidic applications.

5.2 The design of the Lego-like stabiliser system

The novel modular stabiliser system has the following characteristics: first, it

has the ability to reduce the oscillation error in a rapid and low-cost way. Second, the MSS is controllable with multiple working stages in order to meet various amplitude modulation requirements. Third, the system provides well-fitted working curves with theoretical values by controlling stabilisation ratios with the RC constants. To encapsulate these features and showcase the MSS as an effective instrument for microfluidic applications, a modular design reminiscent of a Lego-like system has been conceived as shown in Fig. 5-1. This plug-and-play design philosophy not only facilitates the integration of the aforementioned characteristics but also promotes ease of assembly, disassembly, and customisation, thereby enhancing the accessibility and user-friendliness of the MSS for a wider range of users and applications within the microfluidic field.

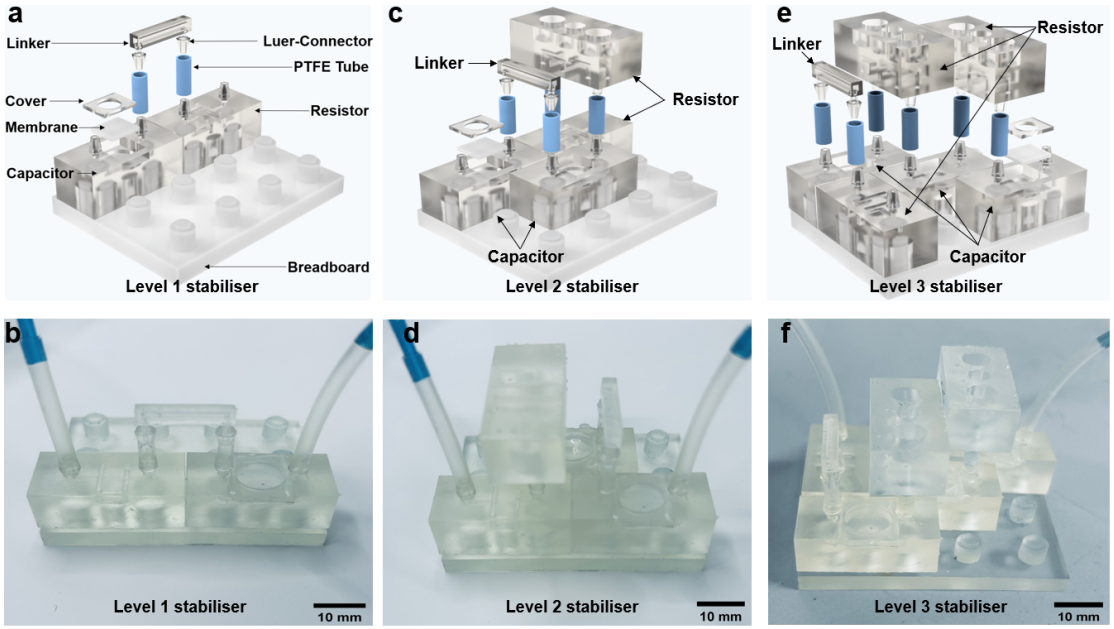

Fig. 5-1 The exploded view of the modular microfluidic stabiliser system: (a) the exploded view of level 1 Lego-like stabiliser system; (b) the assembled level 1 Lego-like stabiliser system; (c) the exploded view of level 2 Lego-like stabiliser system; (d) the assembled level 2 Lego-like stabiliser system; (e) the exploded view of level 3 Lego-like stabiliser system; (f) the assembled level 3 Lego-like stabiliser system.

The system is fabricated using 3D printing technology. Fig. 5-1(a), (c), and (e) depict the optimised design based on the modular design in Chapter 4. The modular stabiliser system comprises several components, including a Lego-like microfluidic capacitor, a Lego-like microfluidic resistor, a linker, and a breadboard. The microfluidic capacitor is a combination of three principal constituents, as depicted in Figure 5-1(a): (1) a cubic main body, measuring 15×12×12 mm in dimensions and featuring internal micro-channels with a diameter of 1 mm (Clear V4, Asiga, USA); (2) a silicone rubber membrane of 500 μm thickness and 10 mm diameter (Ecoflex00-30, Smooth-On, USA), which is designed to provide flexibility, thereby enabling the device to manifest capacitive characteristics in response to fluctuations; and (3) a 3D printed upper cover measuring 11.8×11.8 mm with a height of 1.2 mm, designed to fix the compliant Ecoflex membrane in place. The assembly of these three components was facilitated by hydrophobic photoresist (RZ304, Rui Hong Electronic Chemicals, China). Experimental evidence suggests that the devices are capable of operating at a pressure of 69 mBar or a flow rate of 1100 μl/min without leakage, thereby achieving the maximum sensitivity threshold of the sensor (Fluigent FlowEZ69mbar, France). The modular resistor provides extra fluidic resistance to reduce partial pressure on the flexible membrane. The breadboard and linker with pillars are introduced as a novel organisational framework for the modular units to provide standardised connections for different microfluidic devices such as micropumps, flow sensors or microfluidic chips. This design paradigm simplifies the creation of various combinations of fluidic capacitors and resistors, allowing for the generation of adjustable stabilisation ratios through the use of hard-linking

connectors. This modular approach is better than the direct soft tubing connector as the hard channels and luer-connectors offer superior plugging capabilities and user-friendly interconnectivity without extra capacitance provided by the soft tubes. Furthermore, the breadboard's design enables the efficient and ordered integration of different device combinations within a confined space. This not only enhances the portability of the system but also expands its operational versatility, solidifying the Lego-like system's position as a highly adaptable and user-friendly solution for microfluidic applications.

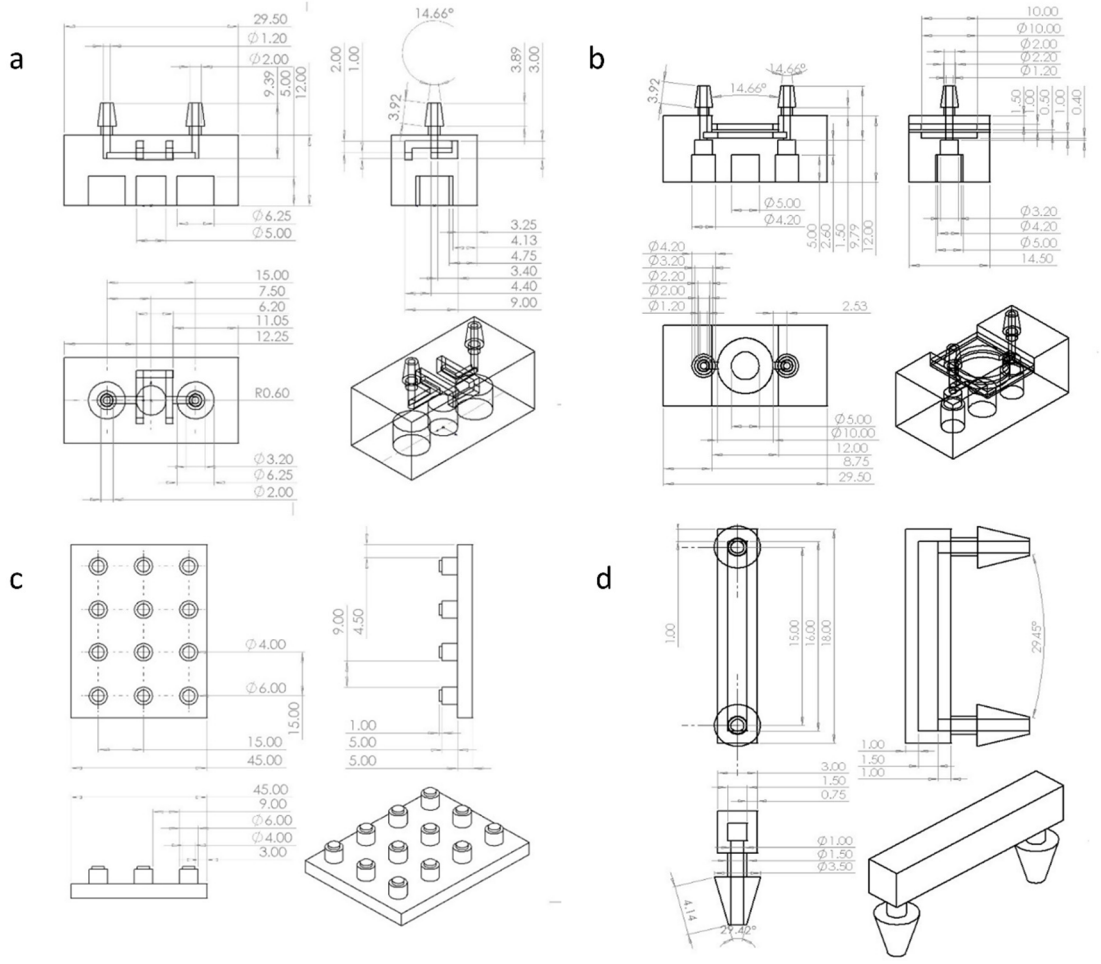

Fig. 5-2 The 2D-schematic diagrams: (a) the fluidic resistor; (b) the fluidic capacitor; (c) the breadboard; (d) the linker.

Due to the reconfigurability of the Lego-like design, multi-levels of RC

constants and stabilisation ratios could be achieved by simply connecting a certain number of capacitors and resistors on demand as shown in Fig. 5-1(b), (d), and (f). The exploded views in Fig. 5-1(a), (c), and (e) are illustrated to show the connection between each device. The 2D-schematic diagram of the MSS is given in Fig. 5-2(a) to (d). By changing the number of resistors shown in Fig. 5-2(a) and capacitors shown in Fig. 5-2(b), different working states with adjustable stabilisation ratios could be assembled on the breadboard shown in Fig. 5-2(c). To avoid the extra capacitance caused by soft tubes, a hard linking unit with standardised luer-connectors is illustrated in Fig. 5-2(d) to provide connections during the assembling of different levels of stabilisers.

5.3 Model set-up

To control the stabilisation ratio by the Lego-like system, it is necessary to know the working mechanism first. Incorporated with a flow source, the MSS is compared with the electrical filter illustrated in Fig. 5-3(a). The classic electrical filter system, depicted in Fig. 5-3(a), consists of a signal generator and a simple RC circuit. When the input signal is in the form of sine waves, the output signal is described as being in the form of sine waves with a specific smaller amplitude that is determined by the RC circuit's RC constant. In a microfluidic sense, the proposed MSS could function similarly. As shown in Fig. 5-3(b), when a given input flow enters the pluggable MSS, its amplitude property can be modulated based on the RC constant of the MSS, with a larger RC constant resulting in a smaller amplitude.

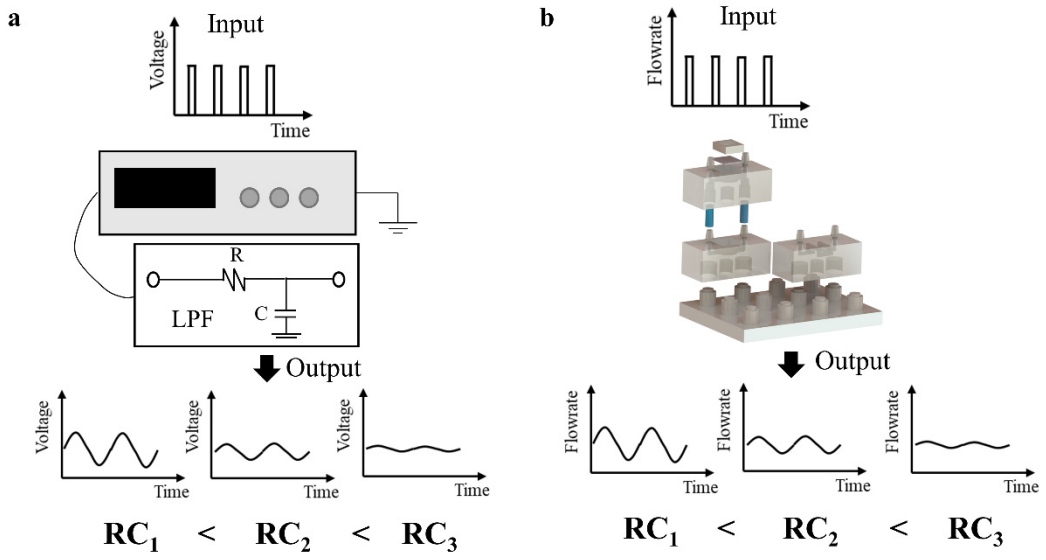

Fig. 5-3 Schematic illustrations of outputs with different RC constants for: (a) a classical electronic RC filter circuit; and (b) a modular fluidic stabiliser filter system.

In this study, features from an RC circuit were used to predict experimental outcomes, which was inspired by the results in Chapter 4. As shown in equation (5-1), it is the ideal transfer function of an RC circuit[30, 35]:

$$|H(j\omega)| = \left|\frac{1}{1 + j\omega R_f C_f}\right| \qquad (5-1)$$

where the ω means the angular frequency of input signal; R_f refers to the fluidic resistance of the low-pass-filter system; C_f is the capacitance of the fluidic capacitor, and j is an imaginary number. The value of RC constant can be regarded as response time τ.

In a real case, according to equation (4-8) and the idea of using an imaginary domain to describe the oscillation, the amplitude ratio of a membrane-based system as the common formula in s domain can be described as follows:

$$H(j\omega) = R_A = \frac{1}{A_1 s} + \frac{1}{A_2 + s} \qquad (5-2)$$

where the A_1 and A_2 are constants for the imaginary domain s. In Section 4.5.3, it is noticed from the filtered exponential decay function in equation (4-9), $\frac{1}{A_1 s}$ can be ignored, since the experimental result of $\frac{1}{A_1}$ is as small as 0.0617, which leads to an ignorable absolute value when calculating R_A.

The simplified $R_A = \frac{1}{A_2+s}$ which presents the transfer function for amplitude, is presumed to be the general form of all magnitude-related formulas in this specific membrane-based system because all the features of the flow are highly relative to the oscillation and displacement of the membrane.

To connect this broad interpretation to measurable variables such as flow rate, RC constant, and frequency, it is assumed that the amplitude between flow rate has a transfer function $H(j\omega RC)$, and can be expressed similarly as in an imaginary domain as follows:

$$H(j\omega RC) = \frac{1}{A_3+j\omega RC} \qquad (5-3)$$

where $H(j\omega RC)$ is the transfer function and A_3 is constant. To simplify the model, the constant A_3 is set to be 1, and an imaginary number s can be supposed as equalling $\omega\mathrm{RC}$ as the ideal transfer function of an RC circuit. Then this equation is achieved:

$$R_{Af} = \left|\frac{1}{(1+j\omega rc)}\right| \qquad (5-4)$$

The simplified equation just has the same absolute value and formula as the one with the ideal transfer function of an RC circuit. R_{Af} presents the ratio between the input and output of the system at frequency f.

To validate this hypothesis, the extracted RC constant and the experimental

working curve of the MSS will be compared with the simplified model in order to see the difference between the real-case response and the simplified theoretical model response in the experimental part.

5.4 Model validation and characteristics of Lego-like microfluidic stabiliser

To determine the RC constant and the stabilisation ratio of the proposed system and compare them with the simplified transfer function model, an experiment was conducted using 3 levels of MSS which consisted of three capacitors and three resistors. To get the working curve based on the RC constant and frequency of input, the experiment was designed to extract both the amplitude response and the RC constant with different levels of MSS. The experimental set-up was illustrated in Fig. 5-4. During the experiment, both the inlet flow and output flow rates were recorded by a flow sensor (Fluigent, France). All the input waves were provided by a gas pump (Fluigent, Oxgen, France). The experiments were conducted with input waves that all shared the same offset of 5 mbar and amplitude of 2 mbar, with the sole variable being the frequency of the input signal. The experiment involved applying a sine pressure wave with a fixed amplitude and a frequency ranging from 0.05 Hz to 4 Hz to different levels of stabilisers. RC constants of each level of stabiliser at various working frequencies were recorded to calculate the theoretical value of the amplitude response according to equation (5-4). This

consistent approach ensures that any observed changes in the system's response can be attributed to the change of input frequencies, thereby providing a clear and controlled assessment of the system's performance across a range of frequencies.

Fig. 5-4 The experimental set-up for extracting stabilisation ratios and RC constants of different levels of stabilisers.

For example, Fig. 5-5 illustrates how to extract the stabilisation ratio and the RC constant of Lego-like stabilisers. For each test, the data is recorded since the pump started working at t = 0 s. After the charging process, the stabiliser works at steady state as shown in the red dotted frame in Fig. 5-4. By using Origin software, the amplitude responses of different levels of stabiliser at various frequencies are fitted, recorded and calculated. In this example, the fitted amplitude response is $105.11 \pm 0.24\ \mu l$ with 0.99 R-square value. Then, the pump is turned off at 50 s in order to use the LSM mentioned in Section

4.4 to extract the RC constant during the discharging process. The discharging process is shown in the green dotted frame in Fig. 5-5. In the example, the stabiliser works at 0.2 Hz with an average flow rate of $521.35 \pm 0.17\ \mu l$, a LSM fitted slope of -0.57 ± 0.01, which leads to a $1.76 \pm 0.03\ s$ RC constat and a 0.55 ± 0.001 stabilisation ratio.

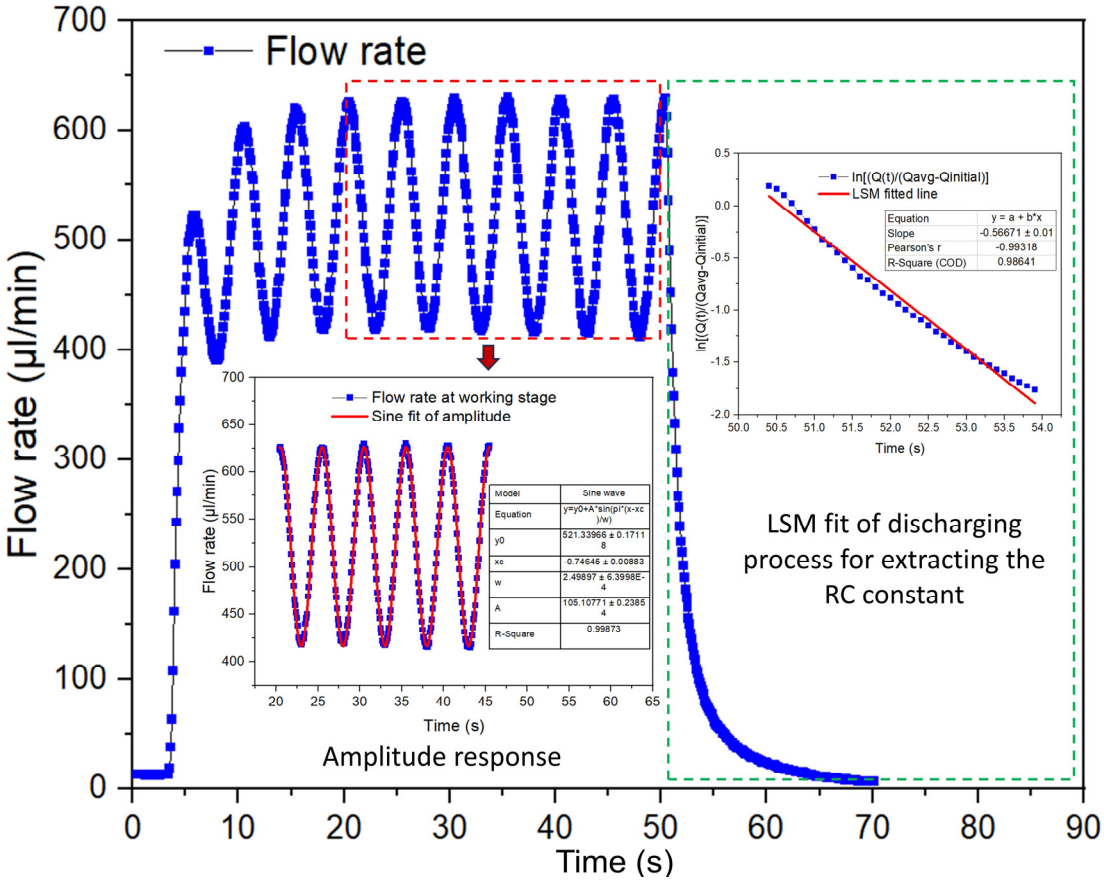

Fig. 5-5 The example of data analysing process of the level 2 Lego-like stabiliser system working at 0.2Hz.

By extracting both RC constants and stabilisation ratios of different levels of stabilisers working at different input frequencies, the working curves of different levels of stabiliser systems can be illustrated and compared with the theoretical value to show the fitting degree of the model.

In Fig. 5-6, there is an example of how to calculate the stabilisation ratio at each input frequency for different levels of stabiliser by equation (5-4). The background signal provided by the gas pump has the same average flow rate and amplitude at each input frequency as shown in Fig. 5-6(a). Fig. 5-6(b) depicts the relationship between amplitudes and corresponding frequencies in the steady stage when the pump is connected to a level 1 Lego-like stabiliser. It can be noticed that with the stabiliser, the amplitude response decreases with the increase of the input frequency, while the amplitude of the background signal stays steady with the input frequency.

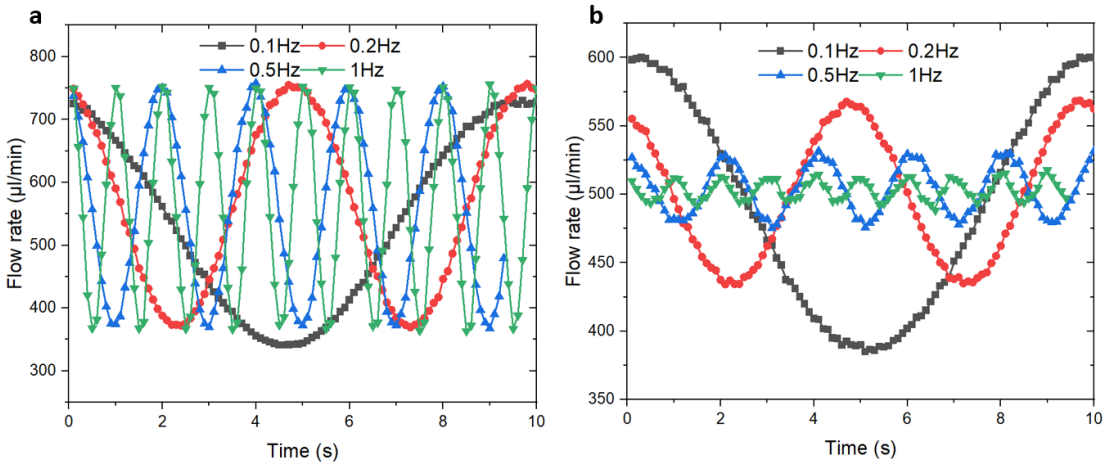

Fig. 5-6 Amplitude response: (a) the background flow recorded from the flow sensor with the frequencies of the input signal varying from 0.05 Hz to 1 Hz; (b) the steady-state flowrate of level 1 Lego-like stabiliser at various driving frequencies.

According to equations (5-1) and (5-4), the theoretically predicted working curves were calculated and compared with the experimental values. The results for each level of modular stabiliser were listed in Fig. 5-7. The overall RC constants of each level of stabiliser were calculated by the LSM fitting

during the discharging process as shown in the green dotted frame of Fig. 5-5.

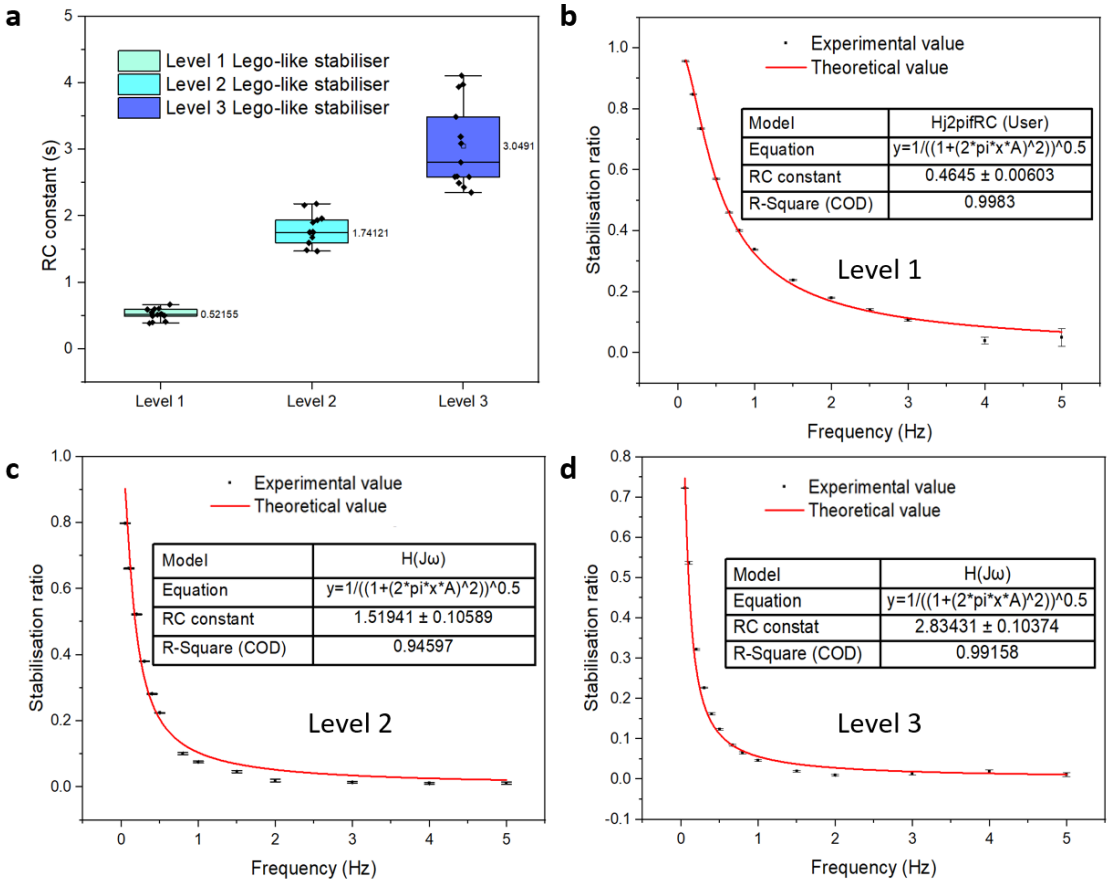

Fig. 5-7 The theoretical curves compared with the experimental curves: (a) the distribution of experimental RC constants extracted at different working frequencies for 3 levels of stabilisers; (b) the working curve of level 1 stabiliser; (c) the working curve of level 2 stabiliser; (d) the working curve of level 3 stabiliser.

The models depicted in Fig. 5-7 all exhibit R-squared values exceeding 0.94, thereby proving the precision of the hypothesis. With different levels of stabiliser combinations, the modular stabilisation system is capable of providing adjustable stabilisation ratios across a range of operating frequencies. Furthermore, the optimal stabilisation ratio achieved is 0.93 ± 0.025%, particularly when the operational frequency is higher than 2 Hz with a level 2 stabiliser. The performance provides the best stabilisation ratios in the

existing literature. In summary, the model presented provides a qualitative analysis view which is capable of preliminary controllable stabiliser devices' development and optimisation in pragmatic applications. The experimental results proved that the designed MSS significantly reduces fluctuations in a microfluidic system.

5.5 System characterisation

In this section, to show the potential for expanding more levels of stabilisation combinations on the system breadboard, 12 discrete RC constants are realised based on the experimental configuration by combining predesigned modular capacitors and resistors in a specific pattern with a piezoelectric pump to take advantage of controlling stabilisation ratios by RC constants. To further illustrate the potential for expanding the levels of stabilisation combinations, stabilisers that incorporate membranes with varying thicknesses and diameters are analysed to provide more choices of capacitance and resistance to form different RC constants and stabilisation ratios.

The established system with Lego-like modular stabilisers is assembled on the motherboard. Fig. 5-8 depicts the experimental setup for analysing the dynamic behaviour of the piezoelectric micropump system with an MSS. The system consists of a pump as the flow source (Healtell, China), an MSS, a

flow sensor (Fluigent, France), tubes, and a water container.

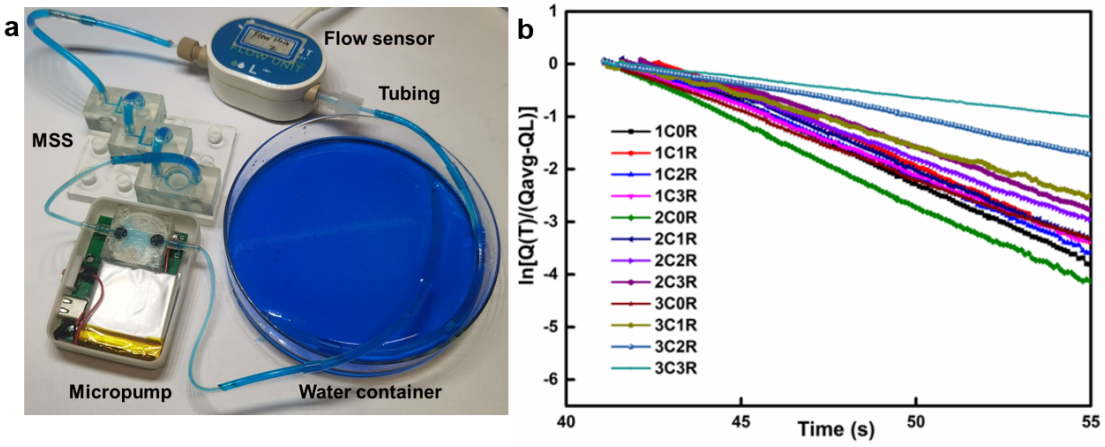

Fig. 5-8 The experimental set-up and results: (a) experimental set-up for the characterisation of RC constants of the MSS system; (b) the LSM fitting results.

The set-up was shown in Fig. 5-8(a). The working frequency of the micropump was set at 2 Hz to provide a constant flowrate of 350 μl/min for each RC combination. The extracted 12 LSM fitted line were illustrated in Fig. 5-8(b).

For each combination state, the RC constant is rigorously measured and extracted. The value of $-\frac{1}{\tau}$, which helps obtain the value of the RC constant τ is calculated. As shown in Fig. 5-8(b), each line indicates the specific RC constant of each combination, and the high linearity shows that excellent fitting quality is attained in experiments. The RC constant $\boldsymbol{\tau}$ ranges from 3.24 s to 12.57 s in the proposed system, and each state has a unique RC constant calculated from the slope of the LSM fitted curve shown in Table 6. Consequently, the modular design offers the flexibility to adjust the RC constant within this range, which facilitates the system's amplitude modulation

function.

Table 6 RC constants calculated from 12 working states by LSM fitted curves.

Working state	Slope	τ（s）
1C0R	-0.31	3.24
1C1R	-0.28	3.53
1C2R	-0.28	3.56
1C3R	-0.25	4.07
2C0R	-0.30	3.31
2C1R	-0.26	3.90
2C2R	-0.20	4.90
2C3R	-0.22	4.48
3C0R	-0.20	4.90
3C1R	-0.19	5.33
3C2R	-0.12	8.14
3C3R	-0.08	12.57

Drawing from the findings, the MSS is capable of serving as a flow modulator, featuring adjustable RC constants that are pivotal in determining the flow amplitude modulation range, as delineated by equation (5-3). This capability gives the proposed MSS with the flexibility to adapt to situations where on-demand amplitude modulation is necessary.

For example, if there is a requirement to diminish the fluctuation by 10%, the system can achieve this by adjusting the input frequency to 0.5 Hz with any levels of stabiliser, or by selecting the 3C3R state configuration and ensures that all inputs are above 0.2 Hz. This demonstrates the system's adeptness in providing precise control over amplitude modulation in response to specific

demands. All the required amplitude ratios can be mapped on the working surface of the MSS in Fig. 5-9.

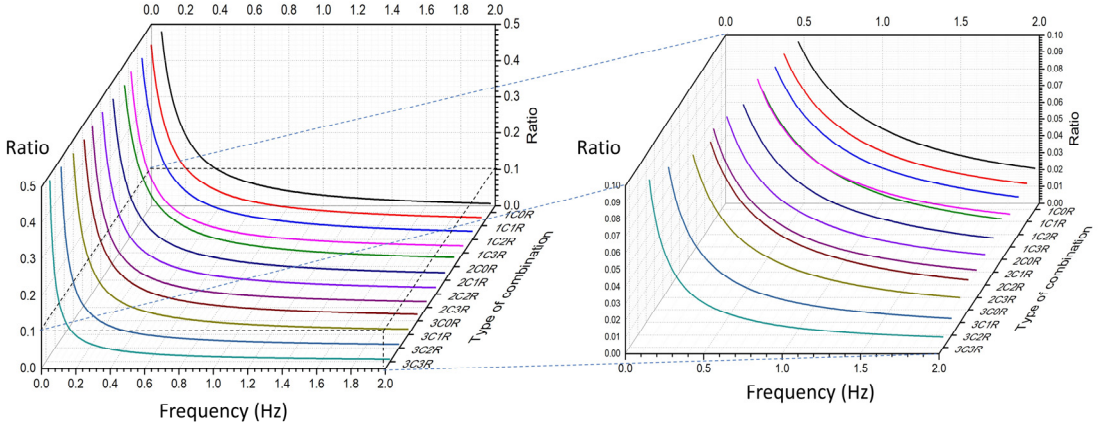

Fig. 5-9 The working curves of the Lego-like device with different stabilisation ratios.

Fig. 5-10 shows the fluctuation reduction ability of the MSS combination. With 3 levels of stabiliser linked to the piezoelectric pump, the unsteady pulse wave can be filtered into a linear output with less than 1% fluctuation.

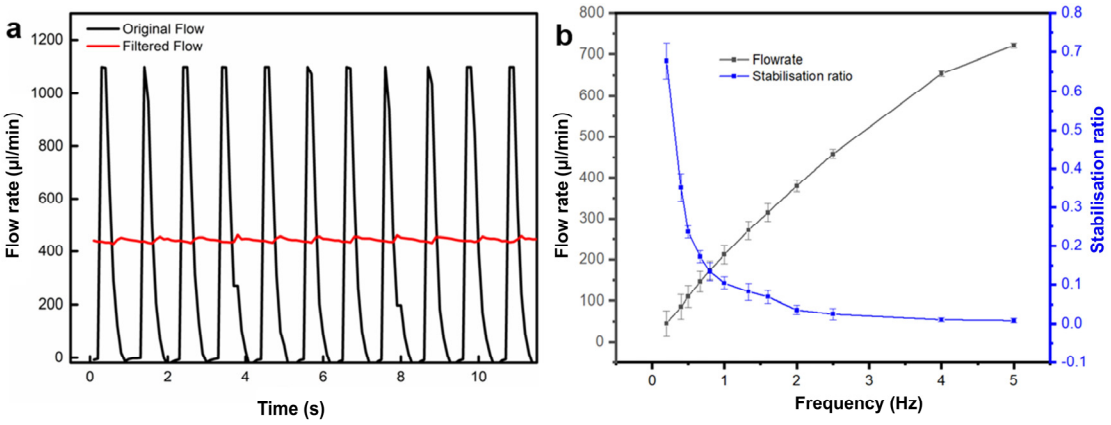

Fig. 5-10 Results of fluctuation reduction test: (a) the example of filtered flow working at 2 Hz; (b) the working curve of stabilised piezoelectric pump system at different input frequencies.

To show the potential for expanding more levels of stabilisation combinations, the hydraulic resistance and capacitance of the MSS are analysed. By adding different numbers of resistors to the pumping system, it can be known that the resistance is linear with the increasing device number. By extracting the slope, the hydraulic resistance of the resistor can be calculated as $1.86 \times 10^8 \pm$

$9.3 \times 10^6\ Pa * s * m^{-3}$ as shown in Fig. 5-11.

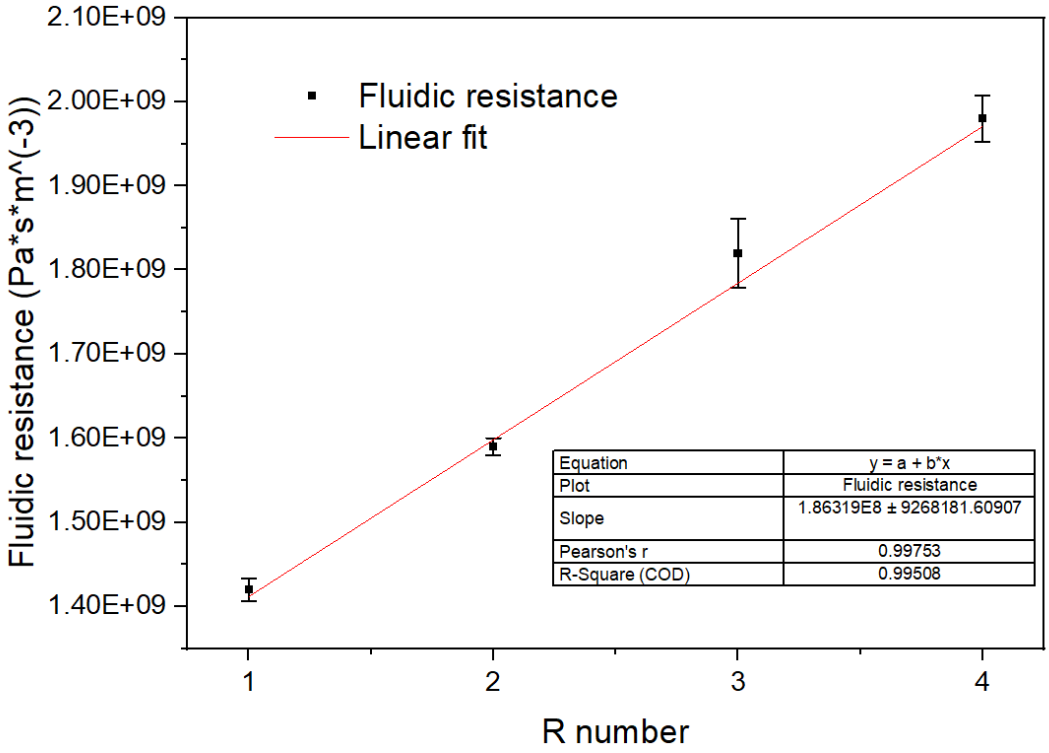

Fig. 5-11 The hydraulic resistance of the designed resistor.

To expand the levels of stabilisation combinations with controllable RC constants and stabilisation ratios, the capacitance of the modular capacitor with different geometric features is analysed. The capacitance of devices assembled with membranes of varying diameters (6 mm, 8 mm, 10 mm) and thicknesses (300 μm, 500 μm, 800 μm, 1000 μm) are listed in Fig. 5-12. The analysis employs the RC constant, derived from the experimental resistance to evaluate the system's capacitive properties and provide customised choice of RC constants.

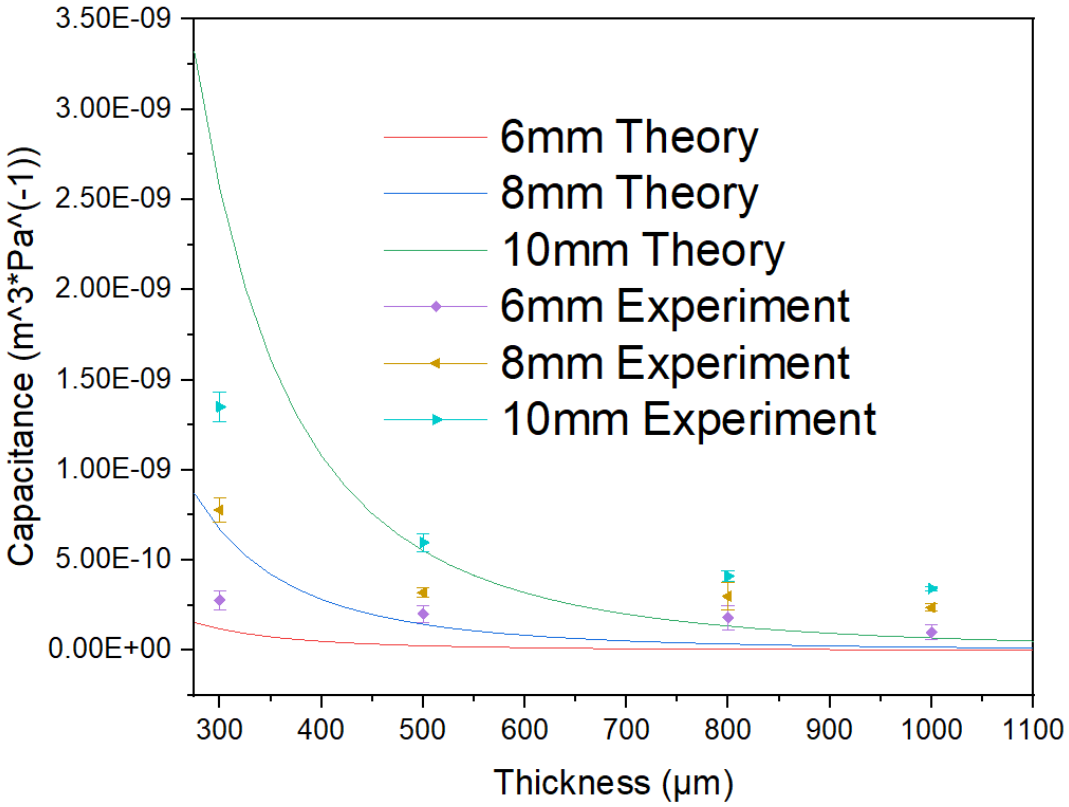

Fig. 5-12 The experimental capacitance vs theoretical value of membranes with different thickness (μm) and diameter (mm).

Illustrated in Figure 5-12, it is observable that there is a direct relationship between the diameter and the thickness of the component with its capacitance. The capacitance decreases as the diameter decreases, and the capacitance decreases as the thickness increases. This trend is an important characteristic which helps to choose the suitable design during applications. The experimental outcomes exhibit a discrepancy when compared to the theoretical values that are calculated from equations (3-4) and (3-16) in Section 3. Specifically, this deviation becomes more pronounced when the thickness of the component exceeds 500 μm. The discrepancy observed might be due to the fact that as the thickness of the film increases or the

radius decreases, the elastic properties of the film are reduced. This reduction in elasticity causes the device to behave more akin to an elastic wall rather than functioning as a fluidic damper. The change in behaviour is significant as it affects the device's ability to absorb fluctuations or oscillations effectively.

Furthermore, as the thickness of the film increases, the capacitance of the device decreases exponentially. This significant reduction in capacitance can make the impact of background noise and additional capacitance from the pump system more pronounced. The extra capacitance from the experimental set-up will lead to an error in the system's response, which influences the model's predictions and leads to a less accurate representation of the actual capacitance.

In summary, as the thickness increases when the diameter decreases, the capacitance drops sharply, which can amplify the effects of background capacitance in the system. This can result in a model that does not accurately reflect the device's performance, particularly when the thickness exceeds certain thresholds (approximately 500 μm in this experiment). Thus, it is suggested to use membranes with a diameter larger than 8 mm and a thickness between 300 to 800 μm to avoid the background noise caused by the pumping system.

5.6 Summary

In this work, a 3D-printed Lego-like pluggable MSS with 3 levels of working states for providing a range of controllable discrete stabilisation ratios and RC constants for fluidic circuits was developed. The best stabilisation ratio is 0.93%, which reaches the best stabilised flow from previous literature. A simplified model extracted from the transfer function of an RC circuit was derived to describe the performance of the system, and experiments were conducted to evaluate the accuracy of the circuit model.

In the model validation part, the calculated stabilisation ratio from extracted RC constants of the MSS fitted the experimental working curve well with an R-square value over 0.94. The comparison of the theoretical and experimental values of the stabilisation ratios at different operating frequencies indicates that the circuit model is accurate. By extracting the RC constant straightforwardly, the simplified fluidic analogy model is used to predict the stabilisation ratio of the MSS without intricate calculations of fluidic resistance and capacitance. The experimental results show that the Lego-like MSS is advantageous for rapidly modifying and controlling its stabilisation ratio over 0 to 5 Hz for its reconfigurable design.

To show the potential for expanding more levels of stabilisation combinations in the system characterisation part, the MSS provides 12 controllable RC

constants with exchangeable stabilisation ratios, which leads to an optimal result of providing a stabilised pumping system with customised working curves. By controlling the diameter and thickness of the membrane and the number of resistors, the RC constant can be controlled from 3.24 s to 12.57 s, which provides a large range of stabilisation combinations.

CHAPTER 6 APPLICATION

6.1 Introduction

After establishing the Lego-like MSS, it is essential to highlight the advantages of its reconfigurability for microfluidic applications. This section explores the MSS's flow control capabilities and applications, focussing on the stabilisation of both piezoelectric and syringe pumps. The system's ability to generate droplets using these pumps is analysed and presented. During the experiment, the polydispersity[121] of droplets produced with various configurations of the Lego-like stabiliser is recorded and discussed. The results indicate that the MSS has successfully minimised the standard deviation in the diameter of the droplets, thereby enhancing their uniformity, as evidenced by an improved polydispersity index. This demonstration underscores the MSS's potential to optimise droplet generation processes, offering a versatile solution for microfluidic applications that demand precise on-chip fluid control.

6.2 Experimental setup

In addition to the amplitude modulation capability realised by the discrete RC range based on 3 levels of the proposed MSS, the easy reconfigurability offers advantages for working with different microfluidic devices. To give an example of how to take advantage of the MSS, the ability to reduce the

fluctuation of piezoelectric pumps and syringe pumps was studied. Droplet generation experiments using a cross-junction generator to improve droplet uniformity were demonstrated.

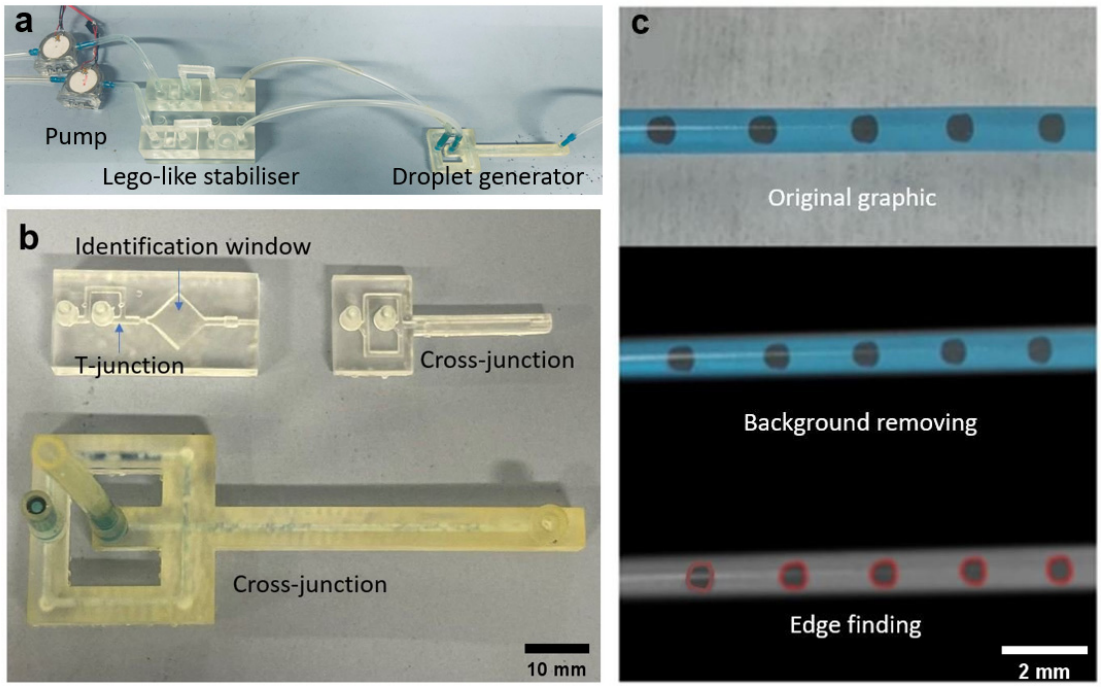

Fig. 6-1 Experiment set-up: (a) the set-up for droplet generation using microfluidic pump; (b) the illustration of droplet generators; (c) the example of counting process.

Typically, the generation of a droplet requires a steady flow input in order to maintain droplet quality stability. However, the flow generated by both piezoelectric pumps and syringe pumps has an inevitable pulsatile property due to their inherent mechanisms.

In Fig. 6-1(a), the experimental set-up for stabilising a droplet generator is illustrated. Microfluidic pumps (LongerPump, Model LSP01-1A and Healtell, China) were tested to show the stabilisation ability. The droplet can be generated by generators as shown in Fig. 6-1(b). In this case, the two cross-junction generators were linked behind the MSS to take advantage of the stabilised flow. The oil continued phase (VPO-68, 0.65cst) and ink dispersed

phase were connected to the MSS respectively to generate droplets with a flow rate ratio of 1:2. As shown in Fig. 6-1(c), the equivalent diameter of the droplets was analysed by Python and ImageJ to calculate the polydispersity and standard deviation. Besides, the distribution of the droplet generation varies with different types of MSS combinations were recorded.

6.3 Result and discussion

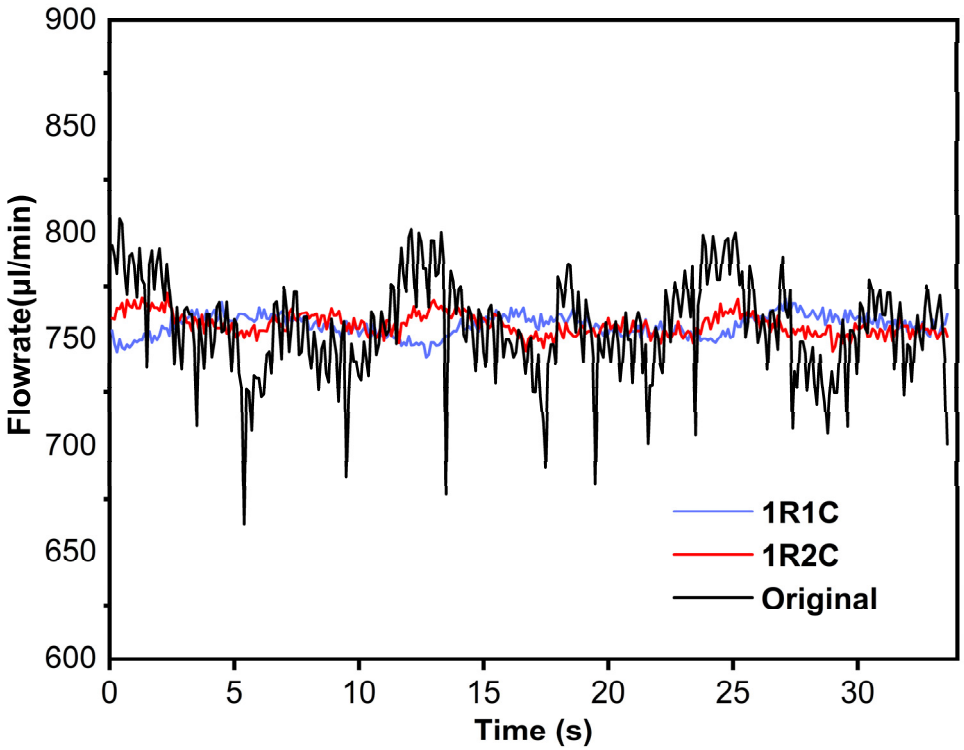

Fig. 6-2 Illustration of flowrate vs time for original state, 1R1C state and 1R2C state respectively.

Fig. 6-2 presents a comparison of the flow rates in three different operational states. The 'original' in the figure denotes the baseline output of the syringe pump (LongerPump, Model LSP01-1A) when not equipped with a MSS. The terms '1R1C' and '1R2C' refer to the configurations of the MSS, indicating one resistor with one capacitor stage and one resistor with two capacitor stages,

respectively. The syringe pump was used to inject a volume of 5 ml at an average flow rate of 750 μl/min. A flow sensor connected to the MSS measures the flow rate at the outlet.

To evaluate the effectiveness of the MSS, the pump's performance was tested under both the 1R1C and 1R2C stages. The original flow rate exhibits fluctuations within a range of 150 μl/min. Upon integration with the MSS, these fluctuations were significantly reduced to less than 20 μl/min, demonstrating the system's ability to stabilise the flow rate.

To show how to benefit from the fluctuation reduction ability of the MSS and to compare the diameter distribution between different states of the MSS, a typical droplet generation experiment was done by the pump (LongerPump, Model LSP01-1A) with the cross-junction generator. During the test, the ink-dispersed phase and the oil-continued phase were driven at a flowrate ratio of 2:1. In Fig. 6-3(a), the illustration of the cross-junction droplet generator is shown. In Fig. 6-3(b), the process of the droplet generation is exhibited. The inner square channel of the generator has a $1 \times 1\ mm$ cross-section area. Besides, a tiny neck with a cross-sectional area of $0.5 \times 0.5\ mm$ is formed at the end of $1 \times 1\ mm$ channel to facilitate droplet generation.

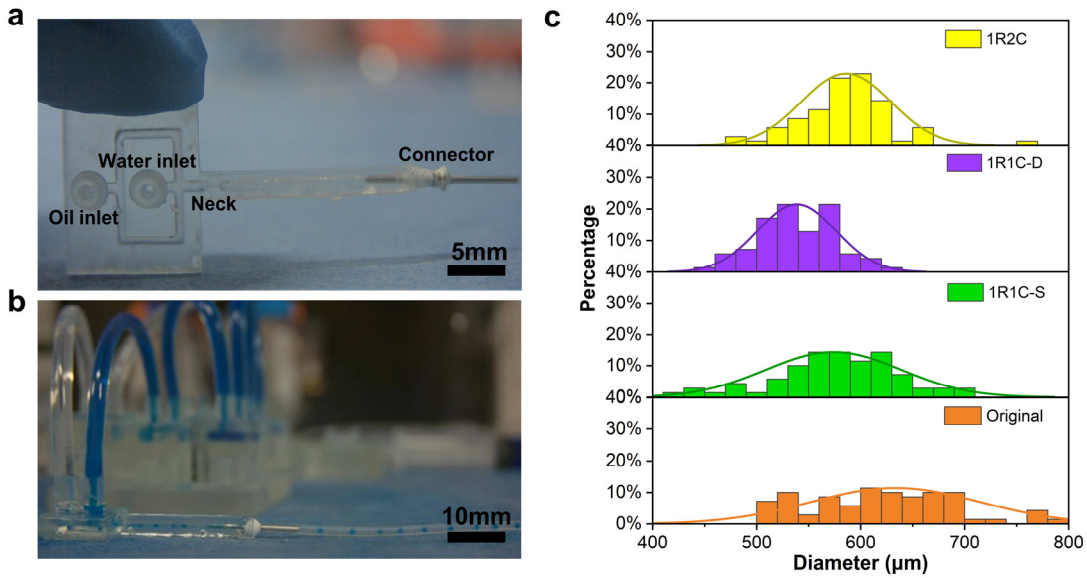

Fig. 6-3 Droplet generation via Cross-junction: (a) photograph of the droplet generator used in the experiment; (b) the working state of the cross-flow generation device for testing stability of the adjusted output of syringe pump; (c) histograms of droplet distribution at different states.

Figure 6-3(c) illustrates the distribution of droplets across four distinct working states. The 1R1C-S state refers to a single flow scenario where the ink-dispersed phase is connected to a 1R1C MSS, while the oil-continuous phase remains in its original state. In contrast, the 1R1C-D state involves both flows being connected to the 1R1C MSS. The 1R2C-S state denotes a configuration where only the ink-dispersed phase is connected to a 1R2C MSS, with the oil-continuous phase still connected to the 1R1C MSS. The process of droplet generation is achieved by mixing an ink-dispersed phase with an oil-continuous phase within the generator. Once formed, these droplets are quantified by using the counting method previously described in Fig. 6-1(c). The quality of droplet distribution is evaluated using the droplet polydispersity, which is defined as $\text{polydispersity} = \frac{Standard\ deviation}{Mean\ droplet\ size}$, with the relevant data presented in Table 7. As shown in Table 7, the original state

exhibits the highest polydispersity index of 0.13. There is a significant improvement in polydispersity as the states progress from 1R1C-S to 1R2C-S, with the best polydispersity index achieved in the experiment being 0.07. This improvement is attributed to the 1R2C configuration reaching the limit of stable flow in the experimental setup. Furthermore, the oil-continuous phase could not function under states with more than three capacitors due to the increased pressure on the membrane. As a result, only three combination states of the MSS were tested in the experiment.

Table 7 Polydispersity and standard deviation of the generated droplets under different cases

Configuration	Standard deviation(μm)	Polydispersity
Original state	81.8	0.13
1R1C-S	62.9	0.11
1R1C-D	44.5	0.08
1R2C-S	48.2	0.07

As a comparison, effective and predictable control of droplet size is nearly impossible when using piezoelectric pumps because the pulse wave provided by piezoelectric pumps has huge fluctuations (see Fig. 5-10 for example), while droplet generation requires a steady and accurate input flow. By linking the MSS with piezoelectric pumps to stabilise the fluid, droplet generation with controllable distribution becomes possible for pulse wave inputs.

Fig. 6-4(a) illustrates the process of droplet generation when using piezoelectric pumps (Healtell, China) with the MSS, which is achieved by mixing an ink-dispersed phase with an oil-continuous phase within the generator.

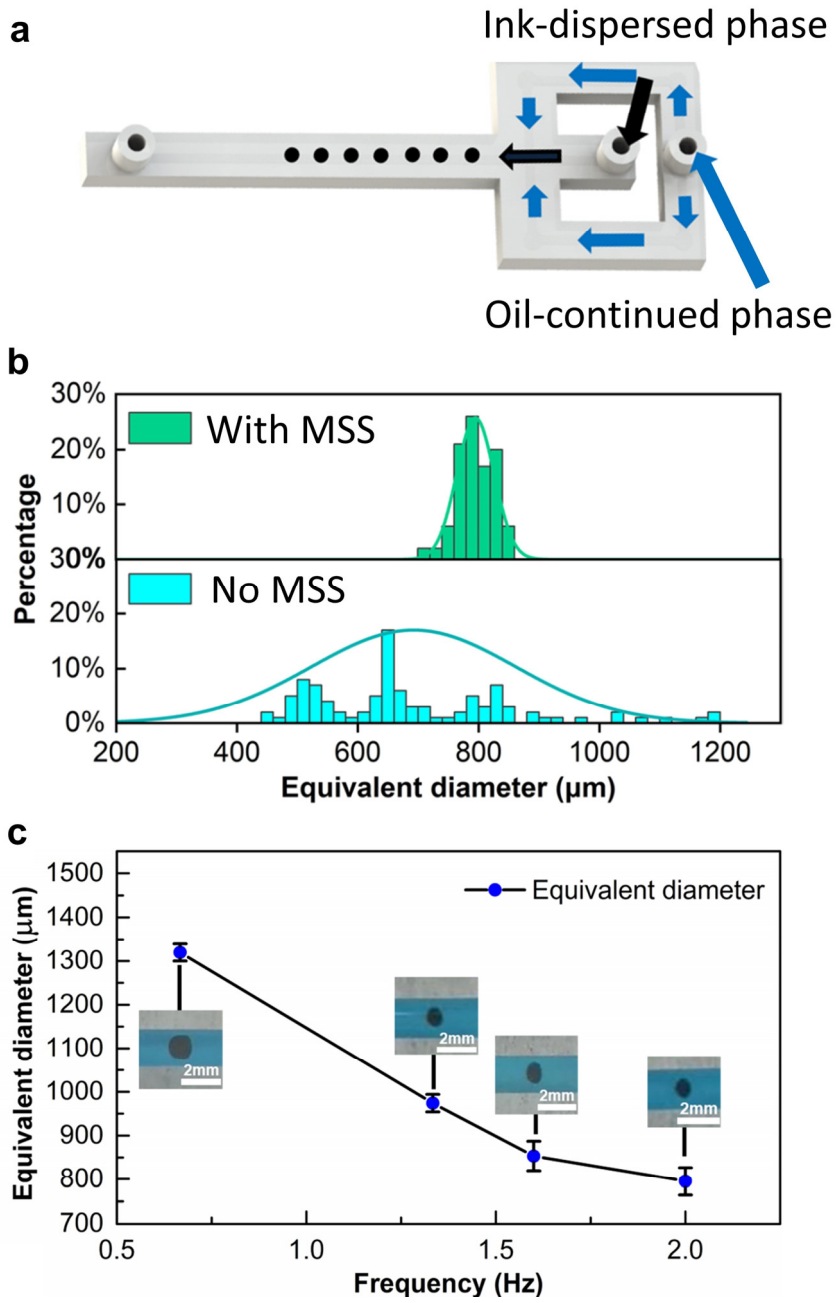

Fig. 6-4 The droplet generation of syringe pump with MSS: (a) The illustration of droplet generation process; (b) the example of droplet generation with and without the MSS when working at 2 Hz; (c) the results of the cross-junction generator at different working frequencies.

Fig. 6-4(b) is the result of droplet generation with and without the MSS. It is obvious that with the MSS linked to the system, the droplet size is more centralised. Fig. 6-4(c) is the results of droplet generation. As the operating frequency of the micropump increases, the system successfully generates

four distinct types of droplets, with average diameters ranging from 800 μm to 1400 μm. The results demonstrated the system's capability to control droplet size, showcasing the effectiveness of the proposed system when integrated with piezoelectric pumps. As shown in Table 8, both the droplet size and polydispersity can be controlled.

Table 8 Polydispersity and standard deviation of droplets generated by piezoelectric pumps.

Mean droplet size(μm)	Standard deviation(μm)	Polydispersity
795.35	31.01	0.039
853.15	33.85	0.040
973.99	20.08	0.021
1319.56	19.61	0.015

6.4 Summary

In this chapter, the MSS was used to provide a stabilisation solution for a typical syringe pump and successfully reduced the oscillation. Then the system was applied for droplet generation by the fluidic cross-junction droplet generators. The polydispersity of the diameter of the droplets was reduced from 0.13 to 0.07 for the syringe pump. Furthermore, the system enables the piezoelectric pump, traditionally limited in producing irregular droplets, to effectively generate uniform droplets with a polydispersity of less than 0.04. This enhancement broadens the capabilities of micropumps, making it suitable for a wider range of microfluidic applications. The result of the droplet

diameter statistics revealed that selecting an appropriate working state for the MSS can improve the uniformity of the droplet distribution. The experimental results demonstrate that the microfluidic stabiliser system markedly diminishes flow fluctuations and improves the uniformity of droplets. By offering a tunable stabilisation ratio, this system paves a novel path for flow control solutions inside microfluidic chips. Its modular, plug-and-play design facilitates its versatile application, enabling precise control over driving fluid within microfluidic devices. Thus, the Lego-like pluggable MSS could be further integrated into various microfluidic platforms to fully exploit the tunable RC constants of the MSS, where facile and flexible modulations of flowrates and pressure amplitudes are needed.

CHAPTER 7 CONCLUSIONS AND FUTURE WORK

7.1 Contributions and conclusions

The overall aim of this study was to study stabiliser systems in a systematic way and provide a novel flow-control solution by establishing a new microfluidic stabiliser system with a simplified prediction model. The following are the contributions and the conclusions:

1. To the author's knowledge, this thesis introduces a Lego-like modular stabiliser system for the first time. The research presents a unified solution for flow control scenarios within microfluidic systems. A 3D-printed Lego-like modular stabilisation system has been designed and manufactured, offering adjustable and predictable working curves in a rapid and cost-effective manner. In contrast to conventional stabilisers that are tailored for specific applications with a fixed working curve, the Lego-like system facilitates controllable stabilisation ratios with a standardised linker and can be connected to customised systems. The MSS enables the amplitude to be fine-tuned to within 1%, which reaches the best stabilisation ratio in previous literature, making it suitable for a range of applications including gas pumps, piezoelectric pumps, and syringe pumps. The system achieves this versatility by offering a multitude of working curve combinations, thereby enhancing

the universality and compatibility of microfluidic systems that must operate under diverse flow control conditions.

2. This study investigates the deflection and geometric characteristics of the membrane in a modular stabiliser, providing insights into the design of a standard Lego-like stabiliser unit for the modular stabilisation system with a specific RC constant. By studying the membrane deflection and drawing a simplified analogy with digital circuits, a common formula for the transfer function between the amplitude response and the input signal is extracted. By using RC constat to predict the stabilisation ratio, the MSS can provide controllable stabilisation ratios without calculating the resistance or capacitance of each microfluidic device. This results in a relatively accurate prediction of the working curve for the novel Lego-like MSS, with a R-square coefficient of 0.95. The predictive model developed by the system offers three levels of working curves, and the stabilisation ratios can be adjusted by employing different combinations of Lego-like devices. Consequently, the Lego-like stabiliser system is capable of providing a range of combinations to achieve a customised stabilisation ratio.

3. In practical applications, it has been demonstrated that the Lego-like microfluidic stabiliser system can enhance the performance of a variety of flow suppliers, including gas pumps, piezoelectric pumps, and

syringe pumps. Specifically, when integrated with pumps in a typical cross-junction droplet generator with a neck, the system exhibited improved performance. The pump's fluctuation was reduced to less than 13%, and the polydispersity index of the droplets was decreased from 0.13 to 0.07. These findings underscore the potential of the Lego-like system for further integration into a range of microfluidic platforms. Its versatility makes it a promising candidate for applications such as drug delivery processes and biological cell culture microfluidic platforms.

7.2 Future work

After establishing such a controllable, pluggable, and standardised modular microfluidic stabiliser, the Lego-like pluggable MSS could be further integrated into various microfluidic platforms, such as a biological cell culture microfluidic platform, to fully exploit the tunable RC constants of the MSS where facile and flexible modulations of flow rates and pressure amplitudes are needed.

For example, the MSS could be integrated within a flow generator, a concentration generator[106] for an accurately controlled mixing of solutions, or for high throughput drug preparation and delivery systems[122]. Those applications are usually designed with multiple microchannels, fluidic resistors, and functional units, and require a steady flow to achieve the designed

performance. For example, in Fig. 7.1(a) and (b), which is an ideal simulation process for a concentration generator designed for mixing nanofluids, the inlets of the two solutions were set to be the same in simulation. But in the real case illustrated in Fig. 7.1(c), obviously the inlet performance is vibrating, which is influenced by the unsteady syringe pump. Thus, further studies about the integration of the MSS with microfluidic platforms would be valuable. Another potential field is the standardisation of other functional microfluidic devices, such as the Lego-like units, which could be used to form a modular microfluidic platform, as shown in Fig. 7.1(d).

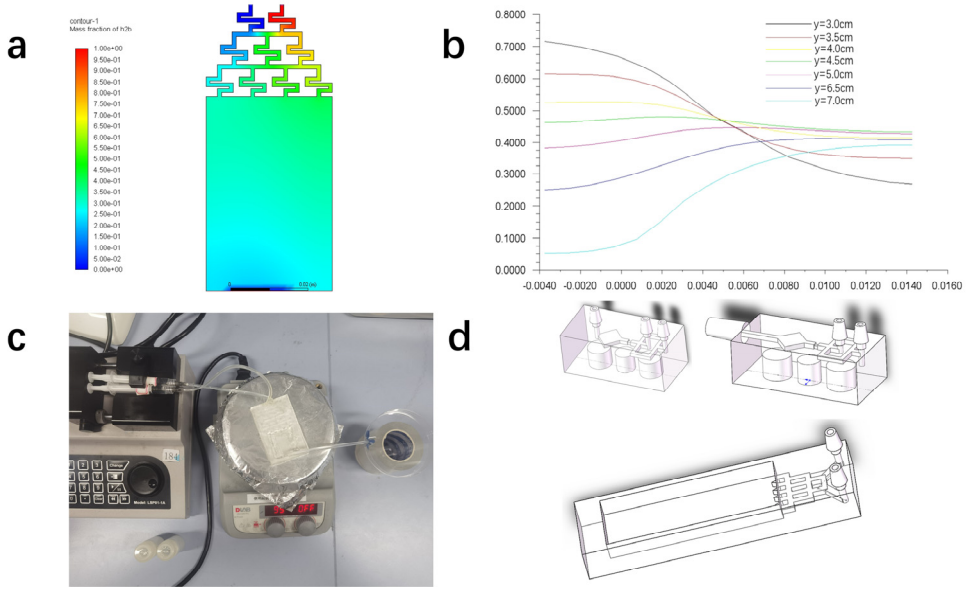

Fig. 7-1 Examples of future work: (a) the concentration gradient of a simulated concentration generator; (b) the ratio curve of two solutions inside the mixer at different positions; (c) the concentration generator working with a syringe pump; (d) standardised Lego-like microfluidic platforms.

In addition to focussing on the performance of the stabiliser, its extreme environmental behaviours, such as the study of amplitude response and

membrane deflection at very high frequency, high pressure, and high temperature conditions, can be investigated in the future. Additionally, the properties of stabilisers made from multi-layer membranes or anisotropy materials can be investigated.

Furthermore, because the RC constant of a stabiliser varies with the thickness and diameter of the membrane, the next generation of Lego-like stabilisers could be modular stabilisers with controllable membranes. If the RC constant of a specific stabiliser can be numerically controlled without connecting other devices, the mobility of the stabiliser will be greatly improved and can be integrated within tiny devices such as wearable blood pressure detectors or wearable insulin infusion pumps.

REFERENCE

1. Weisgrab G, Ovsianikov A, Costa PF. Functional 3D printing for microfluidic chips. Advanced Materials Technologies. 2019;4(10):1900275.
2. Yang B, Metier JL, Lin Q. Using compliant membranes for dynamic flow stabilization in microfluidic systems. In18th IEEE International Conference on Micro Electro Mechanical Systems, 2005. MEMS 2005. 2005 Jan 30 (pp. 706-709). IEEE.
3. Nge PN, Rogers CI, Woolley AT. Advances in microfluidic materials, functions, integration, and applications. Chemical reviews. 2013;113(4):2550-83.
4. Rhee M, Light YK, Yilmaz S, Adams PD, Saxena D, Meagher RJ, et al. Pressure stabilizer for reproducible picoinjection in droplet microfluidic systems. LAB ON A CHIP. 2014;14(23):4533-9.
5. Yang B, Lin Q. A Compliance-Based Microflow Stabilizer. JOURNAL OF MICROELECTROMECHANICAL SYSTEMS. 2009;18(3):539-46.
6. Xiang N, Ni Z. Hand-Powered Inertial Microfluidic Syringe-Tip Centrifuge. Biosensors. 2021 Dec 29;12(1):14.
7. Xia HM, Wu JW, Zheng JJ, Zhang J, Wang ZP. Nonlinear microfluidics: device physics, functions, and applications. LAB ON A CHIP. 2021;21(7):1241-68.
8. Sen AK, Bhardwaj P. Microfluidic System for Rapid Enumeration and Detection of Microparticles. JOURNAL OF FLUIDS ENGINEERING-TRANSACTIONS OF THE ASME. 2012;134(11):111401.
9. Chong ZZ, Tan SH, Gañán-Calvo AM, Tor SB, Loh NH, Nguyen N-T. Active droplet generation in microfluidics. Lab on a Chip. 2016;16(1):35-58.
10. Lin L, Wu X, He W, Chen L. Methods and Experimental Research of Eliminating the Pulse of Piezoelectric Micro-fluidic System. In2018 IEEE 18th International Conference on Nanotechnology (IEEE-NANO) 2018 Jul 23 (pp. 1-4).
11. Lee C-Y, Chang C-L, Wang Y-N, Fu L-M. Microfluidic mixing: a review. International journal of molecular sciences. 2011;12(5):3263-87.
12. Sochol RD, Sweet E, Glick CC, Wu S-Y, Yang C, Restaino M, et al. 3D printed microfluidics and microelectronics. Microelectronic Engineering. 2018;189:52-68.
13. Comina G, Suska A, Filippini D. PDMS lab-on-a-chip fabrication using 3D printed templates. Lab Chip. 2014;14(2):424-30.
14. Choudhury S, Dutta S, Chatterjee S. Cost-effective template development for the microfluidic device. Micro & Nano Letters. 2019;14(8):860-4.
15. Monaghan T, Harding MJ, Harris RA, Friel RJ, Christie SDR. Customisable 3D printed microfluidics for integrated analysis and optimisation. Lab on a Chip. 2016;16(17):3362-73.
16. Xie X, Maharjan S, Liu S, Zhang YS, Livermore C. A modular, reconfigurable microfabricated assembly platform for microfluidic transport and multitype cell culture and drug testing. Micromachines. 2019 Dec 18;11(1):2.

17. Au AK, Lee W, Folch A. Mail-order microfluidics: evaluation of stereolithography for the production of microfluidic devices. Lab Chip. 2014;14(7):1294-301.
18. Ho CMB, Ng SH, Li KHH, Yoon YJ. 3D printed microfluidics for biological applications. Lab on a Chip. 2015;15(18):3627-37.
19. Nie J, Fu J, He Y. Hydrogels: the next generation body materials for microfluidic chips? Small. 2020;16(46):2003797.
20. Waheed S, Cabot JM, Macdonald NP, Lewis T, Guijt RM, Paull B, et al. 3D printed microfluidic devices: enablers and barriers. Lab on a Chip. 2016;16(11):1993-2013.
21. Kitson PJ, Rosnes MH, Sans V, Dragone V, Cronin L. Configurable 3D-Printed millifluidic and microfluidic 'lab on a chip'reactionware devices. Lab on a Chip. 2012;12(18):3267-71.
22. Nielsen AV, Beauchamp MJ, Nordin GP, Woolley AT. 3D printed microfluidics. Annual Review of Analytical Chemistry. 2020 Jun 12;13(1):45-65.
23. Bhargava KC, Thompson B, Malmstadt N. Discrete elements for 3D microfluidics. Proceedings of the National Academy of Sciences. 2014;111(42):15013-8.
24. Adamski K, Kubicki W, Walczak R. Inkjet 3D printed microfluidic devices. In2016 MIXDES-23rd International Conference Mixed Design of Integrated Circuits and Systems 2016 Jun 23 (pp. 504-506). IEEE.
25. Jeong OC, Konishi S. The self-generated peristaltic motion of cascaded pneumatic actuators for micro pumps. Journal of Micromechanics and Microengineering. 2008 Jul 18;18(8):085017.
26. Wu C-H, Chen C-W, Kuo L-S, Chen P-H. A Novel Approach to Measure the Hydraulic Capacitance of a Microfluidic Membrane Pump. Advances in Materials Science and Engineering. 2014;2014:1-8.
27. Oh KW, Lee K, Ahn B, Furlani EP. Design of pressure-driven microfluidic networks using electric circuit analogy. Lab on a Chip. 2012;12(3):515-45.
28. Mosadegh B, Kuo C-H, Tung Y-C, Torisawa Y-s, Bersano-Begey T, Tavana H, et al. Integrated elastomeric components for autonomous regulation of sequential and oscillatory flow switching in microfluidic devices. Nature physics. 2010;6(6):433-7.
29. Abgrall P, Gue AM. Lab-on-chip technologies: making a microfluidic network and coupling it into a complete microsystem—a review. Journal of micromechanics and microengineering. 2007 Apr 24;17(5):R15.
30. Kim D, Chesler NC, Beebe DJ. A method for dynamic system characterization using hydraulic series resistance. Lab Chip. 2006;6(5):639-44.
31. Wang YN, Fu LM. Micropumps and biomedical applications–A review. Microelectronic Engineering. 2018 Aug 5;195:121-38.
32. Raj A, Suthanthiraraj PP, Sen AK. Pressure-driven flow through PDMS-based flexible microchannels and their applications in microfluidics. Microfluidics and Nanofluidics. 2018 Nov;22(11):128.
33. Phillips RH, Jain R, Browning Y, Shah R, Kauffman P, Dinh D, et al. Flow control using audio tones in resonant microfluidic networks: towards cell-phone controlled lab-on-a-chip devices. LAB ON A CHIP. 2016;16(17):3260-7.
34. Kang YJ, Yang S. Fluidic low pass filter for hydrodynamic flow stabilization in microfluidic

environments. Lab Chip. 2012;12(10):1881-9.
35. Leslie DC, Easley CJ, Seker E, Karlinsey JM, Utz M, Begley MR, et al. Frequency-specific flow control in microfluidic circuits with passive elastomeric features. Nature Physics. 2009;5(3):231.
36. Zeng W, Fu H. Precise measurement and control of the pressure-driven flows for microfluidic systems. Electrophoresis. 2020;41(10-11):852-9.
37. Lim YC, Kouzani AZ, Duan W. Lab-on-a-chip: a component view. Microsystem Technologies. 2010 Dec;16:1995-2015.
38. Naderi A, Bhattacharjee N, Folch A. Digital manufacturing for microfluidics. Annual review of biomedical engineering. 2019;21:325.
39. Samiei E, Tabrizian M, Hoorfar M. A review of digital microfluidics as portable platforms for lab-on a-chip applications. Lab on a Chip. 2016;16(13):2376-96.
40. Martinez-Garcia S, Juan Dede-Garcia E, Carlos Campo-Rodriguez J, Joseph Bradley P, Rueda-Boldo P, Monteso-Fernandez S, et al. Present and future of the power electronics (I). Introduction and high-power applications. DYNA. 2010;85(4):315-30.
41. Niculescu A-G, Chircov C, Bîrcă AC, Grumezescu AM. Fabrication and applications of microfluidic devices: A review. International Journal of Molecular Sciences. 2021;22(4):2011.
42. Yeo LY, Chang HC, Chan PP, Friend JR. Microfluidic devices for bioapplications. small. 2011;7(1):12-48.
43. Sanjay ST, Zhou W, Dou M, Tavakoli H, Ma L, Xu F, et al. Recent advances of controlled drug delivery using microfluidic platforms. Advanced drug delivery reviews. 2018;128:3-28.
44. Chen B, Li G, Wang W, Wang P. 3D numerical simulation of droplet passive breakup in a micro-channel T-junction using the Volume-Of-Fluid method. Applied Thermal Engineering. 2015;88:94-101.
45. Chen X, Glawdel T, Cui N, Ren CL. Model of droplet generation in flow focusing generators operating in the squeezing regime. Microfluidics and Nanofluidics. 2015;18(5-6):1341-53.
46. Lee C, Kim M, Kim YJ, Hong N, Ryu S, Kim HJ, et al. Soft robot review. International Journal of Control, Automation and Systems. 2017;15(1):3-15.
47. Cianchetti M, Laschi C, Menciassi A, Dario P. Biomedical applications of soft robotics. Nature Reviews Materials. 2018;3(6):143-53.
48. Hubbard JD, Acevedo R, Edwards KM, Alsharhan AT, Wen Z, Landry J, et al. Fully 3D-printed soft robots with integrated fluidic circuitry. Science Advances. 2021;7(29):eabe5257.
49. Kim SJ, Lai D, Park JY, Yokokawa R, Takayama S. Microfluidic Automation Using Elastomeric Valves and Droplets: Reducing Reliance on External Controllers. SMALL. 2012;8(19):2925-34.
50. Jiao, Z., Zhao, J., Chao, Z., You, Z., & Zhao, J. (2019). An air-chamber-based microfluidic stabilizer for attenuating syringe-pump-induced fluctuations. *Microfluidics and Nanofluidics*, *23*, 1-10.

51. Araci IE, Agaoglu S, Lee JY, Yepes LR, Diep P, Martini M, et al. Flow stabilization in wearable microfluidic sensors enables noise suppression. Lab on a Chip. 2019;19(22):3899-908.
52. Kalantarifard A, Alizadeh Haghighi E, Elbuken C. Damping hydrodynamic fluctuations in microfluidic systems. Chemical Engineering Science. 2018;178:238-47.
53. Zhu HL, Fohlerova Z, Pekarek J, Basova E, Neuzil P. Recent advances in lab-on-a-chip technologies for viral diagnosis. Biosensors & Bioelectronics. 2020;153.
54. Ren K, Zhou J, Wu H. Materials for microfluidic chip fabrication. Accounts of chemical research. 2013;46(11):2396-406.
55. Boonyaphon K, Takayama S, Kim S-J. Microfluidic random number generator driven by water-head pressure and human finger push. Sensors and Actuators A: Physical. 2020;302:111802.
56. Zhang B, Korolj A, Lai BFL, Radisic M. Advances in organ-on-a-chip engineering. Nature Reviews Materials. 2018;3(8):257-78.
57. Jen CP, Lin YC, Wu WD, Wu CY, Wu GG, Chang CC. Improved design and experimental demonstration of a bi-directional microfluidic driving system. Sensors and Actuators B-Chemical. 2003;96(3):701-8.
58. Paschew G, Schreiter JR, Voigt A, Pini C, Chávez JP, Allerdi?En M, et al. Autonomous Chemical Oscillator Circuit Based on Bidirectional Chemical-Microfluidic Coupling. Advanced Materials Technologies. 2016;1(1).
59. Kim S-J, Yokokawa R, Takayama S. Microfluidic oscillators with widely tunable periods. Lab on a Chip. 2013;13(8):1644-8.
60. Wu C, Chen R, Liu Y, Yu Z, Jiang Y, Cheng X. A planar dielectrophoresis-based chip for high-throughput cell pairing. Lab Chip. 2017;17(23):4008-14.
61. Tzekaki E, Tsolaki M, Pantazaki A. Technical characteristics of Alzheimer model based on organ technology (organoid). Hellenic Journal of Nuclear Medicine. 2019;22:195-208.
62. Khorsandi D, Nodehi M, Waqar T, Shabani M, Kamare B, Zare EN, et al. Manufacturing of Microfluidic Sensors Utilizing 3D Printing Technologies: A Production System. Journal of Nanomaterials. 2021;2021.
63. Xiang N, Han Y, Jia Y, Shi Z, Yi H, Ni Z. Flow stabilizer on a syringe tip for hand-powered microfluidic sample injection. LAB ON A CHIP. 2019;19(2):214-22.
64. Lee J, Rahman F, Laoui T, Karnik R. Bubble-induced damping in displacement-driven microfluidic flows. PHYSICAL REVIEW E. 2012;86(2).
65. Gruner P, Riechers B, Orellana LAC, Brosseau Q, Maes F, Beneyton T, et al. Stabilisers for water-in-fluorinated-oil dispersions: Key properties for microfluidic applications. CURRENT OPINION IN COLLOID & INTERFACE SCIENCE. 2015;20(3):183-91.
66. Ma C, Peng YS, Li HT, Chen WQ. Organ-on-a-Chip: A New Paradigm for Drug Development. Trends in Pharmacological Sciences. 2021;42(2):119-33.
67. Zhou Y, Liu J, Yan J, Zhu T, Guo S, Li S, Li T. Standing air bubble-based micro-hydraulic capacitors for flow stabilization in syringe pump-driven systems. Micromachines. 2020 Apr 10;11(4):396.
68. Södergren S, Svensson K, Hjort K. Microfluidic active pressure and flow stabiliser.

Scientific Reports. 2021 Nov 18;11(1):22504.
69. Tung TT, Karunagaran R, Tran DNH, Gao B, Nag-Chowdhury S, Pillin I, et al. Engineering of graphene/epoxy nanocomposites with improved distribution of graphene nanosheets for advanced piezo-resistive mechanical sensing. JOURNAL OF MATERIALS CHEMISTRY C. 2016;4(16):3422-30.
70. Marck J. A nonlinear dynamical model of borehole spiraling (Doctoral dissertation, University of Minnesota).
71. Belhaiba A, El Ghazal N, Chraygane M, Bahani B, Ahmedou MO, Ferfra M. Modeling of a power Balance for microwaves generator with one magnetron. 2012 INTERNATIONAL CONFERENCE ON MULTIMEDIA COMPUTING AND SYSTEMS (ICMCS); 20122012. p. 1024-8.
72. Groisman A, Enzelberger M, Quake SR. Microfluidic memory and control devices. SCIENCE. 2003;300(5621):955-8.
73. Iyer V, Raj A, Annabattula RK, Sen AK. Experimental and numerical studies of a microfluidic device with compliant chambers for flow stabilization. Journal of Micromechanics and Microengineering. 2015 May 22;25(7):075003.
74. Cousseau P, Hirschi R, Frehner B, Gamper S, Maillefer D, editors. Improved micro-flow regulator for drug delivery systems. Technical Digest MEMS 2001 14th IEEE International Conference on Micro Electro Mechanical Systems (Cat No 01CH37090); 2001: IEEE.
75. Cerdeira ATS, Campos JBLM, Miranda JM, Araujo JDP. Review on Microbubbles and Microdroplets Flowing through Microfluidic Geometrical Elements. MICROMACHINES. 2020;11(2).
76. Gao D, Chang R, Lu B, Ma J. Progress on Controllable Preparation of Janus Nanomaterials. Polymer Materials Science & Engineering. 2019;35(1):168-75.
77. Lee M, Lee EY, Lee D, Park BJ. Stabilization and fabrication of microbubbles: applications for medical purposes and functional materials. SOFT MATTER. 2015;11(11):2067-79.
78. Tao J, Chow SF, Zheng Y. Application of flash nanoprecipitation to fabricate poorly water-soluble drug nanoparticles. ACTA PHARMACEUTICA SINICA B. 2019;9(1):4-18.
79. Deng B, de Ruiter J, Schroen K. Application of Microfluidics in the Production and Analysis of Food Foams. FOODS. 2019;8(10).
80. Choi A, Seo KD, Kim DW, Kim BC, Kim DS. Recent advances in engineering microparticles and their nascent utilization in biomedical delivery and diagnostic applications. LAB ON A CHIP. 2017;17(4):591-613.
81. Cairone F, Sanalitro D, Bucolo M, Ortiz D, Cabrales PJ, Intaglietta M. DPIV analysis of RBCs flows in serpentine micro-channel. In2017 European Conference on Circuit Theory and Design (ECCTD) 2017 Sep 4 (pp. 1-4). IEEE.
82. Afrasiab H, Movahhedy MR, Assempour A. Fluid-structure interaction analysis in microfluidic devices: A dimensionless finite element approach. International Journal for Numerical Methods in Fluids. 2012;68(9):1073-86.
83. Zhang DD, Wei SS, Wang GL, Wei CZ. Dynamics Research of Ultrasonic Peristaltic Micro-Fluid Driving Model. Advanced Materials Research. 2011 Apr 20;199:1391-6.
84. Wang YC, Lin SH, Jang D. Unsteady Analysis of the Flow Rectification Performance of

Conical Microdiffuser Valves for Valveless Micropump Applications. Journal of Mechanics. 2010;26(3):299-307.

85. Bai G, Wei S, Jiang C, Jiang X. Dynamic characteristic research of traveling wave driving microfluid model. In2006 IEEE International Conference on Information Acquisition 2006 Aug 20 (pp. 430-434). IEEE.
86. Yang X, Zhou Z, Ye X. Simulation and experimental studies on a micro diaphragm air pump actuated by PZT. InMicrofluidics, BioMEMS, and Medical Microsystems III 2005 Jan 22 (Vol. 5718, pp. 283-290). SPIE..
87. Li W, Zhuge W, Jiang Y, Jiang K, Ding J, Cheng X. A compact modularized power-supply system for stable flow generation in microfluidic devices. Microfluidics and Nanofluidics. 2023;27(12):80.
88. Zhang X, Zhu Z, Xiang N, Ni Z. A microfluidic gas damper for stabilizing gas pressure in portable microfluidic systems. Biomicrofluidics. 2016 Sep 1;10(5).
89. Wu J, Hirai Y, Kamei KI, Tsuchiya T, Tabata O. Novel microfluidic device integrated with a fluidic-capacitor to mimic heart beating for generation of functional liver organoids. Electronics and Communications in Japan. 2019;102(10):41-9.
90. Jackson WC, Tran HD, O'Brien MJ, Rabinovich E, Lopez GP. Rapid prototyping of active microfluidic components based on magnetically modified elastomeric materials. Journal of Vacuum Science & Technology B: Microelectronics and Nanometer Structures Processing, Measurement, and Phenomena. 2001 Mar 1;19(2):596-9.
91. Ghosal S. Lubrication theory for electro-osmotic flow in a microfluidic channel of slowly varying cross-section and wall charge. JOURNAL OF FLUID MECHANICS. 2002;459:103-28.
92. Ajdari A. Steady flows in networks of microfluidic channels: building on the analogy with electrical circuits. Comptes Rendus Physique. 2004;5(5):539-46.
93. Lam EW, Cooksey GA, Finlayson BA, Folch A. Microfluidic circuits with tunable flow resistances. APPLIED PHYSICS LETTERS. 2006;89(16).
94. Lee K, Kim C, Ahn B, Panchapakesan R, Full AR, Nordee L, et al. Generalized serial dilution module for monotonic and arbitrary microfluidic gradient generators. Lab on a Chip. 2009;9(5):709-17.
95. Leslie DC, Easley CJ, Seker E, Karlinsey JM, Utz M, Begley MR, et al. Frequency-specific flow control in microfluidic circuits with passive elastomeric features. NATURE PHYSICS. 2009;5(3):231-5.
96. Tsuda S, Jaffery H, Doran D, Hezwani M, Robbins PJ, Yoshida M, et al. Customizable 3D printed 'plug and play'millifluidic devices for programmable fluidics. PLoS One. 2015;10(11):e0141640.
97. Toepke MW, Abhyankar VV, Beebe DJ. Microfluidic logic gates and timers. LAB ON A CHIP. 2007;7(11):1449-53.
98. Mosadegh B, Kuo CH, Tung YC, Torisawa YS, Bersano-Begey T, Tavana H, et al. Integrated elastomeric components for autonomous regulation of sequential and oscillatory flow switching in microfluidic devices. NATURE PHYSICS. 2010;6(6):433-7.
99. Kim SJ, Yokokawa R, Cai Lesher-Perez S, Takayama S. Multiple independent

autonomous hydraulic oscillators driven by a common gravity head. Nature communications. 2015 Jun 15;6(1):7301.

100. Zhou Z, Xu M, Zhu C, He G, Zhang K, Sun D. Multistage Digital-to-Analogue Chip Based on a Weighted Flow Resistance Network for Soft Actuators. Micromachines. 2021 Aug 26;12(9):1016.
101. Capel AJ, Edmondson S, Christie SD, Goodridge RD, Bibb RJ, Thurstans M. Design and additive manufacture for flow chemistry. Lab on a Chip. 2013;13(23):4583-90.
102. Farahani RD, Dube M, Therriault D. Three-Dimensional Printing of Multifunctional Nanocomposites: Manufacturing Techniques and Applications. Advanced Materials. 2016;28(28):5794-821.
103. Huang LB, Yung KL, Xu Y, Xie YC. Injection molded plastic microfluidic biochips with integrated pumping electrode. In2010 IEEE 5th International Conference on Nano/Micro Engineered and Molecular Systems 2010 Jan 20 (pp. 1017-1020). IEEE.
104. Shahrubudin N, Lee TC, Ramlan R. An overview on 3D printing technology: Technological, materials, and applications. Procedia Manufacturing. 2019;35:1286-96.
105. Zhou LY, Fu J, He Y. A review of 3D printing technologies for soft polymer materials. Advanced Functional Materials. 2020;30(28):2000187.
106. Wang X, Jiang H, Chen Y, Qiao X, Dong L. Microblower-based microfluidic pump. Sensors and Actuators A: Physical. 2017;253:27-34.
107. Kitson PJ, Rosnes MH, Sans V, Dragone V, Cronin L. Configurable 3D-Printed millifluidic and microfluidic 'lab on a chip' reactionware devices. Lab Chip. 2012;12(18):3267-71.
108. Mehta V, Rath SN. 3D printed microfluidic devices: a review focused on four fundamental manufacturing approaches and implications on the field of healthcare. Bio-Design and Manufacturing. 2021;4(2):311-43.
109. Eren O, Çuhadaroğlu MB, Sezer K. Additive Manufacturing of Microfluidic Lab-on-a-Chip Devices. International Journal of 3D Printing Technologies and Digital Industry. 2021;5(3):692-708.
110. Au AK, Huynh W, Horowitz LF, Folch A. 3D-Printed Microfluidics. Angewandte Chemie-International Edition. 2016;55(12):3862-81.
111. Vittayarukskul K, Lee AP. A truly Lego®-like modular microfluidics platform. Journal of Micromechanics and Microengineering. 2017;27(3):035004.
112. Sochol R, Sweet E, Glick C, Venkatesh S, Avetisyan A, Ekman K, et al. 3D printed microfluidic circuitry via multijet-based additive manufacturing. Lab on a Chip. 2016;16(4):668-78.
113. Kanitthamniyom P, Zhou A, Feng S, Liu A, Vasoo S, Zhang Y. A 3D-printed modular magnetic digital microfluidic architecture for on-demand bioanalysis. Microsystems & Nanoengineering. 2020;6(1):48.
114. Lee Y, Kim B, Oh I, Choi S. Optofluidic Modular Blocks for On-Demand and Open-Source Prototyping of Microfluidic Systems. Small. 2018;14(52):1802769.
115. Kato N, Oka R, Sakai T, Shibata T, Kawashima T, Nagai M, Mineta T, Makino E. Experimental and computational analysis of water-droplet formation and ejection process using hollow microneedle. Japanese Journal of Applied Physics. 2011 Jun

20;50(6R):067202.
116. Celata GP, Cumo M, McPhail S, Zummo G. Characterization of fluid dynamic behaviour and channel wall effects in microtube. International Journal of Heat and Fluid Flow. 2006;27(1):135-43.
117. Zengerle R, Richter M. Simulation of microfluid systems. Journal of Micromechanics and Microengineering. 1994;4(4):192.
118. Vaicekauskaite J, Mazurek P, Vudayagiri S, Skov AL. Mapping the mechanical and electrical properties of commercial silicone elastomer formulations for stretchable transducers. Journal of Materials Chemistry C. 2020;8(4):1273-9.
119. Vaicekauskaite J, Mazurek P, Vudayagiri S, Skov AL. Silicone elastomer map: Design the ideal elastomer. InElectroactive Polymer Actuators and Devices (EAPAD) XXI 2019 Mar 13 (Vol. 10966, pp. 297-305). SPIE.
120. Herren B, Saha MC, Altan MC, Liu Y. Development of ultrastretchable and skin attachable nanocomposites for human motion monitoring via embedded 3D printing. Composites Part B: Engineering. 2020 Nov 1;200:108224.
121. Li Z, Mak SY, Sauret A, Shum HC. Syringe-pump-induced fluctuation in all-aqueous microfluidic system implications for flow rate accuracy. Lab on a Chip. 2014;14(4):744-9.
122. Zhou B, Gao Y, Tian J, Tong R, Wu J, Wen W. Preparation of orthogonal physicochemical gradients on PDMS surface using microfluidic concentration gradient generator. Applied Surface Science. 2019;471:213-21.